Non-nucleosidic Polyaromatic Building Blocks as DNA Base Surrogates

Inauguraldissertation
der Philosophisch-naturwissenschaftlichen Fakultät
der Universität Bern

vorgelegt von
Simon Matthias Langenegger
von Langnau i. E. (BE)

Leiter der Arbeit:
Prof. Dr. R. Häner
Departement für Chemie und Biochemie der Universität Bern

Non-nucleosidic Polyaromatic Building Blocks as DNA Base Surrogates

Inauguraldissertation
der Philosophisch-naturwissenschaftlichen Fakultät
der Universität Bern

vorgelegt von
Simon Matthias Langenegger
von Langnau i. E. (BE)

Leiter der Arbeit:
Prof. Dr. R. Häner
Departement für Chemie und Biochemie der Universität Bern

Von der Philosophisch-naturwissenschaftlichen Fakultät angenommen.

Bern, den 11. Mai 2005 Der Dekan:

Prof. Dr. P. Messerli

List of Publications and Patents

Publications

S. M. Langenegger, R. Häner
The effect of a non-nucleosidic phenanthrene building block on DNA duplex stability.
Helv. Chim. Acta. **2002**, *85*, 3414-3421.

A. Stutz, S. M. Langenegger , R. Häner
Phenanthrene-derived DNA hairpin mimics.
Helv. Chim. Acta. **2003**, *86*, 3156-3163.

S. M. Langenegger, L. Moesch, F. Natt, J. Hall, R. Häner
A novel oxime-derived solid support for the synthesis of 3'-phosphorylated oligonucleotides.
Helv. Chim. Acta. **2003**, *86*, 3476-3481.

S. M. Langenegger, R. Häner
A simple, non-nucleosidic base surrogate increases duplex stability of DNA containing an abasic site.
Chem. Biodiv. **2004**, *1*, 259-264.

S. M. Langenegger , R. Häner
DNA containing phenanthroline- and phenanthrene-derived, non-nucleosidic base surrogates.
Tetrahedron Lett. **2004**, *45*, 9273-9276.

S. M. Langenegger, R. Häner
Excimer formation by interstrand stacked pyrenes.
Chem. Commun. **2004**, *45*, 2792 - 2793.

S. M. Langenegger, R. Häner
Remarkable stabilization of duplex DNA containing an abasic site by non-nucleosidic phenanthroline and pyrene building blocks.
ChemBioChem, **2005**, in press

Patent

S. Langenegger, R. Häner

Molecular Beacons

Case UB-06/076 (24.09.04)

Table of Contents

Summary 1
1. Introduction 3
1.1. Structure of DNA 4
1.2. π-π Interactions/ Aromatic Interactions 7
1.2.1. A Theoretical Model for π-π Interactions 7
1.2.2. Experimental Determination of Stacking Energies 9
1.3. Non-hydrogen-bonding Base Pairs and their Thermodynamic Stability 14
1.3.1. Non-hydrogen-bonding Base Pairs with a Deoxyribose Backbone 14
1.3.2 Non-hydrogen-bonding Base Pairs with a Non-nucleosidic Backbone 15
1.3.3. Stretches of Non-hydrogen-bonding Base Pairs 16
1.4. Aim of the Work 18
2. The Effect of a Non-nucleosidic Phenanthrene Building Block on DNA Duplex Stability 23
2.1. Abstract 23
2.2. Introduction 23
2.3. Results and Discussion 24
2.4. Experimental Section 29
3. DNA Containing Phenanthroline- and Phenanthrene-derived, Non-nucleosidic Base Surrogates 35
3.1. Abstract 35
3.2. Introduction 35
3.3. Results and Discussion 36
3.4. Conclusions 40
4. A Simple, Non-Nucleosidic Base Surrogate Increases Duplex Stability of DNA Containing an Abasic Site 43
4.1. Abstract 43
4.2. Introduction 43
4.3. Results and Discussion 44
4.4. Conclusions 49
4.5. Experimental Section 49

5. Remarkable stabilization of duplex DNA containing an abasic site by non-nucleosidic phenanthroline and pyrene building blocks 53
5.1. Introduction 53
5.2. Results and Discussion 54
5.3. Conclusions 57
5.4. Experimental Section 58
6. Stretches of Interstrand Stacked Phenanthrenes in DNA 71
6.1. Introduction 71
6.2. Results and Discussion 71
6.3. Conclusions 75
6.4. Experimental Section 75
7. Excimer Formation by Interstrand Stacked Pyrenes 79
7.1. Introduction 79
7.2. Results and Discussion 79
7.3. Conclusions 83
7.4. Experimental Section 84
8. Control of Excimer Formation by Interstrand Stacking 89
8.1. Introduction 89
8.2. Results and Discussion 89
8.3. Conclusions 94
8.4. Experimental Section 94
9. Towards A New Type of Molecular Beacon 97
9.1. Introduction 97
9.2. Results and Discussion 98
9.3. Conclusions 101
9.4. Experimental Section 102
10. Phenanthrene-derived DNA Hairpin Mimics 105
10.1. Abstract 105
10.2. Introduction 105
10.3. Results and Discussion 106
10.4. Conclusions 111
10.5. Experimental Section 111
11. Conclusions and Outlook 119

Summary

Three different polyaromatic residues (phenanthrene **1**, phenanthroline **2**, pyrene **3**) with different linker lengths were synthesized and incorporated into oligodeoxynucleotides. Duplexes containing these flexible, non-nucleosidic polyaromatic building blocks in opposite positions can be used as base pair surrogates. Thermal denaturation experiments showed that every polyaromatic residues with optimized linkers, placed in opposite positions, stabilizes the duplex to a similar extent as an A/T base pair.

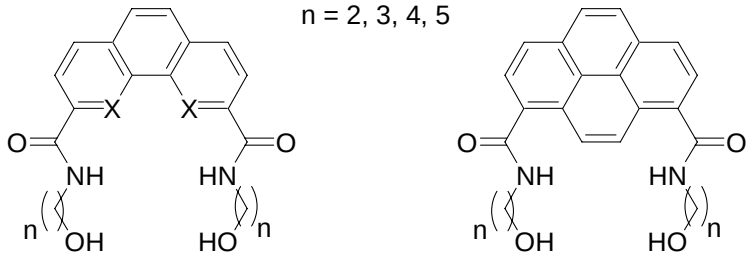

1 X = C-H
2 X = N

3

Based on spectroscopic data, a model of a duplex containing interstrand stacked polyaromatic residues was proposed. Furthermore, an increasing number of replacements of natural base pairs in a DNA duplex by phenanthrene-derived building blocks (**1**) showed a lengthening of the duplex in gel shift experiments, which is a consequence of the proposed interstrand stacking. Finally, the model could be further strengthened by the detection of excimer fluorescence in duplex DNA duplexes containing two pyrenes (**3**) in opposite positions.

Combinations of phenanthrene (**1**) and pyrene (**3**) derived building blocks were used for the development of a new type of a molecular beacon. The natural base pairs in the stem region of the molecular beacon were replaced by phenanthrene and pyrene derived building blocks, which serve as stabilizer of the stem and, at the same time, take the function of the fluorophor/quencher system.

In a further study, the different polyaromatic building blocks showed a significant effect on the stability of an abasic site-containing DNA duplex. The non-nucleosidic building blocks were positioned opposite to the abasic site. In comparison to a duplex containing a natural nucleotide (adenosine) opposite to abasic site, all building blocks led to a significant increase of the melting temperature as analyzed by thermal denaturation experiments.

Finally, self-complementary oligodeoxynucleotides containing a phenanthrene-derived building block (**1**) adopt highly stable, hairpin-like structures. The thermodynamic stability of these hairpin mimics is higher than the one of comparable hairpins with a dT_4- or dA_4-tetraloop.

1. Introduction

The era of the nucleic acid chemistry started in the year 1869 when Friedrich Miescher from Tübingen isolated from human pus cells and then from sperm of Rhine salmon a phosphorus containing substance, which he later on called nucleic acid [1]. In the following years, more and more articles about DNA were published; slowly, but inexorably, the mystery of the extensive supramolecular structure of DNA was solved. In the year 1952 *Todd et al.* could show that the primary structure of DNA is a linear polynucleotide in which each deoxribonucleoside is linked to the next by means of a 3'- to 5'- phosphodiester[2]. *Erwin Chargaff* investigated a very different aspect of order in DNA structure. He studied the base composition from a variety of sources and he found that the proportion of purines (A, G), is always equal to the proportion of pyrimidines (C, T) [3]. This observation was important for *Astbury* [4] and *Wilkins* [5] for the interpretation of the X-ray diffraction pattern. By combining all this data, *Watson* and *Crick* [6] proposed in the year 1953 the model of the double helix, in which the base adenine pairs specific with thymine and guanine with cytosine *via* hydrogen bonds. The individual base pairs were stacked with a distance of 3.4Å (*Figure 1.1.*). In that irregular sequence of nucleotide bases in the DNA of a cell all the information is stored, which is needed to carry out the function of that cell.

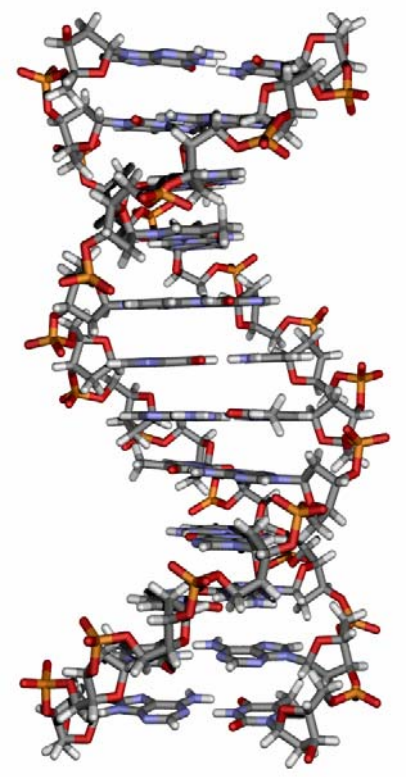

Figure 1.1. Model of a regular DNA Duplex.

In 1962, *Watson*, *Crick* and *Wilkins* received the *Nobel* price in medicine for their work. This started an era of intensive research of nucleic acids in chemistry, biochemistry and biology. One important role in this field was the chemical synthesis of nucleic acids. In 1956 *Khorana et al.* achieved the first synthesis of a thymine dimer [7]. In the eighties, the automated DNA synthesis was developed by *Caruthers* and *Köster*, which was based on phosphoramidite chemistry [8]. This method was further improved and by now, a huge variety of modified types of nucleic acids can be synthesized in an automated way.

1.1. Structure of DNA

DNA is a linear polynucleotide, in which each deoxribonucleoside is linked to the next by means of a 3', 5'- phosphodiester. The nucleotides are composed of three parts: a heterocyclic base, a pentose sugar, and a phosphate residue. There are four major nucleosides: Adenosine (A), thymidine (T), guanosine (G), and cytidine (C, *Figure 1.2.*). Two DNA single strands can form a duplex, in which the bases of one strand pair with the bases of the other strand through hydrogen bonds.

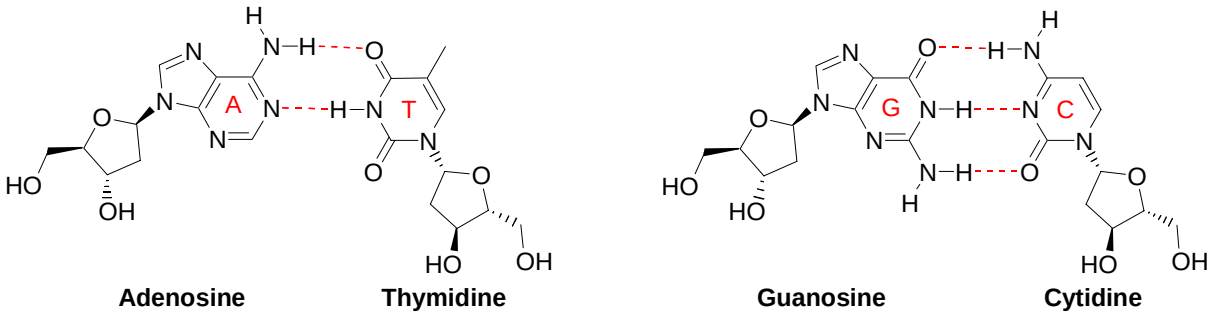

Figure 1.2. Watson-Crick base pairs for A/T and G/C.

DNA double helices posses two grooves of different depth and width, formed by the two sugar phosphate backbones of each strand. One is called minor groove and the other is the major groove, which is located on the opposite side (*Figure 1.3.*).

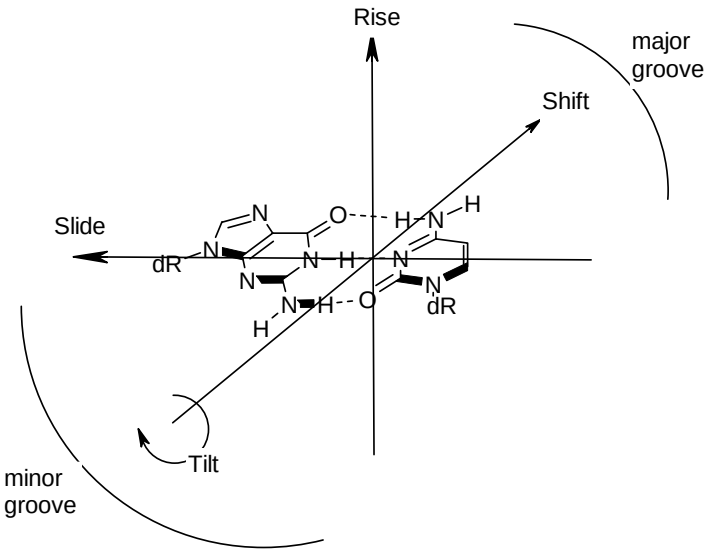

Figure 1.3. Major and minor groove of the DNA.

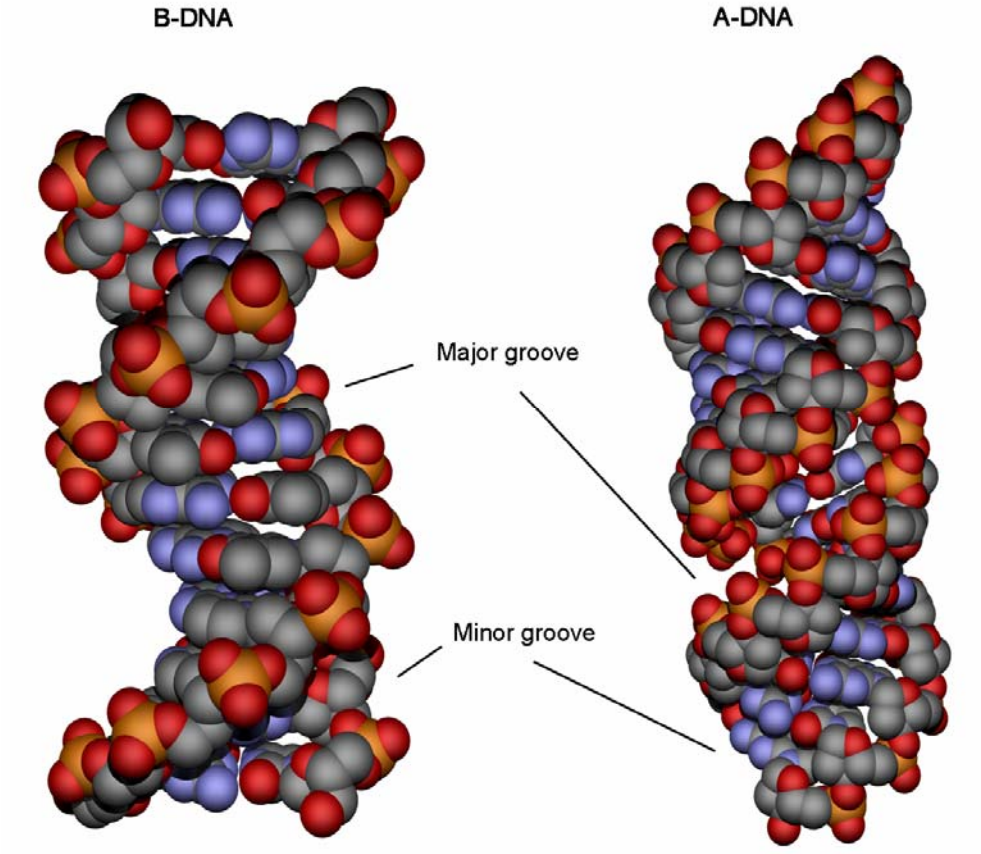

Figure 1.4. B-DNA (left) and A-DNA (right).

Three major types of DNA conformers exist: A-DNA, B-DNA and Z-DNA. A- and B-DNA form a right-handed double helix, whereas Z-DNA forms a left-handed helix. The B-DNA is the structure commonly adopted by DNA/DNA duplexes in the fully hydrated form. A-DNA is usually observed when DNA is dehydrated *in vitro*. Under high salt concentration, Z-DNA can be formed in G/C alternating DNA sequences. B-DNA has 10 bases per turn with little tilting of the bases to enhance the base stacking whereas the A-type helix has 11 bases per turn. The major groove of B-DNA is wide and the minor groove is narrow, in A-DNA the major groove is narrow and deep and the minor groove is broad and shallow (*Figure 1.4.*). In all DNA conformers, the grooves are solvated.

A difference between the A- and the B-duplex is also found in the sugar puckering mode (*Figure 1.5.*). In an A-form duplex, the sugar is predominantly in a C(3')-*endo* conformation whereas in a B-form duplex, it prefers a C(2')-*endo* conformation.

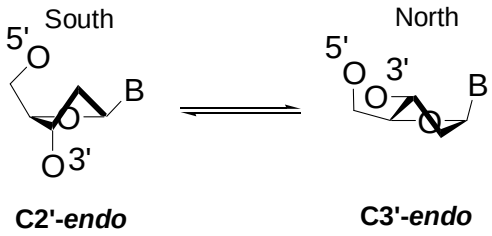

Figure 1.5. The sugar puckering modes.

In *Table 1.1.,* the characteristic geometrical differences between the DNA conformers are summarized.

Entry	A-DNA	B-DNA	Z-DNA
Helicity	Right-handed	Right-handed	Left-handed
Sugar puckering	C(3')-*endo*	C(2')-*endo*	C(2')-*endo* in pyrimidine and C(3')-*endo* in purine
Number of bases per turn	11	10	12
Distance between neighbouring base-pairs (Å)	2.9	3.3 - 3.4	3.7
Dislocation of base-pairs from the axis (Å)	4.5	-0.2 to -1.8	-2 to -3
Tilt of bases (°)	20	-6	7

Table 1.1. Comparison of helix parameters.

In all DNA duplex conformations, the helix is stabilized by two major interactions: The hydrogen bonds and the stacking interactions between the nucleotide bases.

1.2. π-π Interactions/ Aromatic Interactions [9-11]

Strong attractive interactions between π-systems have been known for over half a century. They control such diverse phenomena as: Double helical structures of DNA, the tertiary structures of proteins, intercalation of drugs in DNA, the packing of aromatic molecules in crystals, complexation in many host-guest systems, and porphyrin aggregation. But the understanding and prediction of these interactions are difficult, because it is not an electrostatic point-to-point interaction like a hydrogen bond; it is rather a framework of interactions, which is summarized as π-π interactions.

1.2.1. A Theoretical Model for π-π Interactions

In order to understand aromatic stacking interaction, it is important to consider the relative contribution of each of these forces to the interaction. The following part is overview on the different interactions, which are combined in the stacking interactions.

Van der Waals Interaction. This highly attractive interaction, which is the sum of the dispersion and repulsion energies, varies with r^{-6} and constrains the aromatic residues in *Van der Waals* contact. The *Van der Waals Interaction* also includes a repulsive exponential term, which is only important when the molecules are compressed to within *Van der Waals* contact distance.

Electrostatic interactions between partial atomic charges. Electronegative atoms like nitrogen and oxygen polarize the electron density and so these and neighboring atoms are associated with partial atomic charges. These interactions vary with r^{-1} and so are relatively long range effects. In highly polarized aromatics, such as DNA bases, the partial atomic charges are large. Thus, these are usually the largest single electrostatic interactions.

Electrostatic interactions between the charge distributions associated with the out of plane π-electron density. Aromatic molecules have a characteristic charge distribution. The nuclei form a positively charged σ-framework, which is sandwiched between two regions of negatively charged π-density (*Figure 1.6.*). Electrostatic interactions between these charge

distributions are unfavorable in face-to-fa.ce stacked geometries since repulsion between the π-electrons dominates. However, they can be favorable in *offset stacking* and *T-shape* geometries. These interactions vary roughly with r^{-5} and they are strongly geometry dependent.

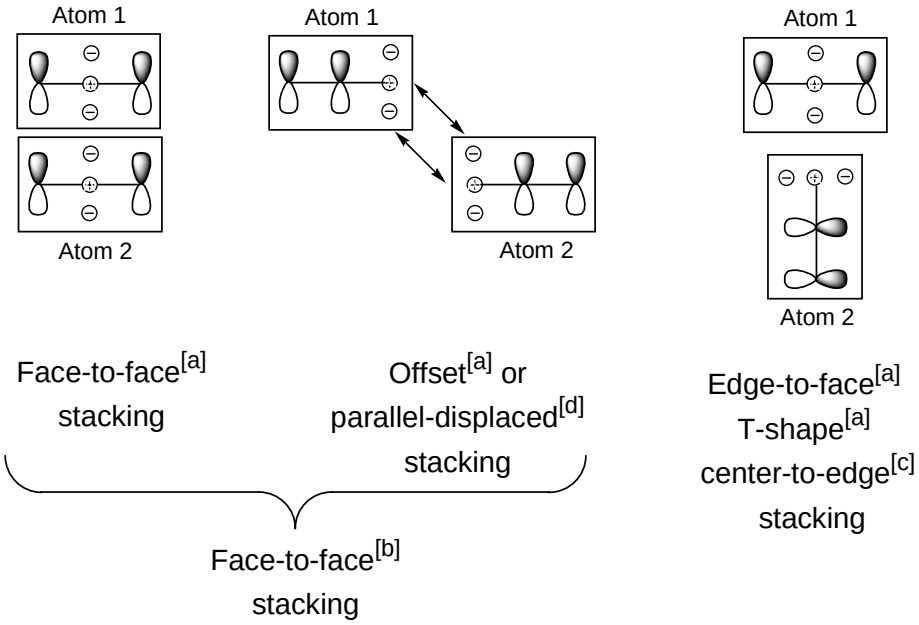

Figure 1.6. Electrostatic interactions in a face-to-face stacking geometry, in an offset stacking geometry or in an edge-to- face stacking geometry. [a] termed by Hunter [b], Kool [c], Siegel [d] and Diederich (illustration adopted from C. Brotschi [12])

Electrostatic interactions between the charge distributions associated with the out of plane - electron density and the partial atomic charges. This term varies roughly r^{-4} and so is quite sensitive to geometry. It is also relatively large due to the large partial atomic charges.

Charge-transfer. Although charge-transfer bands are common in aromatic complexes. Charge-transfer is not always observed, indicating that it is not related to the mechanism of interactions. Theoretical calculations suggest that these effects make a very small contribution to the stability of the ground state of molecular complexes.

Induction. There is little experimental evidence to suggest that induction effects are important in aromatic interactions.

The interaction of aromatic residues and solvent. In literature these effects are also called; solvation effect, desolvation, solvophobic force, solvation-driven force or hydrophobic effect.

Already the number of terms that exist leads to the assumption of controversial debate in literature. For example, *Hunter* argues that the flat π-electron surfaces of aromatic molecules are non-polar so that solvophobic forces favor stacking interaction. *Diederich et al.* also concluded that water is the best solvent for apolar bonding by studying host-guest systems of pyrene and cyclophane [13]. These findings are in contrast to *Gellman*'s experiments with linked aromatic residues, which suggest no significant solvent-induced interactions [14,15].

1.2.2. Experimental Determination of Stacking Energies

A large variety of experiments were done to gain a better view into stacking interactions. For example *Hunter* and *Sanders* proposed 1990 a simple model of the charge distribution in a π-system to explain the strong geometrical requirements for interactions between aromatic molecules [10]. The key features of the model is that it considers the σ-framework and the π-electrons separately and demonstrates that the net favorable π-π interactions are actually the result of π-σ attractions that overcome π-π repulsions (*Figure 1.6.*). They could show that the calculations correlate with the observation that porphyrines offset stacked, in crystals as well as in solution (*Figure 1.7.*).

Figure 1.7. Two porphyrins that stack in an offset arrangement. The π-stacked porphyrins are not rotated relative to one another. The distance between them is 3-4Å.

Overall, the conclusion was, that the π-σ attraction rather than the π-π interaction leads to favorable interactions. These electrostatic effects determine the geometry of interaction, while *Van der Waals* interactions and solvophobic effects make the major contribution to the magnitude of the observed interaction. Further they deduced that the widespread simple *electron-donor-acceptor concept* can be misleading since within any one molecule there will

be both electron rich and electron poor regions. The net intermolecular interaction depends critically on how such regions are aligned.

In a different study, *Cozzi* and *Siegel* demonstrated the importance of the electrostatic contributions [16-18]. They synthesized series of substituted 1,8-diarylnaphthalenes and studied the variation of the barrier to aryl-naphthalene bond rotation as a function of the aryl substitution (*Figure 1.8.*).

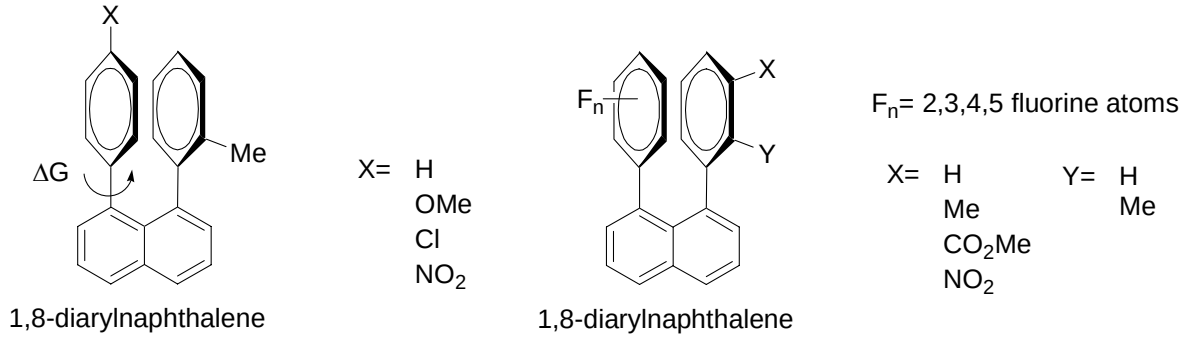

Figure 1.8. Substituted diarylnaphthalenes to study the aromatic stacking interactions.

The results showed that the acceptor-donor interaction is not the most favourable interaction. Rather, an acceptor-acceptor arrangement results in the most favourable interaction. The explanation for this is that an electron withdrawing substituent (NO_2) decreases the electron density and thereby two electron deficient π-systems are best due to reduced repulsion forces. Electron donating substituents (OMe, NMe_2) are increasing the electron density, which leads to an increase in π-repulsion and thereby to a less favourable interaction due to electronic repulsion. To determine the importance of quadrupolar effects in aromatic interactions, experiments with fluorinated diarylnaphthalene have been carried out. Increasing fluorination of one phenyl ring leads to an increase of the rotation barrier, which is plausible since fluorine acts as an electron-withdrawing group and therefore minimizes π-repulsion. The perfluorinated ring reversed the trend in the rotation-barrier as a function of substitutes (H, NO_2 etc.). These findings underline that electrostatic effects are an important contribution. But, in contrast to the work of *Hunter* and *Sanders*, the investigated stacking moieties were geometrically restrained in this study.

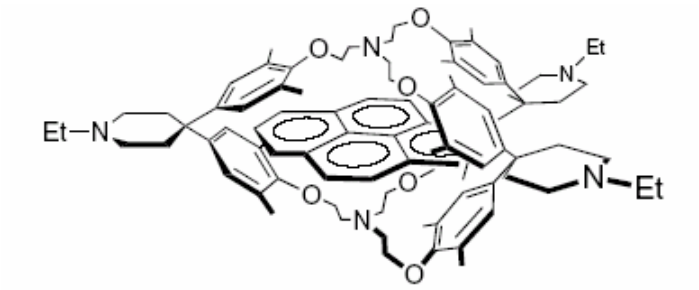

Figure 1.9. Pyrene cyclophane complex.

To get a deeper view insight into solvation effects, *Diederich et al.* [19] investigated host-guest systems (*Figure 1.9.*). They compared the free enthalpy of complexation of pyrene and cyclophane in different solvents [20]. They found a strong linear relationship between the free enthalpy and the solvent polarity. The most polar solvent, water, was the best for apolar bonding.

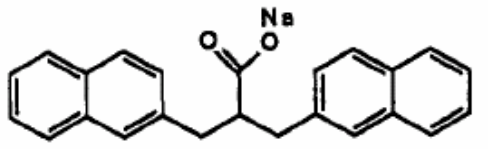

Figure 1.10. Flexible dinaphthyl carboxylates**.**

Another approach to investigate the hydrophobic effect was chosen by *Gellman et al.*. They synthesized flexible dinaphthyl carboxylates (*Figure 1.10.*) and measured their stacking properties by NMR in water [21]. No evidence of intramolecular naphtyl-naphtyl association was detected in aqueous solution. Later, the three-atom linker was replaced by a four-atom linker for which they observed an edge to face geometry of the flexible dinaphthyl carboxylate in the crystal, in water, in benzene and also in chloroform [22]. From this, they concluded that there were no significant solvent-induced interactions.

Kool et al. [23,24], studied the stacking interaction of dangling nucleotides. Single nucleotides of interest were placed at the ends of a duplex (*Figure 1.11.*). The resulting stabilization of the duplex by the dangling base can be measured by thermal denaturation experiments and can be compared to the stability of the duplex lacking the added nucleotide. The energetics of stacking can, thus, be measured separately from hydrogen bonding.

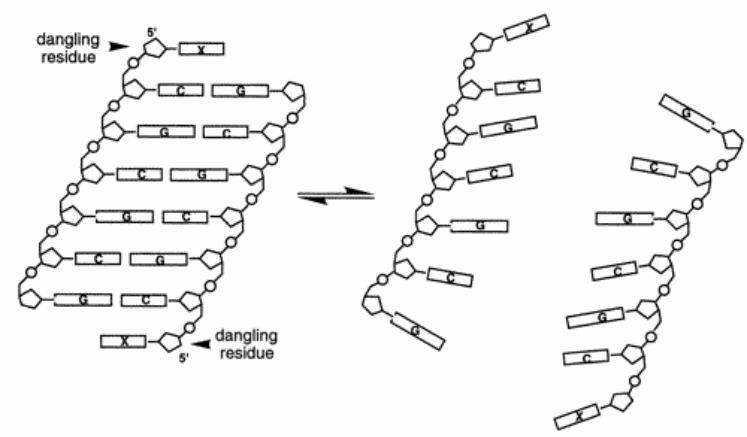

Figure 1.11. Illustration of dangling ends in a duplex (left) and when melted into two single strands (right).

The authors investigated different natural and unnatural nucleotides as dangling ends (*Figure 1.12.*). The different moieties varied in sizes, shape and polarity.

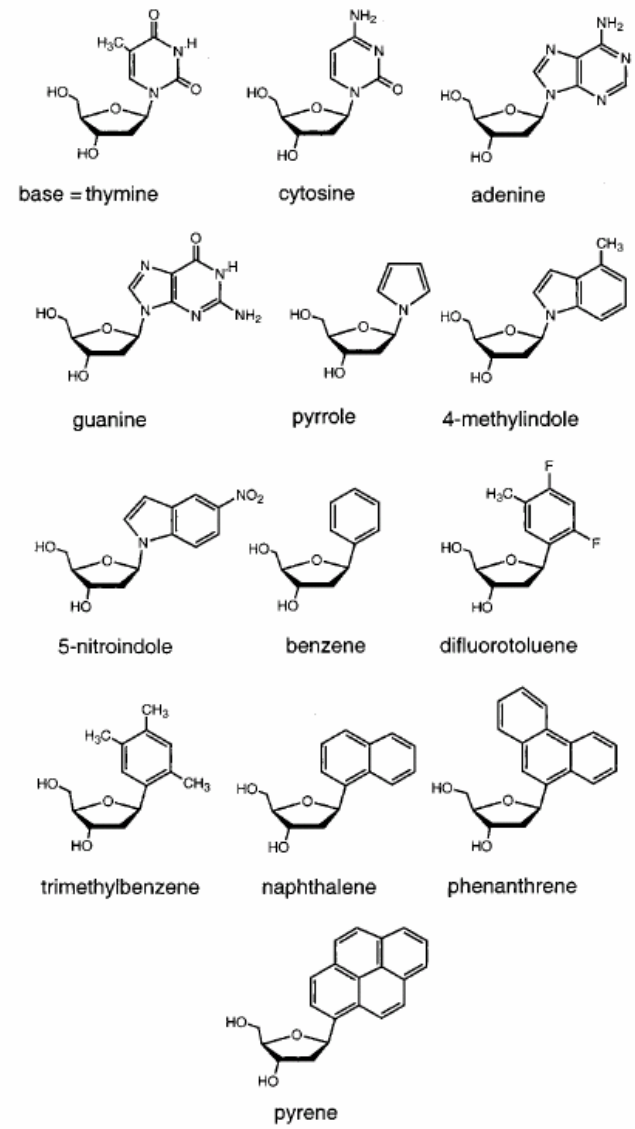

Figure 1.12. Structures of the dangling ends.

To test for general correlations between these relative apparent stacking free-energy values and calculated physical properties of the aromatic bases, they plotted the various properties (log P, polarizability, surface area excluded, dipole moment) as a function of the experimental stacking energies (*Figure 1.13.*).

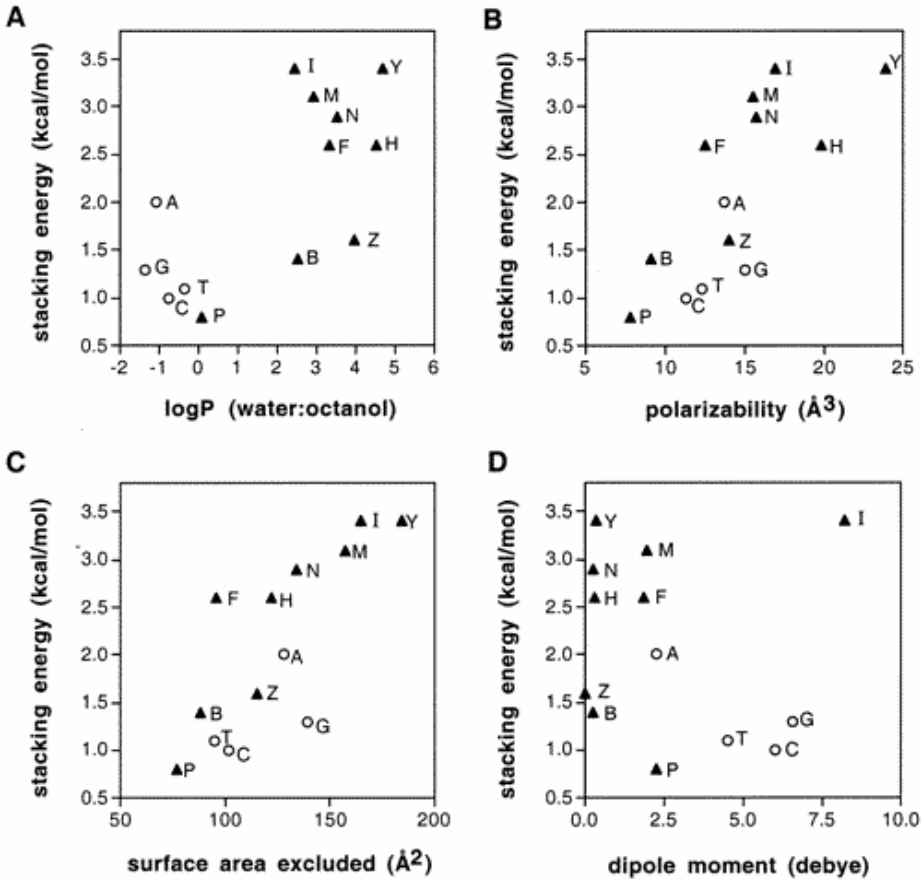

Figure 1.13. Relationship between the stacking free energies and calculated physical properties of the DNA bases and aromatic analogs. (A) Hydrophobicity, as measured by log P for the methylated bases; (B) calculated polarizability; (C) estimated surface area of the dangling residue excluded from the solvent on stacking; (D) dipole moment of the methylated bases. Data for natural bases are given by circles, data for other analogs by triangles. Abbreviations are as follows; A (adenine), B (benzene), C (cytosine), F (difluorotoluene), G (guanine), H (phenanthrene), I (5-nitroindole), M (4-methylindol), N (naphthalene), P (pyrrole), T (thymine), Y (pyrene), Z (trimethylbenzene).

There appears to be no quantitatively close linear correlation between any single property and stacking ability, indicating that more than one property is important in the energetic of stacking. But, in general, *Kool et al.* concluded that the hydrophobic effects are larger than electrostatic effects and dispersion forces. Similar experiments were also done by *Seela et al.*, who used modified nucleobases as dangling ends. Their conclusion was that a higher

polarizability leads to a higher thermal stability of the duplex and consequently better stacking abilities [25].

1.3. Non-hydrogen-bonding Base Pairs and their Thermodynamic Stability

1.3.1. Non-hydrogen-bonding Base Pairs with a Deoxyribose Backbone

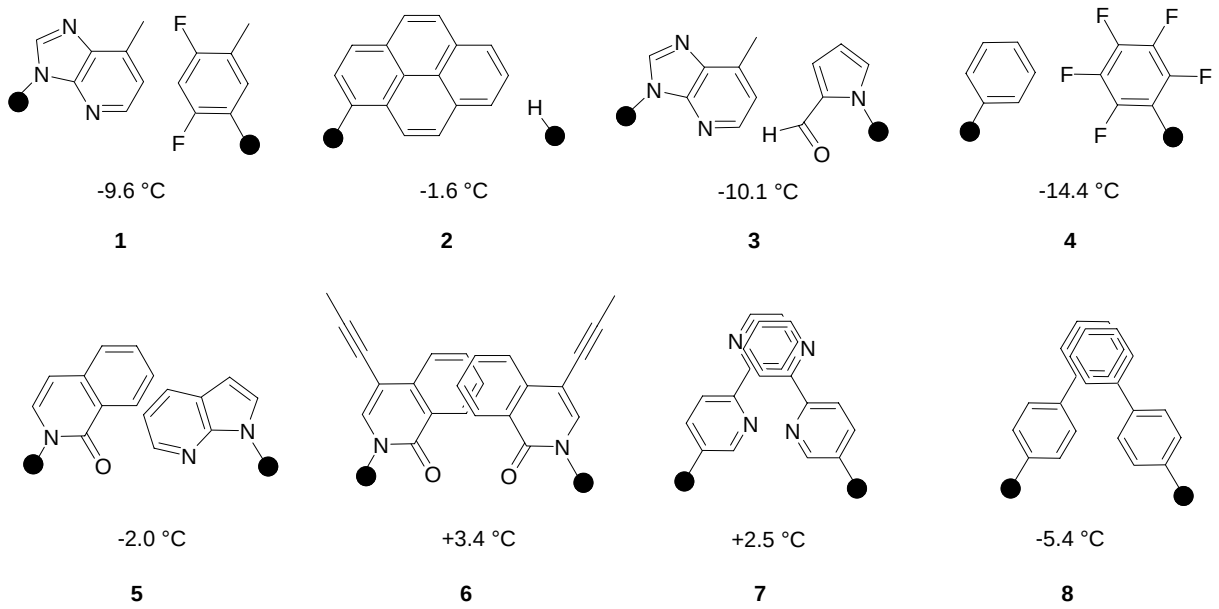

Figure 1.14. Non-hydrogen-bonding base-pairs. The values report the difference in T_m between the base-pairs and the natural A/T base pair in the given context (negative values indicates a lower affinity, positive values a higher affinity than a natural A/T base pair). The filled cycle marks the deoxyribose.

The first non-hydrogen-bonding base pairs with a sugar backbone were developed, because they are orthogonal to the natural base pairs and are selectively replicated by polymerase enzymes [26,27]. In 1998, *Kool et al.* described the first non-hydrogen bonding base-pair (**1**, *Figure 1.14.*), an isoster of the A/T base-pair. It shows a decreased duplex stability compared to the natural A/T base-pair by 9.6 °C in the given context [28]. Another base-pair analog developed by *Kool et al*. is the pyrene/abasic site pair (**2**). This is not a base pair in the classical sense, since only one of the nucleosides is carrying a base, while the other partner is an abasic site (a stable tetrahydrofuran-abasic site analog). Such a pair is only 1.6 °C less stable than a natural A/T base-pair. In that case the pyrene moiety interacts with the complementary strand by stacking interaction which implies that interstrand stacking can stabilize a DNA-duplex [29]. *Yokoyama et al.* developed a hydrophobic base-pair (**3**) between

pyrrole-2-carbaldehyde and 9-methylimidazol[(4,5)-b]pyridine, which destabilizes the duplex by about 10°C compared to an A/T base pair [30]. *Hunziker et al.* investigated the base pair **4** [31]. The idea was that the inverse quadrupolar moments of benzene and hexafluorobenzene, leading to an edge-to-edge attractive intermolecular force, should compensate for the loss of the hydrogen bonds. Destabilization of about 15 °C compared to a natural A/T base pair in the given duplex was observed. *Schultz, Romesberg et al.* also investigated non-natural hydrophobic base pairs in an effort to find new orthogonal base pairs, which might be used to expand the genetic code [32, 33]. Of particular interest was **5**, which consists of isocarbostyril and 7-azaindole. Compared to a natural A/T base pair, **5** is only slightly less stable. The base-pair number **6** [34] has a duplex stability, which excels that of a A-T base-pair or G/C base-pair by 3.4 °C or 0.8 °C, respectively. This is due to partial overlap of the extended aromatic surface area leading to interstrand stacking between the units [35]. *Leumann et al.* studied the base pairs **7** and **8**, for which they proposed interstrand stacking as the duplex stabilizing force [36, 37].

1.3.2 Non-hydrogen-bonding Base Pairs with a Non-nucleosidic Backbone

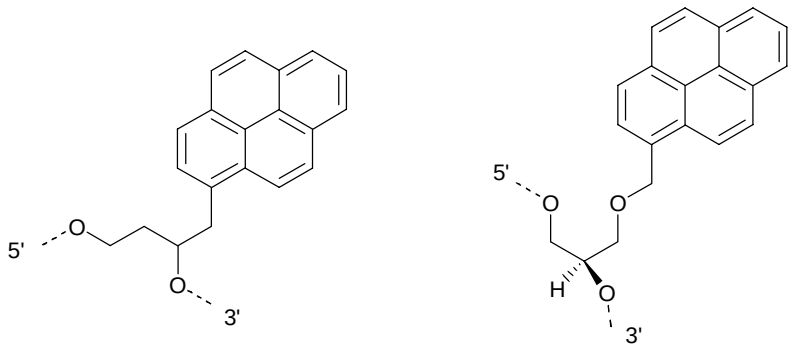

Figure 1.15. Non-hydrogen bonding base pairs with a flexible backbone.

Non-hydrogen-bonding base substitutes with a flexible backbone are not so common in the literature. *A priori*, an increase in flexibility will lead to a loss in preorganisation, which should lead to a destabilisation of the DNA duplex. The examples, which are found, are mainly used for diagnostic purposes and not for forming thermodynamically stable base pairs and duplexes. *Korshun et al.* investigated the fluorescence properties of the racemate of 4-(1-pyrenyl)-1,3-butandiol (*Figure 1.15.*) in DNA at different positions. Among other things, they placed the building blocks in opposite positions but didn't measure the thermodynamic

stability of these duplexes [38]. Also *Pedersen et al.* used 1-*O*-(1-pyrenylmethyl)glycerol (*Figure 1.15.*) as a diagnostic tool [39]. In 2004, they reported a NMR structure of two 1-*O*-(1-pyrenylmethyl)glycerols in opposite positions in a DNA duplex (*Figure 1.16.*) [40]. The structure shows that the pyrene moieties are interstrand stacked. The thermodynamic stability is about 0.7°C less stable than the duplex without pyrenes. This observation indicates that it is possible to obtain about the same stabilisation with a flexible backbone as with a sugar backbone if the base surrogates are interstrand stacked.

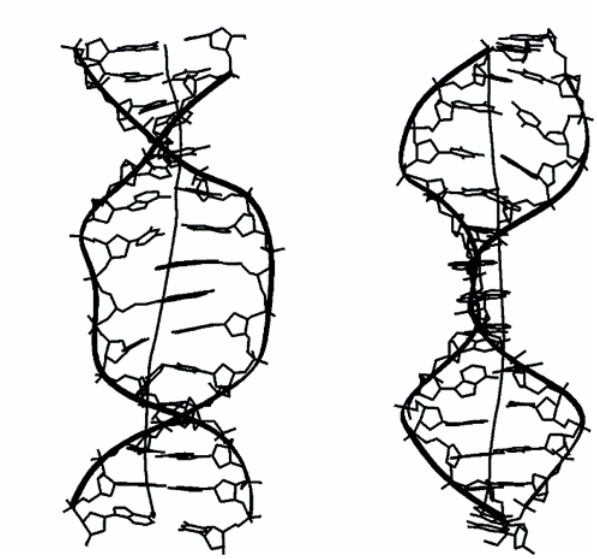

Figure 1.16. NMR structure of two pyrenes in opposite positions.

1.3.3. Stretches of Non-hydrogen-bonding Base Pairs

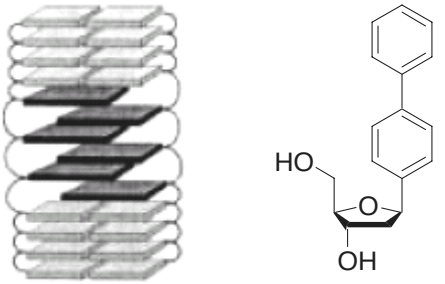

Figure 1.17. Zipper like biphenyls (darkgrey) and natural bases (grey) (left); the biphenyl C-nucleoside residue (right).

As described in the previous chapter, only non-hydrogen-bonding base pairs, which are able to form interstrand stacking interaction are comparably stable as a natural base pair. This is necessary if incorporation of more than one non-hydrogen-bonding base pair is attempted.

Leumann et al. incorporated up to four (per each strand) of their biphenyl C-nucleoside residues (*Figure 1.17.*) into a DNA duplex. They suggested a zipper like motif, in which the biphenyls are interstrand stacked (*Figure 1.16.*) [37].

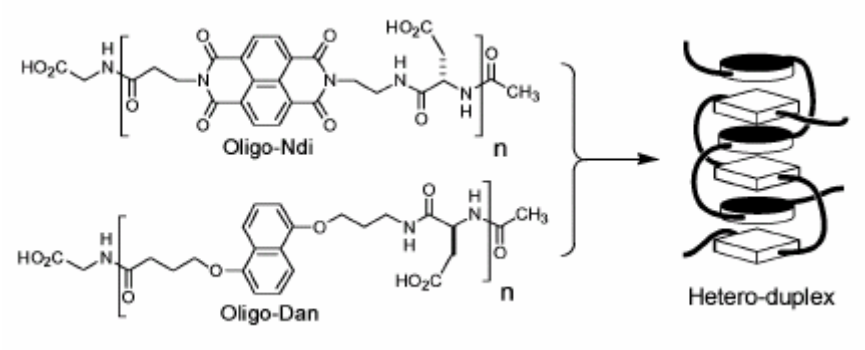

Figure 1.18. Interstrand stacking of eletron rich and electron deficient units.

Iverson et al. investigated something different: in their system, the stacking unit is a part of the backbone. Also in that case the duplex is stabilized by interstrand stacking (*Figure 1.18.*) [41]. They synthesized up to four non-hydrogen-bonding base pairs duplexes and determined the binding constants by NMR and isothermal titration calorimetry (ITC). The binding constant increases about two orders of magnitude from the two-mer ($2.7*10^3$ M^{-1}) to the four-mer ($3.5*10^5$ M^{-1}).

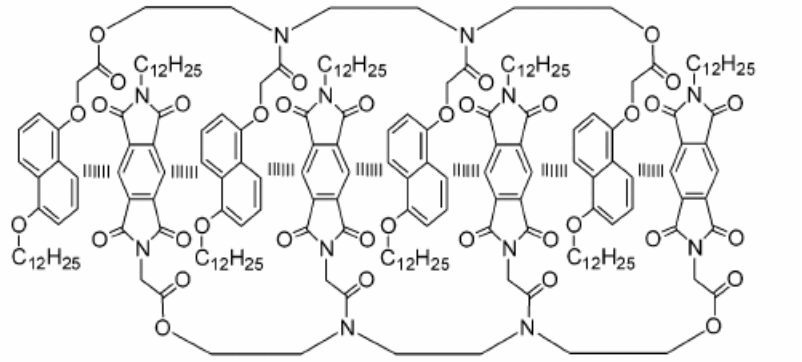

Figure 1.19. Zipper shaped artificial duplex.

Similar experiments were also done by *Li et al.,* but the measurements were done in chloroform and they used a classical linkage from the stacking residue to the backbone (*Figure 1.19.*) [42]. *Li et al.* observed also an eletron-transfer absorbance, which increased by the length of the oligomer.

1.4. Aim of the Work

Beside the hydrogen bonds, stacking interactions are one of the major interactions in DNA [43]. Several approaches were pursued to gain more information on stacking interactions or, alternatively, to use stacking interactions to form stable DNA duplexes (*Chapter 1.3.*). In 2001, when we started the project, most of the work was done with modified nucleosides (*Chapter 1.3.1.*). The aim of the present work was the synthesis and investigation of DNA containing non-nucleosidic, non-hydrogen bonding building blocks. Firstly, not a lot was known about flexible backbones in combination with non-hydrogen bonding bases. Secondly, stacking interactions are the result of several different forces (*Chapter 1.2.1.*), some of which are highly geometry sensitive. Thus, a higher degree of flexibility may well turn out to be an advantage. A further point was an easy synthesis, which would provide simple access to a large variety of different building blocks.

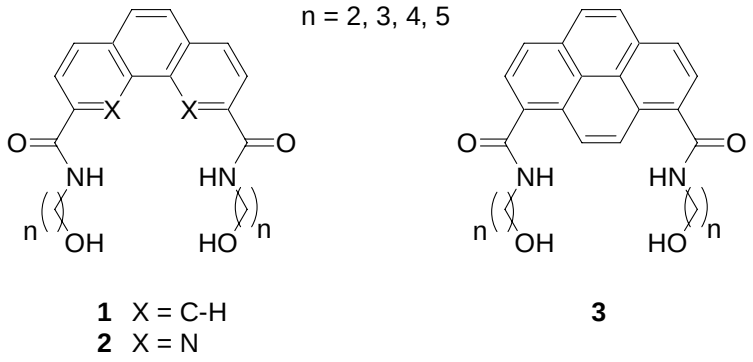

1 X = C-H
2 X = N

3

Figure 1.20. Non-nucleosidic building blocks.

To achieve all the objectives listed above, we decided for the non-nucleosidic building blocks in *Figure 1.20.*. The two isosteric compounds **1** (phenanthrene derived) and **2** (phenanthroline derived), which have different dipol moments, as well as compound **3** (pyrene derived) with an enlarged π-system served as the primary target structures. Furthermore, pyrene is highly fluorescent and is known to give rise to excimer fluorescence if two molecules are stacked. This property can be used to investigate the relative geometry of the pyrene building blocks in the context of a DNA duplex.

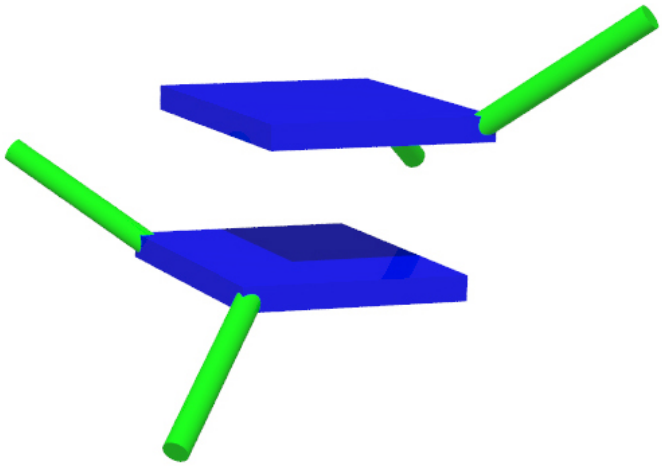

Figure 1.21. Proposed interstrand stacking of the non-nucleosidic building blocks.

In these building blocks, the stacking unit is a part of the backbone (*Figure 1.21.*). The design of the compounds ensures the simple introduction of linkers of different length and type. Incorporation of these building blocks should also help to better further explore the nature of stacking interactions, in particular interstrand stacking modes.

References

[1] F. Miescher Hoppe Seyler's , *Med. Chem. Unters.* **1871**, 441.

[2] A. R. Todd, D. M. Brown, *J. Chem. Soc.* **1952**, *52*, 52.

[3] E. Chargaff, *Fed. Proc.* 1951, *10,* 654.

[4] W. T. Astbury, F. C. Bell, *Nature* **1938**, *141*, 747.

[5] M. H. F. Wilkins, W. E. Seeds, A. R. Stockes, H. R. Wilson, *Nature* **1953**, *172*, 759.

[6] J. D. Watson, F. H. Crick *Nature* **1953**, *171*, 737.

[7] H. G. Khorana, G. M. Teuer, J. G. Moffat, E. H. Pol, *Chem. Ind.* (London) **1956**, 1523.

[8] M. H. Caruthers, M. D. Matteuci, *J. Am. Soc.* **1981**, *103*, 3185.

[9] C. A. Hunter, K. R. Lawson, J. Perkins, C. J. Urch, *J. Chem. Soc. Perkin Trans. 2*, **2001**, 651-669.

[10] C. A. Hunter, J. K. M. Sanders, *J. Am. Chem. Soc.* **1990**, *112*, 5525-5534.

[11] C. A. Hunter, *J. Mol. Biol.* **1993**, *230*, 1025-1054.

[12] Ch. Brotschi, *Thesis University of Bern* **2004**.

[13] D. B. Smithrud, F. Diederich, *J. Am. Chem. Soc*. **1990**, *112*, 339-343.

[14] L. F. Newcomb, S. H. Gellman, *J. Am. Chem. Soc*. **1994**, *116*, 4993-4994.

[15] L. F. Newcomb, T. S. Haque, S. H. Gellman, *J. Am. Chem. Soc*. **1995**, *117*, 6509-6519.

[16] F. Cozzi, M. Cinquini, R. Annunziata, T. Dwyer, J. S. Siegel, J. Am. Chem. Soc. **1992**, 114, 5729-5733.

[17] F. Cozzi, M. Cinquini, R. Annunziata, J. S. Siegel, *J. Am. Chem. Soc.* **1993**, *115*, 5330-5331.

[18] F. Cozzi, J. S. Siegel, *Pure and Appl. Chem.* **1995**, 67, 683-689.

[19] E. A. Meyer, R. K. Castellano, F. Diederich, *Angew. Chem. Int. Ed*. **2003**, 42, 1220-1250

[20] D. B. Smithrud, F. Diederich, *J. Am. Chem. Soc*. **1990**, *112*, 339-343.

[21] L. F. Newcomb, S. H. Gellman, *J. Am. Chem. Soc*. **1994**, *116*, 4993-4994.

[22] L. F. Newcomb, T. S. Haque, S. H. Gellman, *J. Am. Chem. Soc*. **1995**, *117*, 6509-6519.

[23] K. M. Guckian, B. A. Schweitzer, R. X.-F. Ren, C. J. Sheils, P. L. Paris, D. C. Tahmassebi, E. T. Kool, J. Am. Chem. Soc. 1996, 118, 8182-8183.

[24] K. M. Guckian, B. A. Schweitzer, R. X.-F. Ren, D. C. Tahmassebi, E. T. Kool, J. Am. Chem. Soc. 2000, 122, 2213-2222.

[25] H. Rosemeyer, F. Seela, *J. Chem. Soc., Perkin Trans. 2,* **2002**, 746-750.

[26] J. C. Delaney, P. T. Henderson, S. A. Helquist, J. C. Morales, J. M. Essigmann, E. T. Kool, *Proc. Natl. Acad. Sci.* **2003**, *100*, 4468-4473.

[27] E. T. Kool, J. C. Morales, K. M. Guckian, *Angew. Chem. Int. Ed.* **2000**, *39*, 990-1009.

[28] K. M. Guckian, J. C. Morales, E.T. Kool, *J. Org. Chem.* **1998**, *63*, 9652-9656.

[29] T. J. Matray, E. T. Kool, *J. Am. Chem. Soc*. **1998**, *120*, 6191-6192.

[30] T. Mitsui, A. Kitamura, M. Kimoto, T. To, A. Sato, I. Hirao, S. Yokoyama, *J. Am. Chem. Soc.* **2003**, *125*, 5298-5307.

[31] G. Mathis, J. Hunziker, *Angew. Chem. Int. Ed.* **2002**, *41*, 3203-3205.

[32] Y. Wu, A. K. Ogawa, M. Berger, D. L. McMinn, P. G. Schultz, F. E. Romesberg, *J. Am. Chem. Soc*. **2000**, *122*, 7621-7632.

[33] A. K. Ogawa, Y. Wu, D. L. McMinn, J. Liu, P. G. Schultz, F. E. Romesberg, *J. Am. Chem.* Soc. **2000**, *122*, 3274-3287.

[34] M. Berger, A. K. Ogawa, D. L. McMinn, Y. Wu, P. G. Schultz, F. E. Romesberg, *Angew. Chem.* **2000**, *122*, 3069-3071.

[35] A. A Henry, F. E. Romesberg, *Curr. Opin. Chem. Biol*. **2003**, *7*, 727-733.

[36] C. Brotschi, A. Häberli, C. J. Leumann, *Angew.Chem.* **2001**, 113, 3101-3103; *Angew. Chem. Int. Ed.* **2001**, 40, 3012-3014.

[37] C. Brotschi, C. J. Leumann, *Angew. Chem. Int. Ed.* **2003**, 42, 1655-1658.

[38] K. V. Balakin, V. A. Korshun, I. I. Mikhalev, G. V. Maleev, A. D. Malakhov, I. A. Prokhorenko, Yu. A. Berlin, *Biosensors and Bioelectronics* **1998**, 13, 771-778.

[39] U. B. Christensen, E. B. Pedersen, *Nucleic Acid Res.* **2002**, 30, 4918-4925.

[40] C. B. Nielsen, M. Petersen, E. B. Pedersen, P. E. Hansen, U. B. Christensen, *Bioconjugate Chem.* **2004**, 15, 260-269.

[41] G. J. Gabriel, B. L. Iverson, *J. Am. Chem. Soc.* **2002**, 124, 15174-15175.

[42] Q. Z. Zhou, X. K. Jiang, X. B. Shao, G. J. Chen, M. X. Jin, Z. T. Li, *Org. Lett.* **2003**, 5, 1955-1958.

[43] W. Saenger, *Principles of Nucleic Acid Structure*, Springer, New York, **1984**.

2. The Effect of a Non-nucleosidic Phenanthrene Building Block on DNA Duplex Stability

Simon M. Langenegger, Robert Häner, *Helv. Chim. Acta* **2002**, 85, 3414-3421.

2.1. Abstract

Oligonucleotides containing a phenanthrene-derived, non-nucleosidic building block with flexible linkers were synthesized. The effect of the phenanthrene moiety on duplex stability at different positions was investigated. Placement of two phenanthrene residues in opposite positions had a slightly positive effect on duplex stability. This positive effect was further increased when two phenanthrene pairs were placed at juxtaposed positions. In contrast, introduction of a single phenanthrene unit opposite to an adenosine or a thymidine led to a destabilization of the duplex. A model of a phenanthrene-modified duplex is proposed.

2.2. Introduction

Modified oligonucleotides have found widespread applications as diagnostic and research tools. In addition, incorporation of different chemical modifications into oligonucleotides can lead to a better understanding of biological and chemical properties of nucleic acids. Chemical changes of sugar, base or phosphate backbone have been a topic of intense research. Furthermore, combinations of different chemical modifications are well known and have substantially contributed to innovation in the field of antisense technology [1,2]. The influence of nucleoside-linked aromatic and heteroaromatic base analogs on duplex stability and base pairing properties has been reported [3-6] and reviewed [7]. As part of our activities aimed at the development of non-nucleosidic DNA building blocks, we investigated the influence of a phenanthrene unit on duplex stability. Here, we report the synthesis and properties of oligonucleotides containing non-nucleosidic phenanthrene building blocks.

2.3. Results and Discussion

Chemical synthesis of the phenanthrene phosphoramidite building block is shown in *Scheme 2.1.*. The known dimethyl 4,4'-stilbene dicarboxylate **1** was prepared in analogy to the procedures reported in the literature [8]. Formation of the phenanthrene was achieved by oxidative photochemical cyclisation of **1** [9]. The thus obtained phenanthrene diester **2** was treated with 3-amino-1-propanol to afford the corresponding dicarboxamide **3**. Reaction of **3** with 4,4'-dimethoxy tritylchloride under controlled conditions (see *experimental section*) gave the mono-protected intermediate **4**, which was subsequently transformed into the phosphoramidite derivative **5**.

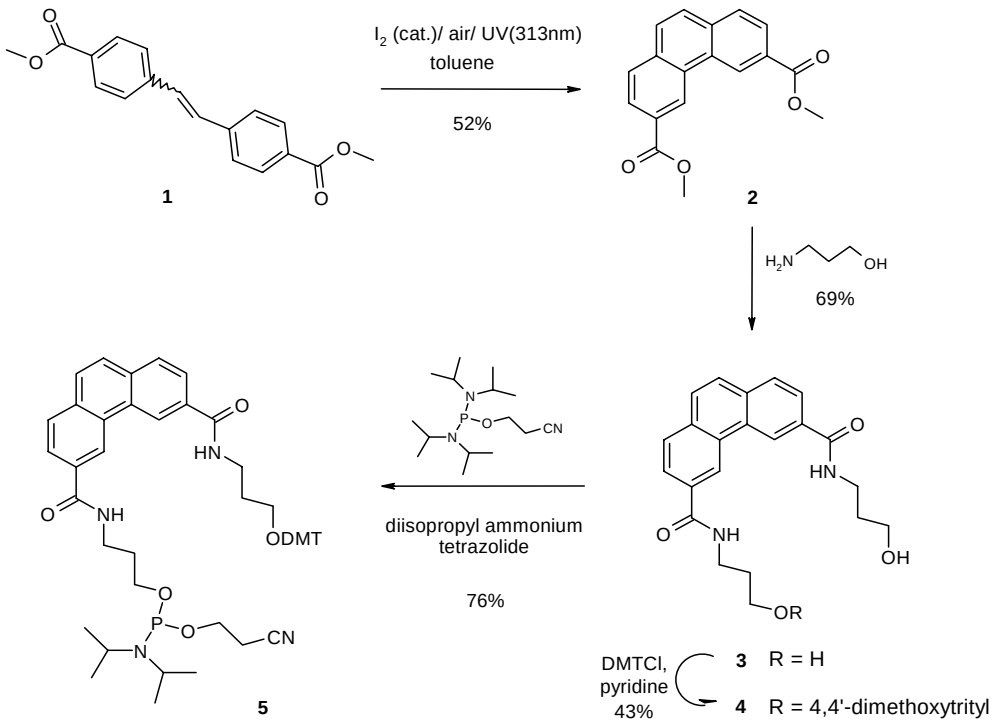

Scheme 2.1. Synthesis of the phenanthrene dicarboxamide-derived phosphoramidite building block **5**.

For control purposes, we synthesized an open chain linker lacking the phenanthrene moiety. Thus, dimethyl malonate was treated with 3-amino-1-propanol to yield diamide **6**, which was directly transformed into the mono-protected **7**. Phosphitylation gave the desired phosphoramidite **8**.

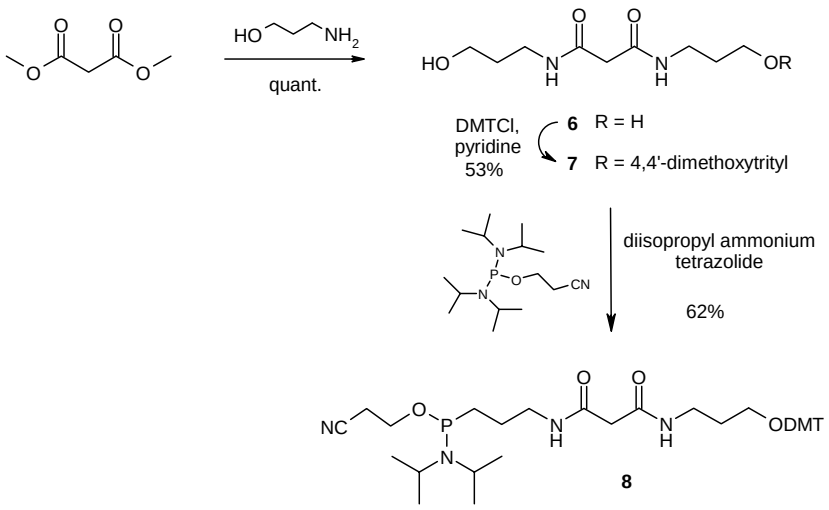

Scheme2.2. Synthesis of the malonamide-derived phosphoramidite building block **8**.

Building blocks **5** and **8** were incorporated into oligonucleotides at various positions. Assembly of the different oligonucleotides involved the standard phosphoramidite procedure [10,11]. To ensure a high incorporation yield of the modified building blocks, a longer coupling time was allowed in the respective cycles (see *experimental section*). Deprotection (*conc*. ammonia, 55°C), followed by standard HPLC purification yielded oligonucleotides **9-20** (*Table 2.1.*). The effect of the building block **5** on duplex stability was analysed by thermal denaturation experiments. As can be seen from *Table 2.1.*, placement of a phenanthrene (**P**) opposite to a canonical base (thymine or adenine, entries 2 and 3) results in a considerable destabilisation (ΔTm -3.7 and -5.4°C, respectively). On the other hand, no destabilization is observed if two phenanthrenes are placed at opposite sites in the duplex (ΔTm +0.3°C, entry 4). Surprisingly, two pairs of phenanthrenes in juxtaposed positions lead to a clear stabilisation of the duplex (ΔTm/mod +1.3°C, entry 5). Other combinations of **P-P** pairs, which are not placed in juxtaposed positions (entries 6 and 7) have a marginal effect. To better understand the contribution of the phenanthrene moiety to duplex formation, we synthesized oligonucleotides **19** and **20** containing the linker **L**, in which a simple methylene unit has replaced the phenanthrene. A strong decrease (ΔTm -17.7°C) in duplex stability was observed if **L** was placed opposite to a natural base (adenine; see *Table 2.1.*, entry 8), which is well in agreement with data observed with a similar linker [12]. A duplex containing two **L**‘s in opposite positions (entry 9) shows an even larger destabilization (ΔTm -20.7°C). On the other hand, placement of **P** opposite to **L** (entry 10) partially reduces this destabilization (ΔTm -12.3°C). Thus, the phenanthrene moiety significantly contributes to duplex stability.

Entry	Oligo #	Duplex	Tm (°C)	ΔTm (°C)	ΔTm/mod (°C)
1	**9** **10**	5' AGC TCG GTC ATC GAG AGT GCA 3' TCG AGC CAG TAG CTC TCA CGT	67.7		
2	**9** **11**	5' AGC TCG GTC ATC GAG AGT GCA 3' TCG AGC CAG T**P**G CTC TCA CGT	64.0	-3.7	**-3.7**
3	**12** **10**	5' AGC TCG GTC A**P**C GAG AGT GCA 3' TCG AGC CAG TAG CTC TCA CGT	62.3	-5.4	**-5.4**
4	**12** **11**	5' AGC TCG GTC A**P**C GAG AGT GCA 3' TCG AGC CAG T**P**G CTC TCA CGT	68.0	0.3	**0.3**
5	**13** **14**	5' AGC TCG GTC **PP**C GAG AGT GCA 3' TCG AGC CAG **PP**G CTC TCA CGT	70.3	2.6	**1.3**
6	**15** **16**	5' AGC TCG GT**P** A**P**C GAG AGT GCA 3' TCG AGC CA**P** T**P**G CTC TCA CGT	67.3	-0.4	**-0.2**
7	**17** **18**	5' AGC TCG G**P**C A**P**C GAG AGT GCA 3' TCG AGC C**P**G T**P**G CTC TCA CGT	68.3	0.6	**0.3**
8	**19** **10**	5' AGC TCG GTC A**L**C GAG AGT GCA 3' TCG AGC CAG TAG CTC TCA CGT	50.0	-17.7	**-17.7**
9	**19** **20**	5' AGC TCG GTC A**L**C GAG AGT GCA 3' TCG AGC CAG T**L**G CTC TCA CGT	47.0	-20.7	**-20.7**
10	**19** **11**	5' AGC TCG GTC A**L**C GAG AGT GCA 3' TCG AGC CAG T**P**G CTC TCA CGT	55.4	-12.3	**-12.3**
P =	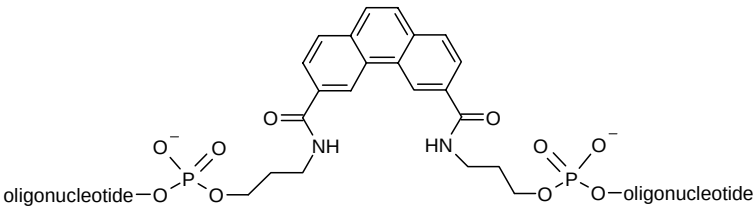				
L =	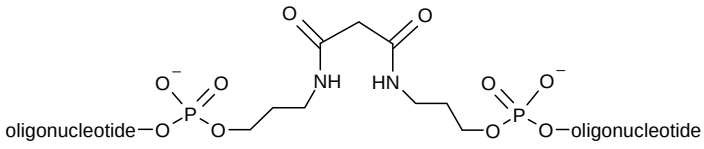				

Table 2.1. Hybridisation data (Tm, °C) of different oligonucleotides duplexes containing a phenanthrene based building block (**P**) or a linker without aromatic residue (**L**). All measurements were carried out at pH 7.5 and 100mM NaCl; for detailed conditions see experimental part.

The data obtained can be interpreted as a consequence of favorable stacking effects of the phenanthrene residue within the duplex. This is supported by the fact, that the duplex containing two **P-P** pairs (duplex **13**/**14**) shows a strongly increased hyperchromic effect compared to the unmodified duplex (duplex **9**/**10**, see *Figure 2.1.*). Circular dichroism (*CD*) spectral analysis of the duplex **13**/**14** is consistent with an overall B-conformation (data not shown).

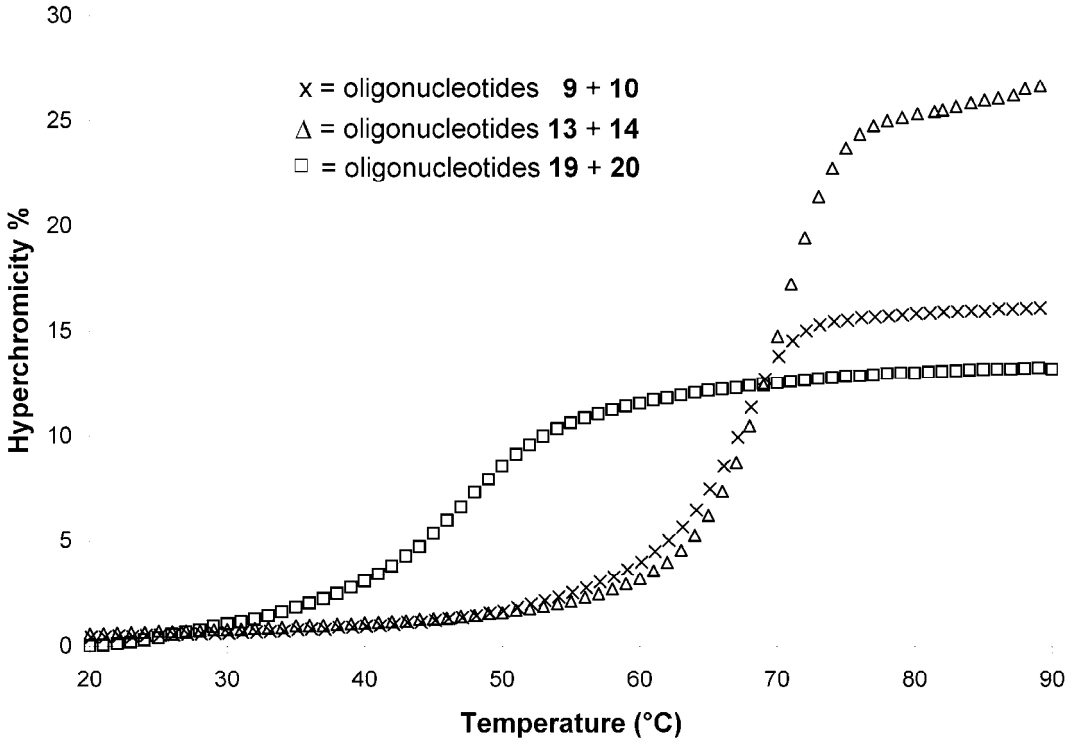

Figure 2.1. Tm curves of three different duplexes; x = unmodified duplex; Δ = duplex containing two **PP** pairs; □ = duplex containing a linker **L** in each strand (*cf.* also *Table 2.1*).

Finally, thermodynamic data were estimated from the thermal denaturation experiments (*see Table 2.2.*). As can bee seen, the parameters obtained by analysis of the melting curves (*curve fitting* method [13]) of the phenanthrene-modified duplex (entry 4) are comparable to the unmodified duplex (entry 1). Although the data obtained from the melting curves have to be interpreted with some caution (estimated error ±5%), they indicate an unfavorable reaction enthalpy for formation of the duplex containing two phenanthrenes (**P**), which is compensated by a favorable entropy term. On the other hand, the ΔH of formation of the duplex containing two linkers without phenanthrenes (**L**, entry 9) is very unfavorable and cannot be offset by a favorable ΔS. The calculated $\Delta G^{25°C}$ are reflecting the observed Tm's (*cf. Table 2.1.*).

Entry	Oligo #	Duplex	ΔH kcal mol^{-1}	ΔS cal mol^{-1} K^{-1}	ΔG$^{25°C}$ kcal mol^{-1}
1	**9** **10**	5' AGC TCG GTC ATC GAG AGT GCA 3' TCG AGC CAG TAG CTC TCA CGT	-129	-351	-24.3
4	**12** **11**	5' AGC TCG GTC A**P**C GAG AGT GCA 3' TCG AGC CAG T**P**G CTC TCA CGT	-117	-314	-23.4
9	**19** **20**	5' AGC TCG GTC A**L**C GAG AGT GCA 3' TCG AGC CAG T**L**G CTC TCA CGT	-63	-167	-13.2

Table 2.2. Comparison of thermodynamic parameters obtained from experimental UV melting curves (*curve fitting* method, estimated error ±5%) [13].

Based on the available data obtained we favor a model of a right-handed duplex in which two opposite aromatic phenanthrene units are stacked in an inter-strand fashion. Simple model considerations suggest that the relatively long and flexible linker arms enable a continuous duplex without loss of stacking interactions (see *Figure 2.2.*).

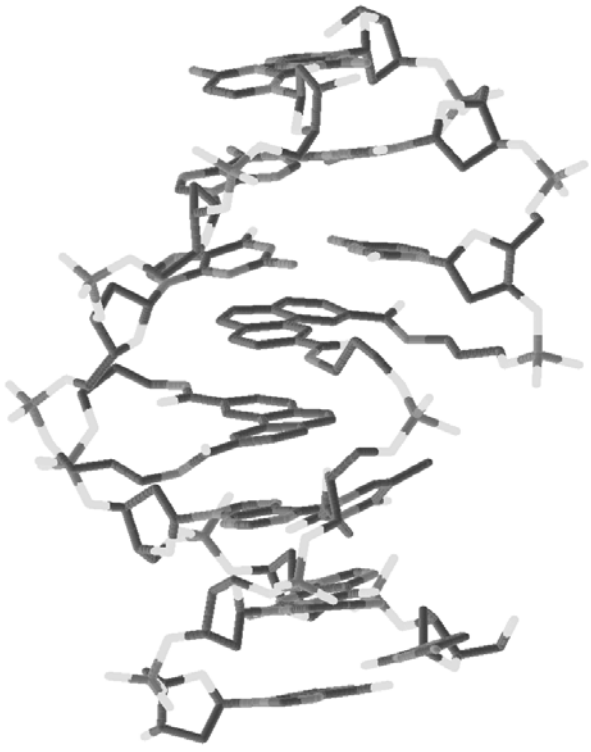

Figure 2.2. Illustration of a modified DNA duplex showing the possibility of inter-strand stacking of two phenanthrenes.

Such a model of a continuous duplex is in agreement with the observed thermodynamic stability, the relatively strong hyperchromicity and the shape of the melting curves, which shows a single, sharp transition indicative of a highly cooperative melting process. Finally, it is worth mentioning that the phenanthrene building block **P** strongly prefers a **P** in opposite position compared to a canonical base (A or T). The relative destabilizations (ΔTm -5.7 and -4.0°C, see *Table 2.1.*, entry 4 compared with entries 3 and 2, respectively) are well comparable to *Watson/Crick* base pair mismatches.

In conclusion, oligonucleotides containing non-nucleosidic phenanthrene building blocks (**P**) form stable duplexes. **P** strongly prefers **P** in opposite position compared to A or T. The data obtained are in agreement with a model of a continuous right-handed duplex with inter-strand stacked phenanthrenes.

2.4. Experimental Section

General

Chemicals, solvents and reagents for reactions were generally from Acros, Aldrich or Fluka, and were the highest quality available. Cyanoethoxy-bis(N,N-dimethylamino)phosphine was prepared according to the literature [14]. Solvents for extraction and chromatographie were of technical grade and distilled prior to use. TLC silica gel 60 F_{254} glass plates (*Merck*); visualisation by UV and or *A*) by dipping in a soln. of H_2SO_4/H_2O/EtOH 14:4:1 or *B*) cerium(IV) sulfate(3mM)/ammonium molybdate (250mM) in aq. H_2SO_4(10%), followed by heating. Flash column chromatography (CC) was performed on silica gel 60 (40-63 μm, 230-400 mesh, *Fluka*) at low pressure. In case of acid-sensitive compounds, the silica gel was pretreated with solvents containing 0.5-1% N-methylmorpholine. ^{1}H- and ^{13}C-NMR: *Bruker AC-300* δ values in ppm (solvents signals as internal standard), *J* [Hz]; ^{31}P-NMR: *Bruker AMX 400* δ values in ppm (85% H_3PO_4 as external standard). EI-MS: *Autospec Q (Micromass)* ionisation energy 70eV; only selected peaks; LSI-MS: *Autospec Q* Cs^+ ion gun. ESI-MS: *VG Platform* single quadrupole ESI-Mass spectrometer. Oligonucleotides were synthesized on a *392 DNA/RNA Synthesizer (Applied Biosystems)* using standard phosphoramidite chemistry [10, 11]. The nucleoside phosphoramidites were from *CHEMGENES (Ashland, MA)*. The standard synthetic procedure (trityl-off mode) was used and only for the non natural phosphoramidites the coupling time was extended to 5 min. Coupling efficiencies for all building blocks, including **5** and **8** were >98%. After standard detachment and deprotection (conc. NH_3, 55°C, 16h) the crude oligomers were purified bye

anion exchange HPLC *(Machery-Nagel, Nucleogen DEAE 60/7)* and desalted over *Sep-Pak cartridges (Waters, Milford, USA).* All oligonucleotides were analysed by electrospray mass spectrometry. The masses were found to be within 0.0005 % of the expected mass. UV melting curves were determined at 260 nm on a *Varian Cary 3e* spectrophotometer that was equipped with a *Peltier* block using the *Varian WinUV* software. Complementary oligonucleotides were mixed to 1:1 stoichiometry and the solutions adjusted to a final duplex concentration of 0.5-0.7 μM in 0.1mM TrisHCl, 100mM NaCl, pH 7.5. A *heating-cooling-heating* cycle in the temperature range 0-90° or 20-90°C was applied with a temperature gradient of 0.5°C/min. All ramps were indicating equilibrium melting processes. T_m values were defined as the maximum of the first derivative of the melting curve. Thermodynamic date were determined directly from the melting curves bye a curve fitting procedure that is based on the two state model for a bimolecular non self-complementary oligonucleotide pair [13]. Abbreviations: DMT: 4,4'-dimethoxytrityl.

Experiments Referring to Scheme 2.1.

Dimethyl 3, 6-phenanthrene dicarboxylate (**2**) [9]. A solution of 4.25 g (14.4mmol) dimethyl 4,4'-stilbene dicarboxylate **1** [8] in 3 l toluene containing 0.42 g (1.6 mmol) iodine, was irradiated for 24 h using a medium-pressure mercury lamp (125 W) in a quartz tube while oxygen was slowly bubbled through the reaction mixture. After removal of the solvent under reduced pressure, the residue was taken up in dichloromethane and passed through a short column of silicagel. Concentration of the eluate followed by addition of methanol precipitated a white solid, which on recrystalization from dichloromethane/methanol mixture, gave the required phenanthrene as white prisms (2.18g, 52% yield). TLC (EtOAc:hexane): R_f 0.34. ^{1}H-NMR (300MHz, $CDCl_3$): 4.07 (6H, s), 7.87 (2H,s), 7.96 (2H,d, J = 8.4), 8.26 (2H, d, J = 8.4), 9.50 (2H, s). ^{13}C-NMR (75MHz, $CDCl_3$): 52.5, 125.2, 127.1, 128.6, 128.8, 128.9, 130.0, 134.9, 167.3. EI-MS: 294 (100, $M^{+\cdot}$), 263(81), 176(79).

Phenanthrene-3,6-dicarboxylic acid bis-[(3-hyroxy-propyl)-amide] (**3**). A suspension of 3 g (10.2 mmol) **2** in 15 ml 3-amino-1-propanol was heated under reflux (160°C) for 30 min. The reaction mixture was acidified with 2 M hydrochloric acid and was extracted 4 × with 250 ml dichloromethane/isopropanol (3:1). The org. phase was dried (Na_2SO_4) and evaporated gave 2.7 g (69%) of a white solid. ^{1}H-NMR (300MHz, MeOD): 1.83 (4H, m), 3.50 (4H,t, J = 7.0), 3.62 (4H, t, J = 6.2), 7.82 (2H,m), 7.95 (4H, m), 9.33 (2H, s). ^{13}C-NMR (75MHz, D_6-DMSO):

32.6, 36.8, 39.5, 122.3, 125.6, 127.9, 128.6, 129.5, 133.1, 133.3, 166.4. EI-MS: 380 (4, $M^{+\cdot}$), 362 (6), 344(95), 288(100).

Phenanthrene-3,6-dicarboxylic acid 3-({3-[bis(4-methoxy-phenyl) -phenyl-methoxy]-propyl}–amide 6-[3-hydroxy-propyl)-amide (**4**). A solution of 2.7 g (7.1 mmol) **3** in 71 ml dry pyridine was placed under nitrogen. A solution of 2.4 g (7.1 mmol) DMT chloride in 45 ml dry pyridine was added slowly over 4 h at r.t. The mixture was stirred over night, then 250 ml EtOAc was added and was washed 3 × with sat. aq. $NaHCO_3$, then dried (Na_2SO_4) and evaporated under reduced pressure. The resulting residue was purified by CC on silica gel (EtOAc, 0.5% N-methylmorpholine). The production fractions were combined, evaporated, and dried under high vacuum to furnish 2.1g (43%) of a white foam. TLC (EtOAc): R_f 0.32. ^{1}H-NMR (300MHz, $CDCl_3$): 1.67(2H, t, *J* = 5.1), 1.98 (2H. t, *J* = 5.8), 3.34 (2H, t, *J* = 5.3), 3.67 (6H, s), 3.72 (4H,m), 3.80 (2H, t, *J* = 5.3), 6.74 (4H,m) 7.2-8.9 (15H,m), 8.92 (1H, s), 9.02 (1H, s). ^{13}C-NMR (75MHz, $CDCl_3$): 29.2, 32.0, 37.9, 55.2, 60.4, 62.6, 86.7, 113.3, 121.6, 122.3, 124.6, 125.6, 126.9, 128.0, 128.2, 128.7, 128.9, 129.6, 129.8, 130.1, 132.6, 133.7, 133.8, 136.2, 144.8, 158.6, 168.0, 168.6. ESI-MS(pos.): 683 (20, $[M+H]^+$) , 303 (100, DMT).

Diisopropyl-phosphoramidous acid 3-[(6-{3-[bis- (4-methoxy-phenyl)-phenyl-methoxy]-propylcarbamoyl}-phenanthrene-3-carbonyl)-amino]-propyl ester 2-cyanoethylester (**5**). A suspension of 345 mg (2.01 mmol) diisopropylammonium tetrazolide and 661 µl (1.84 mmol) cyanoethoxy-bis(N,N-dimethylamino)phosphine in 5 ml dry CH_2Cl_2, was placed under nitrogen, then added slowly a solution of 1 g (1.46mmol) **4** in 10 ml dry CH_2Cl_2 at r.t. After 45 min 100 ml CH_2Cl_2 was added to the reaction mixture, washed with 100ml sat. aq. $NaHCO_3$, dried (K_2CO_3), and evaporated under reduced pressure. The resulting oil purified by CC on silica gel (EtOAc/hexane(1:1), 1% N-methyl-morpholine). The production fractions were combined, evaporated, and dried under high vacuum to furnish 980 mg (76%) of a white foam. TLC (EtOAc/hexane(1:1): R_f 0.21. ^{1}H-NMR (300MHz, $CDCl_3$): 1.08 (12H, m), 1.92 (4H, m), 2.53 (2H,m), 3.26 (2H, m), 3.50 (2H, m), 3.62 (10H, m), 3.72 (2H, m), 3.79 (2H, m), 6.90 (4H, m), 6.89 (2H, m), 7.1-7.4 (7H, m), 7.6-8.0 (6H, m) 9.06 (1H, s), 9.11 (1H, s). ^{13}C-NMR (75MHz, $CDCl_3$): 20.7, 24.7, 24.8, 29.4, 30.7, 38.3, 39.2, 43.1, 43.3, 55.2, 55.6, 58.3, 58.6, 62.3, 62.6, 113.3, 122.2, 122.6, 124.9, 125.3, 126.9, 128.0, 128.17, 128.3, 129.0, 130.1, 133.3, 134.0, 136.2, 158.6, 167.7. ^{31}P-NMR (161.9MHz, $CDCl_3$): 149.3.

Experiments Referring to Scheme 2.2.

N,N'-*Bis-(3-hydroxy-propyl)-malonamide* (**6**). A solution of 1.73 ml (15.1 mmol) dimethyl malonate in 6.8 ml 3-amino-1-propanol was heated under reflux (160°C) for 1 h, then the solvent was removed by vacuum destillation, the white solid residue was the pure product 3.3 g (quant.). ^{1}H-NMR (300MHz, $CDCl_3$): 1.73 (4H,m), 3.20 (2H,s), 3.46 (4H,m), 3.67 (4H, t, *J* = 5.6) ^{13}C-NMR (75MHz, D_6-DMSO): 32.3, 35.9, 43.4, 58.4, 166.9 LSI-MS (DTT/DTE): 219 ($[M+H]^+$).

N-*{3[bis-(4-methoxy-phenyl)-phenyl-methoxy]-propyl}*-N'-*(3-hydroxy-propyl)-malonamide* (**7**). A solution of 2.0 g (9.7 mmol) **6** in 70 ml dry pyridine was placed under nitrogen. A solution of 3.3 g (7.1 mmol) DMT chloride in 45 ml dry pyridine was added slowly over 1h at r.t. The mixture was stirred over night, then 250 ml EtOAc was added and was washed 3 × with sat. aq. $NaHCO_3$, then dried (Na_2SO_4) and evaporated under reduced pressure. The resulting residue was purified by CC on silica gel (EtOAc:MeOH (9:1), 0.5% N-methylmorpholine). The production fractions were combined, evaporated, and dried under high vacuum to furnish 1.71 g (35%) of a colorless oil. TLC (EtOAc:MeOH[9:1]): R_f 0.24. ^{1}H-NMR (300MHz, $CDCl_3$): 1.69 (2H, m), 1.80 (2H, m), 3.05 (2H,s), 3.21 (2H, t, *J* = 5.6), 3.41 (4H, m), 3.61 (2H, t, *J* = 5.6) 3.80 (6H,s), 6.84 (4H, m), 7.2-7.4 (9H, m). ^{13}C-NMR (75MHz, $CDCl_3$): 29.3, 32.1, 36.3, 38.0, 42.8, 46.5, 55.3, 59.4, 61.5, 86.3, 113.3, 126.9, 127.9, 128.1, 130.0, 136.2, 145.0, 158.6, 167.5, 168.0. EI-MS: 520 (2, $M^{+\cdot}$), 303 (100, DMT).

Diisopropyl-phosphoramidous acid 3-[(6-{3-[bis-(4-methoxyphenyl)phenyl-methoxy]propylcarbamoyl}acetylamino)propylester-2-cyanoethylester(**8**). A suspension of 461 mg (2.69 mmol) diisopropylammonium tetrazolide and 880 µl (2.46 mmol) cyanoethoxy-bis(N,N-dimethylamino)phosphine in 8 ml dry CH_2Cl_2, was placed under nitrogen, then added slowly a solution of 1 g (1.97 mmol) **7** in 13.3 ml dry CH_2Cl_2 at r.t. After 3 h 100 ml CH_2Cl_2 was added to the reaction mixture, washed with 100ml sat. aq. $NaHCO_3$, dried (K_2CO_3), and evaporated under reduced pressure. The resulting oil purified by CC on silica gel (EtOAc/hexane(2:1), 1% N-methylmorpholine). The production fractions were combined, evaporated, and dried under high vacuum to furnish 959 mg (69%) of a colorless oil. TLC (EtOAc/hexane(2:1): R_f 0.25. ^{1}H-NMR (300MHz, $CDCl_3$): 1.10 (12H, m), 1.72 (4H, m), 2.57 (2H, t, J = 6.4) 2.96 (2H, s), 3.10 (2H, t, J = 5.7), 3.3-3.6 (6H, m), 3.71 (6H,s), 6.76 (4H, m), 7.15-7.22 (9H, m) ^{13}C-NMR (75MHz, $CDCl_3$): 20.5, 24.7, 24.8, 29.3, 30.6, 30.7, 37.0, 37.9,

42.9, 43.0, 43.2, 55.3, 58.2, 58.5, 61.5, 61.7, 86.2, 113.2, 117.9, 126.9, 127.9, 128.1, 130.0, 136.2, 145.0, 158.5, 167.1, 167.4 ^{31}P-NMR (161.9MHz, $CDCl_3$): 149.0.

References

[1] S. T. Crooke, *Antisense Nucleic Acid Drug Dev.* **1998,** *8* 115-122.

[2] A. De Mesmaeker, R. Häner, P. Martin, H. E. Moser, *Acc.Chem.Res.* **1995,** *28* 366-374.

[3] C. Brotschi, A. Haberli, C. J. Leumann, *Angewandte Chemie-International Edition* **2001,** *40* 3012-3014.

[4] I. Singh, W. Hecker, A. K. Prasad, S. P. A. Virinder, O. Seitz, *Chemical Communications* **2002,** 500-501.

[5] M. Berger, A. K. Ogawa, D. L. McMinn, Y. Q. Wu, P. G. Schultz, F. E. Romesberg, *Angewandte Chemie-International Edition* **2000,** *39* 2940-2942.

[6] D. L. McMinn, A. K. Ogawa, Y. Q. Wu, J. Q. Liu, P. G. Schultz, F. E. Romesberg, *Journal of the American Chemical Society* **1999,** *121* 11585-11586.

[7] E. T. Kool, J. C. Morales, K. M. Guckian, *Angewandte Chemie, International Edition* **2000,** *39* 990-1009.

[8] M. E. Langer, F. Khorshahi, *US Patent 5113010* **1992**.

[9] A. I. Khalaf, A. R. Pitt, M. Scobie, C. J. Suckling, J. Urwin, R. D. Waigh, R. V. Fishleigh, S. C. Young, W. A. Wylie, *Tetrahedron* **2000,** *56* 5225-5239.

[10] S. L. Beaucage, M. H. Caruthers, *Tetrahedron Letters* **1981,** *22* 1859-1862.

[11] N. D. Sinha, J. Biernat, J. McManus, H. Koster, *Nucleic Acids Res.* **1984,** *12* 4539-4557.

[12] I. Pompizi, A. Haberli, C. J. Leumann, *Nucleic Acids Research* **2000,** *28* 2702-2708.

[13] L. A. Marky, K. J. Breslauer, *Biopolymers* **1987,** *26* 1601-1620.

[14] W. Bannwarth, A. Treciak, *Helvetica Chimica Acta* **1987,** *70* 175-186.

3. DNA Containing Phenanthroline- and Phenanthrene-derived, Non-nucleosidic Base Surrogates

Simon M. Langenegger, Robert Häner, *Tetrahedron Lett*. **2004**, 45, 9273-9276.

3.1. Abstract

Simple, non-nucleosidic phenanthroline- and phenanthrene-derivatives have been synthesised and incorporated into oligodeoxynucleotides. Complementary strands containing the modified building blocks in opposite positions form stable hybrids. Thermal denaturation experiments show that the double strands containing the phenanthroline-derivatives are more stable than the ones with the corresponding phenanthrenes. Furthermore, it was found that duplex stability is considerably decreased if the linkers of the modified building blocks are too short.

3.2. Introduction

Besides their importance as the genetic material, nucleic acids are increasingly gaining interest as nanometer-sized, functional matter [1-4]. Due to the repetitive, well-defined arrangement of their building blocks, nucleic acids and related types of oligomers [5-8] are ideal objects for the designed construction of larger assemblies. Thus, they have been used for the spatially well-defined arrangement of gold nanoparticles [9, 10] or for the generation of larger molecular assemblies and architectures [11-14]. Furthermore, they may find applications as molecular metal wires [15-19] and even as molecular computers [20, 21] or machines [22, 23]. The combination of nucleotides with non-natural building blocks enhances the number of possible constructs and their potential applications even further. Recently, we reported the synthesis and properties of a non-nucleosidic, phenanthrene-derived building block and its incorporation into double stranded DNA (*Scheme 3.1.*, **A**) [24, 25]. This simple building block can serve as a base surrogate without destabilizing the DNA duplex nor altering its overall B-DNA structure. Based on the data obtained, a model of interstrand-stacked phenanthrenes was proposed [24]. Since π-stacking interactions should be favored by heteroaromatic derivatives [26], we investigated the effect of the phenanthroline analogs (*Scheme 3.1.*, **B**). Here, we report that the phenanthroline derivatives gives rise to more stable

hybrids than the analogous phenanthrenes and that the length of the non-nucleosidic linker plays an important role.

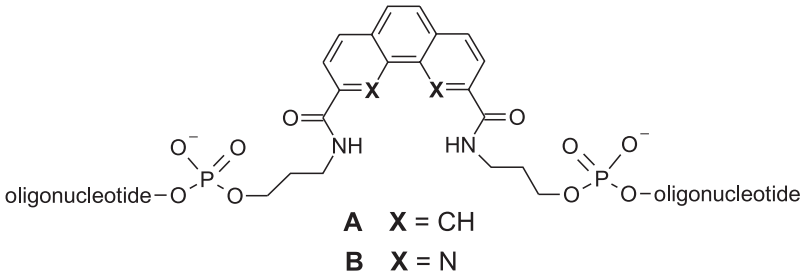

Scheme 3.1. Non-nucleosidic phenanthrene- and phenanthroline-derived building blocks.

3.3. Results and Discussion

The building blocks required for the synthesis of the modified oligonucleotides are shown in *Scheme 3.2.*. The phenanthrene derivatives **1a-c** were prepared as described previously [25, 27]. In addition, **1d** was prepared according to the same procedures. Synthesis of the phenanthroline-derived compounds started from the known **2** [28].

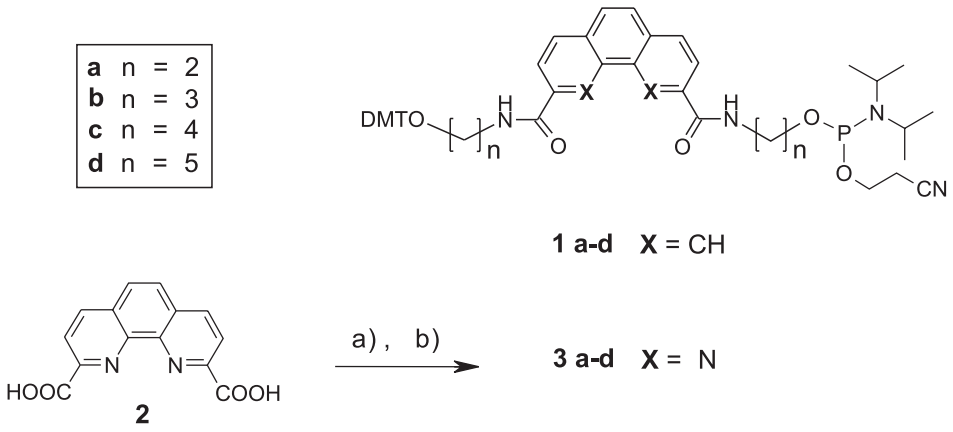

Scheme 3.2. Synthesis of the required phosphoramidites. Conditions: a) $H_2N(CH_2)_nOH/H_2N(CH_2)_nODMT$ (1:1), *Hünig's* base, BOP; b) 2-cyanoethyl diisopropylamidochloridophosphite, *Hünig's* base.

Attachment of the different 4,4'-dimethoxytritylated linkers and subsequent phosphitylation yielded the phosphoramidite compounds **3a-d**.[29] Building blocks **2a-d** and **3a-d** were then used for the synthesis of the oligonucleotides shown in *Table 3.1.*. Assembly of the oligomers involved standard automated oligonucleotide synthesis [30,31]. The crude oligomers were

purified by reverse phase HPLC and their identity was verified by mass spectrometry. The oligonucleotides are sets of complementary 21mers containing a modified building block in the central position of each strand. **Pn** or **Qn** symbolize a phenanthrene or a phenanthroline, respectively, and **n** indicates the length of the alkyl linkers. For comparison, an unmodified reference duplex was synthesised possessing an AT-base pair in the central position.

The influence of the aromatic base surrogates on duplex stability was analysed by thermal denaturation experiments. The melting temperatures (Tm's, see *Table 3.1.*) reveal that the phenanthrene-modified hybrids (entries 2-5) are consistently less stable than the corresponding hybrids containing phenanthroline and analogous linkers (entries 6-9). The difference in Tm's between the two series is in the range of 2-4°C, always in favour of the phenanthroline-modified duplexes. Such a difference is comparable to the contribution of an AT-base pair to duplex stability. Furthermore, in both series the optimal linker length is reached with n=3, i.e with propyl-type linkers. Duplex stability is rather insensitive to a further increase in the linker length. No statistically significant change (exptl. error: ± 0.5°C) is observed among the derivatives containing propyl, butyl or pentyl linkers in both series. In contrast, the stability is considerably diminished if the linker is too short. Thus, going from a propyl to an ethyl linker, the Tm is reduced by 7.0 and 5.5°C in the phenanthrene and the phenanthroline series, respectively (cf. *entries 2/3* and *6/7*).

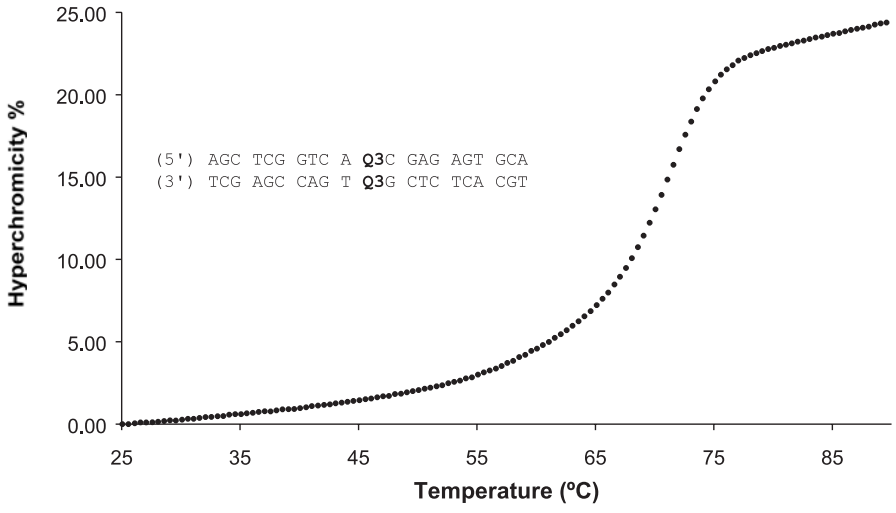

Figure 3.1. Representative thermal melting curve of a duplex containing two non-nucleosidic phenanthroline building blocks (Q3, see also *Table 3.1.*, entry 7) in opposite positions.

Entry	Duplex	Tm (°C)[a,b]	ΔTm (°C)[c]
1	(5') AGC TCG GTC A T C GAG AGT GCA (3') TCG AGC CAG T A G CTC TCA CGT	68.0	-
2	(5') AGC TCG GTC A **P2**C GAG AGT GCA (3') TCG AGC CAG T **P2**G CTC TCA CGT	61.3	-6.7
3	(5') AGC TCG GTC A **P3**C GAG AGT GCA (3') TCG AGC CAG T **P3**G CTC TCA CGT	68.3	0.3[d]
4	(5') AGC TCG GTC A **P4**C GAG AGT GCA (3') TCG AGC CAG T **P4**G CTC TCA CGT	67.3	-0.7
5	(5') AGC TCG GTC A **P5**C GAG AGT GCA (3') TCG AGC CAG T **P5**G CTC TCA CGT	68.7	0.7
6	(5') AGC TCG GTC A **Q2**C GAG AGT GCA (3') TCG AGC CAG T **Q2**G CTC TCA CGT	65.6	-2.4
7	(5') AGC TCG GTC A **Q3**C GAG AGT GCA (3') TCG AGC CAG T **Q3**G CTC TCA CGT	71.1	3.1
8	(5') AGC TCG GTC A **Q4**C GAG AGT GCA (3') TCG AGC CAG T **Q4**G CTC TCA CGT	70.6	2.6
9	(5') AGC TCG GTC A **Q5**C GAG AGT GCA (3') TCG AGC CAG T **Q5**G CTC TCA CGT	70.2	2.2

Pn (phenanthrene)

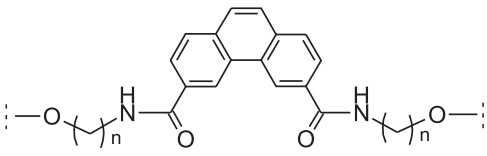

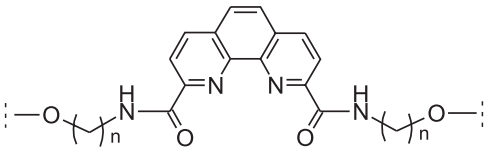

Qn (phenanthroline)

P2,Q2: n = 2
P3,Q3: n = 3
P4,Q4: n = 4
P5,Q5: n = 5

Table 3.1. Influence of phenanthrene and phenanthroline nucleotide surrogates on the thermal stability of duplex DNA. [a] Conditions: oligomer concentration 1.0µM, 10 mM Tris-HCl, 100 mM NaCl, pH 7.4; temp. gradient: 0.5°C/min. [b] Melting temperatures were determined from the maximum of the first derivative of the melting curve (A_{260} against temperature); each Tm is the average of three independent experiments; exptl. error: ± 0.5°C. [c] Difference in Tm relative to the control duplex (entry 1). [d] Value taken from the literature [24].

All oligomers investigated in the study showed a single, cooperative transition. *Fig. 3.1.* shows the melting curve of the duplex containing phenanthrolines with three methylene groups in the linkers (i.e. **Q3**, see also entry 7 in *Table 3.1.*).

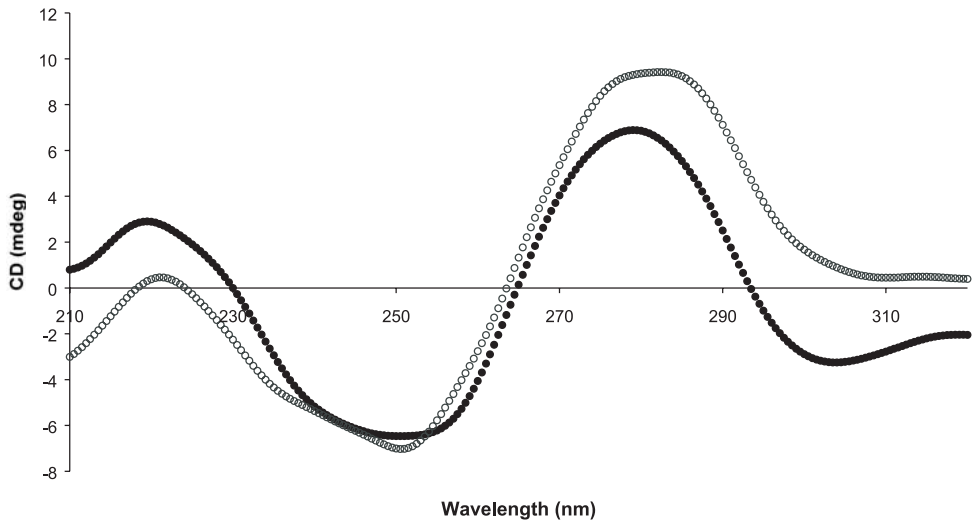

Figure 3.2. CD spectrum of the duplex containing two non-nucleosidic phenanthroline building blocks (filled circles, **Q3**, see also *Table 3.1.*, entry 7) in comparison to the unmodified duplex (open circles, *Table 3.1.*, entry 1).

In addition, the circular dichroism spectra (CD) of the hybrids investigated are all in agreement with a B-form duplex. The CD spectrum of the duplex containing the **Q3** building blocks (see also *Table 3.1.*, entry 7) is shown in *Fig. 3.2.* as a representative example.

All the data obtained support a model of interstrand-stacked, non-nucleosidic building blocks in an otherwise regular B-DNA duplex. An illustration of interstrand-stacked phenanthrolines is shown in *Fig. 3.3.*.

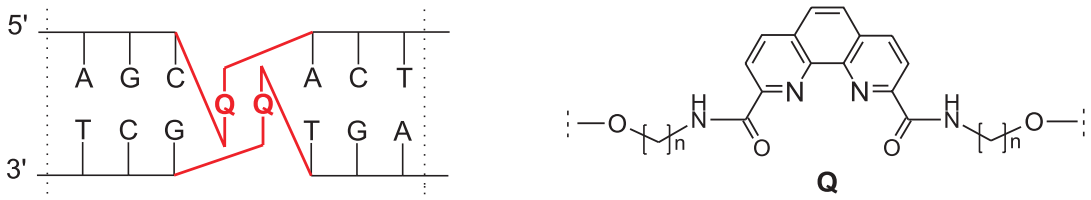

Figure 3.3. Illustration of a duplex containing interstrand-stacked phenanthrolines with flexible, non-nucleosidic linkers.

The flexible linkers connecting the polyaromatic hydrocarbons to the phosphate backbone of the nucleic acid do not compromise the overall stability of the hybrid nor do they substantially alter the overall B-DNA geometry. The increase in Tm, which is observed by going from phenanthrene to the corresponding phenanthroline building blocks is well in agreement with the expectation, since the higher dipole moment present in the heteroaromatic phenanthrolines should lead to stronger stacking interactions [26].

3.4. Conclusions

In conclusion, non-nucleosidic phenanthrene and phenanthroline building blocks are well tolerated in duplex DNA. In general, the phenanthroline derivatives give more stable hybrids than the corresponding phenanthrene analogs. The difference in Tm is most likely a result of the higher dipole moment of the heteroaromatic phenanthroline, compared to the phenanthrene, resulting in stronger interstrand stacking interactions. Finally, the stability of the hybrids is considerably decreased if the linkers of the building blocks are too short.

References and notes

[1] Seeman, N. C. *Acc.Chem.Res.* **1997**, *30*, 357-363.

[2] Seeman, N. C. *Nature* **2003**, *421*, 427-431.

[3] Wengel, J. *Org.Biomol.Chem.* **2004**, *2*, 277-280.

[4] Bashir, R. *Superlattices and Microstructures* **2001**, *29*, 1-16.

[5] Uhlmann, E.; Peymann, A. *Chem.Rev.* **1990**, *90*, 543-584.

[6] Herdewijn, P. *Biochim.Biophys.Acta, Gene Struct.Expr.* **1999**, *1489*, 167-179.

[7] Eschenmoser, A. *Science* **1999**, *284*, 2118-2124.

[8] Leumann, C. J. *Bioorg.Med.Chem.* **2002**, *10*, 841-854.

[9] Mirkin, C. A.; Letsinger, R. L.; Mucic, R. C.; Storhoff, J. J. *Nature* **1996**, *382*, 607-609.

[10] Alivisatos, A. P.; Johnsson, K. P.; Peng, X. G.; Wilson, T. E.; Loweth, C. J.; Bruchez, M. P.; Schultz, P. G. *Nature* **1996**, *382*, 609-611.

[11] Shi, J. F.; Bergstrom, D. E. *Angew.Chem., Int.Ed.Engl.* **1997**, *36*, 111-113.

[12] Shih, W. M.; Quispe, J. D.; Joyce, G. F. *Nature* **2004**, *427*, 618-621.

[13] Li, Y. G.; Tseng, Y. D.; Kwon, S. Y.; D'Espaux, L.; Bunch, J. S.; Mceuen, P. L.; Luo, D. *Nature Mat.* **2004**, *3*, 38-42.

[14] Winfree, E.; Liu, F.; Wenzler, L. A.; Seeman, N. C. *Nature* **1998**, *394*, 539-544.

[15] Meggers, E.; Holland, P. L.; Tolman, W. B.; Romesberg, F. E.; Schultz, P. G. *J.Am.Chem.Soc.* **2000**, *122*, 10714-10715.

[16] Tanaka, K.; Tengeiji, A.; Kato, T.; Toyama, N.; Shionoya, M. *Science* **2003**, *299*, 1212-1213.

[17] Weizman, H.; Tor, Y. *J.Am.Chem.Soc.* **2001**, *123*, 3375-3376.

[18] Zimmermann, N.; Meggers, E.; Schultz, P. G. *J.Am.Chem.Soc.* **2002**, *124*, 13684-13685.

[19] Zimmermann, N.; Meggers, E.; Schultz, P. G. *Bioorg.Chem.* **2004**, *32*, 13-25.

[20] Adleman, L. M. *Science* **1994**, *266*, 1021-1024.

[21] Sakamoto, K.; Gouzu, H.; Komiya, K.; Kiga, D.; Yokoyama, S.; Yokomori, T.; Hagiya, M. *Science* **2000**, *288*, 1223-1226.

[22] Yurke, B.; Turberfield, A. J.; Mills, A. P.; Simmel, F. C.; Neumann, J. L. *Nature* **2000**, *406*, 605-608.

[23] Dittmer, W. U.; Simmel, F. C. *Nano Letters* **2004**, *4*, 689-691.

[24] Langenegger, S. M.; Häner, R. *Helv.Chim.Acta* **2002**, *85*, 3414-3421.

[25] Langenegger, S. M.; Häner, R. *Chem.Biodiv.* **2004**, *1*, 259-264.

[26] Hunter, C. A.; Lawson, K. R.; Perkins, J.; Urch, C. J. *J.Chem.Soc., Perkin Trans.2* **2001**, 651-669.

[27] Stutz, A.; Langenegger, S. M.; Häner, R. *Helv.Chim.Acta* **2003**, *86*, 3156-3163.

[28] Chandler, C. J.; Deady, L. W.; Reiss, J. A. *J.Heterocyclic Chem.* **1981**, *18*, 599-601.

[29] Representative analytical data are given for compound **3b**: light-yellow foam. TLC (AcOEt:hexane 7:3 + 2% Et_3N): R_f 0.28. ^{1}H-NMR(300MHz,$CDCl_3$): 1.10, 1.12 (2*d*, J = 6.7, 2 *Me*CHN); 2.00 (*m*, 2 $CH_2CH_2CH_2$); 2.50 (*t*, J = 6.4, CH_2CN); 3.2-3.8 (*m*, $CH_2CH_2CH_2N$, $CH_2CH_2CH_2N'$, OCH_2CH_2CN, 2 Me_2CHN); 3.67 (*s*, 2MeO); 6.73 (*d*, 4 arom. H); 7.1-7.5 (*m*, 9 arom. H); 7.93 (s, 2 arom H); 8.44 (*m*, 2 arom. H); 8.59 (*m*, 2 arom. H, 2 NH). ^{31}P-NMR(162MHz, $CDCl_3$): 147.78. HR-ESI-MS (*pos. mode*): 907.3943 ($[M+Na]^+$; calc. 907.3924).

[30] Beaucage, S. L.; Caruthers, M. H. *Tetrahedron Lett.* **1981**, *22*, 1859-1862.

[31] Sinha, N. D.; Biernat, J.; McManus, J.; Koster, H. *Nucleic Acids Res.* **1984**, *12*, 4539-4557.

4. A Simple, Non-Nucleosidic Base Surrogate Increases Duplex Stability of DNA Containing an Abasic Site

Simon M. Langenegger, Robert Häner, *Chem. Biodiv*. **2004**, 1, 259-264.

4.1. Abstract

Abasic sites represent a common type of lesion in DNA. If not repaired, they can lead to mutations during replication or to cell death. Due to its biological importance, there is a strong interest in methods of recognizing abasic sites in DNA both, for diagnostic and also for potential pharmaceutical applications. Extended aromatic residues can have a substantial positive influence on the stability of double stranded DNA containing abasic sites. We report here the use of a simple, non-nucleosidic phenanthrene as a base surrogate, which effectively enhances the duplex stability of DNA with an abasic site. The influence of the linker length on the stability of the duplex is investigated. Data and model considerations suggest that stabilization is a result of stacking interactions between the phenanthrene and DNA base pairs.

4.2. Introduction

Loss of a base is one of the most frequent lesions in DNA. It can happen as a spontaneous process [1], as a result of base modification or in an enzymatic repair process [2,3]. The resulting abasic site has a high potential for mutagenicity if not repaired. Furthermore, due to their chemical instability, abasic sites can lead to strand breakage, an event which may result in cell death. From a structural point of view, an abasic site represents a discontinuity of the DNA base string and, thus, leads to a deviation from the regular DNA duplex structure [4]. Due to the biological relevance, there is considerable interest in the investigation of abasic sites in DNA. In particular, the selective binding of intercalating ligands [5,6,7] to such sites by may result in the inhibition of enzymatic repair [4]. Such ligands are investigated for their potential of increasing the effectiveness of cytotoxic agents. Stabilisation of abasic sites in duplex DNA has also been reported using complementary oligonucleotides carrying modified nucleosides. Placement of extended aromatic residues opposite to the abasic site can substitute for the missing nucleobase and maintain the aromatic stacking throughout the duplex [8,9].

Deoxyribofuranosides carrying pyrene and other polyaromatic hydrocarbons have been used for this purpose. All of the reported surrogates are deoxyribose-derived, a fact that originates from the goal of leaving the sugar-phosphate backbone as little changed as possible, compared to the natural DNA backbone [10]. We have recently reported that phenanthrene substituted with flexible aliphatic linkers can act as a non-hydrogen bonding nucleotide surrogate [11]. In a similar approach, Christensen and Pedersen have shown that a glycerol-linked pyrene has a stabilizing effect on double stranded DNA through intercalation [12,13]. In view of these observations, we investigated the possibility of stabilizing abasic sites with simple, non-nucleosidic aromatic building blocks. Besides gaining insight into the requirements or limitations of backbone flexibility, such building blocks might present a considerable practical advantage over the synthetically more demanding sugar-derived analogues. Herein, we report on the stabilizing effect of 3,6-substituted phenanthrenes on the stability of double stranded DNA containing an abasic site.

4.3. Results and Discussion

Synthesis of the phenanthrene based building blocks **1a-c** containing different linkers (see *Scheme 4.1.*) was accomplished following the previously reported procedures [14,11]. In addition, we synthesized phosphoramidite **1d** containing five methylene units in each linker in an analogous way. Assembly of the required oligonucleotides involved the standard phosphoramidite procedure[15,16].

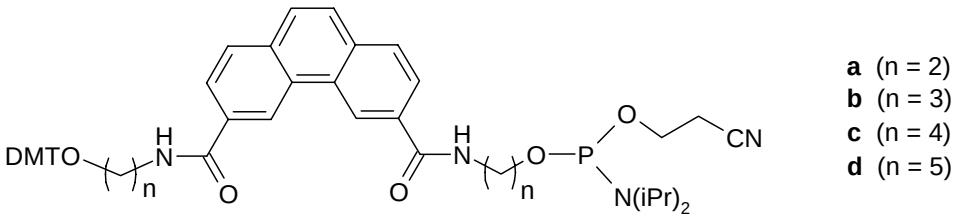

1 a-d

Scheme 4.1. Phenanthrene 3,6-dicarboxamide-derived phosphoramidite building blocks with different linker lengths.

To ensure a high incorporation yield of the modified building blocks **1a-d**, a longer coupling time was allowed in the respective cycles (see *Experimental Section*). For synthesis of the

abasic site (ϕ) containing oligonucleotide[1)] (cf. *Table 4.1.*), we used a commercially available, tetrahydrofuran-derived phosphoramidite. Deprotection (*conc*. ammonia, 55°C), followed by standard HPLC purification gave rise to oligonucleotides **2**-**8** (*Table 4.1.*).

Entry	Oligo #	Duplex	Tm (°C)	ΔTm (°C)
1	**2** **3**	5′ AGC TCG GTC A ϕ C GAG AGT GCA 3′ TCG AGC CAG T **A** G CTC TCA CGT	56.0	-
2	**2** **4**	5′ AGC TCG GTC A ϕ C GAG AGT GCA 3′ TCG AGC CAG T **T** G CTC TCA CGT	57.0	**1.0**
3	**2** **5**	5′ AGC TCG GTC A ϕ C GAG AGT GCA 3′ TCG AGC CAG T **P_2** G CTC TCA CGT	56.4	**0.4**
4	**2** **6**	5′ AGC TCG GTC A ϕ C GAG AGT GCA 3′ TCG AGC CAG T **P_3** G CTC TCA CGT	58.3	**2.3**
5	**2** **7**	5′ AGC TCG GTC A ϕ C GAG AGT GCA 3′ TCG AGC CAG T **P_4** G CTC TCA CGT	61.7	**5.7**
6	**2** **8**	5′ AGC TCG GTC A ϕ C GAG AGT GCA 3′ TCG AGC CAG T **P_5** G CTC TCA CGT	60.9	**4.9**

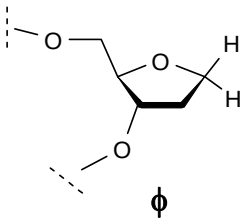

ϕ

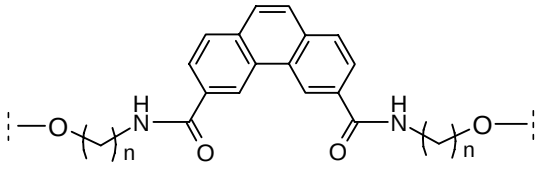

P_n

P_2: n = 2
P_3: n = 3
P_4: n = 4
P_5: n = 5

Table 4.1. Influence of phenanthrene building blocks on duplex DNA containing an abasic site. (Conditions: oligomer concentration 1.5 µM, 10 mM Tris-HCl, 100 mM NaCl, pH 7.5.)

[1)] The building block ϕ is commonly used as a chemically stable model for abasic sites. We therefore refer to this building block as ‘abasic site’ although it is not an abasic site in the strict sense.

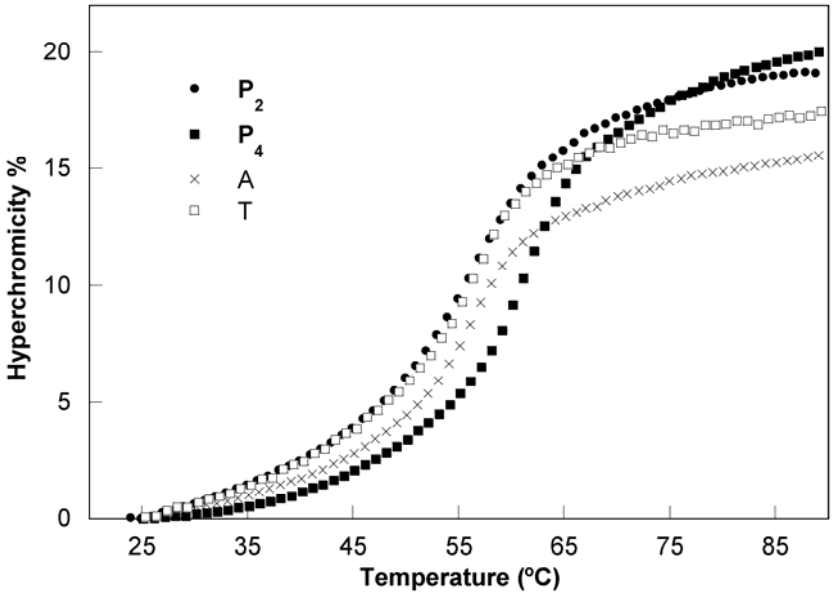

Figure 4.1. Tm curves of DNA duplexes containing phenanthrenes or a natural base opposite an abasic sites: × = A; □ = T; ● = $\mathbf{P_2}$; ■ = $\mathbf{P_4}$ (*cf.* also *Table 4.1*, entries 1, 2, 3 and 5, respectively. (Conditions: oligomer concentration 1.5 μM, 10 mM Tris-HCl, 100 mM NaCl, pH 7.5.)

The effect of the phenanthrene building blocks ($\mathbf{P_n}$) on the stability of an abasic site-containing DNA duplex was then analyzed by thermal denaturation experiments and the data are shown in *Table 4.1.*. Entries 1 and 2 show the Tm values of the duplex with natural bases opposite to the abasic site (**ϕ**). Thymine (**T**) is slightly preferred over adenine (**A**) (ΔTm +1.0°C). The phenanthrene building blocks all have a positive effect on duplex stability, relative to the effect of an adenine. The effect is dependent on the linker, with $\mathbf{P_4}$ being optimal (ΔTm +5.7°C, entry 5). It is noteworthy to mention that the stabilizing effect increases steadily from $\mathbf{P_2}$ to $\mathbf{P_4}$ with increasing length and flexibility of the linkers. A longer linker allows a better placement of the phenanthrene inside the duplex resulting in optimal stacking interactions (see below). Further increasing the linker beyond the optimal length (going from $\mathbf{P_4}$ to $\mathbf{P_5}$) is rather well tolerated; only a modest decrease in stability (ΔTm -0.8°C, entry 6) is observed. The shape of the denaturation curves reveals a cooperative melting process (see *Figure 4.1.*) with hyperchromicities in the range of 15-20%.

NMR investigations of abasic DNA containing a *stacked in* adenine[17,18] or thymine[19] show that the cavity arising from the missing nucleobase leads to a discontinuation of the

stacking interaction within the helix. It is thus likely, that the phenanthrene building blocks are filling this cavity to maintain stacking interactions. The data shown in *Table 4.1.* indicate that a sufficiently flexible linker is required for the proper placement of the phenanthrene in the cavity around the abasic site. This interpretation is supported by model considerations. *Figure 4.2.* shows the *Amber*-minimized structures for the duplexes with $\mathbf{P_2}$ (left) and $\mathbf{P_4}$ (right). In this model, the longer linker in $\mathbf{P_4}$ allows the phenanthrene to reach deeper into the interior of the helix, thereby enabling an optimal positioning for stacking interactions with the neighboring base pairs. The proper orientation required for stacking can be seen in both views in *Figure 4.2.*. The view along the axis (*top*) shows a better overlap of the phenanthrene (green) with the two adjacent base pairs (shown in blue and pink) in the case of the longer linker ($\mathbf{P_4}$, right side of *Figure 4.2.*). The effect of the longer linker is also evident in the view perpendicular to the helical axis (*bottom*). The model agrees well with the structure derived from the NMR structure of a DNA duplex with a sugar-derived pyrene opposite to an abasic site [9]. In this structure, the pyrene is oriented towards the inside of the helix, close to the abasic site. The influence of the proper positioning of the poly-aromatic residue for ideal stacking interactions with the neighboring base pairs is emphasized.

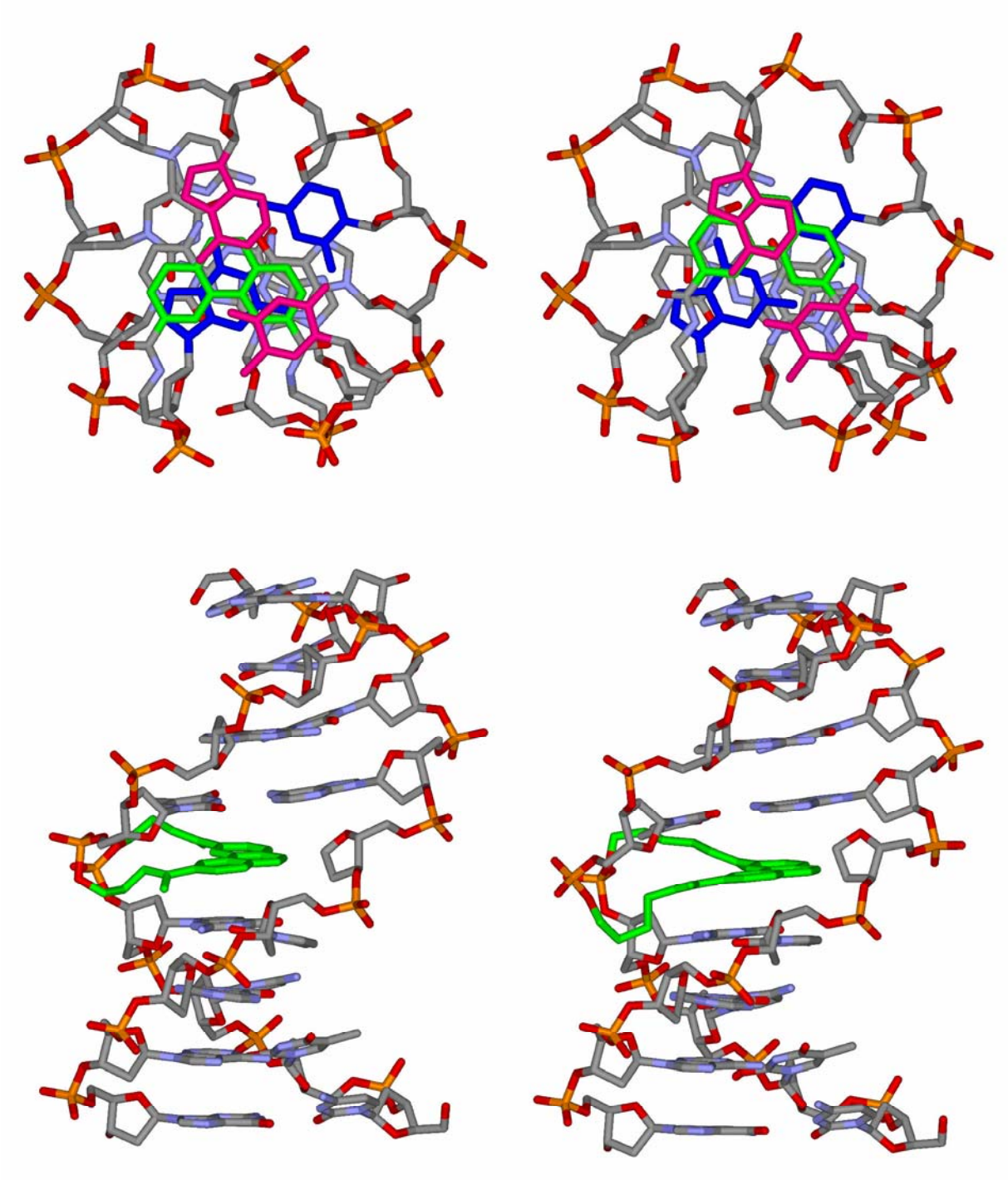

Figure 4.2. *Amber*-minimised model of a DNA duplex containing phenanthrenes $\mathbf{P_2}$ (left) and $\mathbf{P_4}$ (right) opposite to an abasic site. *Top:* View along a truncated helix showing the orientation of the phenanthrene (green) relative to the neighbouring nucleobases (pink and blue). *Bottom:* Influence of the linker length on the positioning of the phenanthrene in the cavity near the abasic site.

4.4. Conclusions

The influence of a phenanthrene-3,6-dicarboxamide derivative with flexible, aliphatic linkers on the duplex stability of abasic DNA has been investigated. The building blocks have been incorporated opposite to the abasic site. Thermal denaturation experiments show that a phenanthrene with an optimized linker length (**P_4**) leads to a significant stabilization of the abasic DNA, relative to the duplex with a natural base opposite to the missing base. Based on model considerations and data from the literature, it can be concluded that the stabilizing effect arises from stacking interactions between the phenanthrene and the adjacent base pairs. Thus, a considerable stabilization is observed even in the absence of a pre-oriented, continuous sugar phosphate backbone.

4.5. Experimental Section

General

Chemicals, solvents, and reagents for reactions were from *Acros*, *Aldrich*, or *Fluka*, and were of the highest quality available. NMR: *Bruker AC-300* δ values in ppm (solvents signals as internal standards), *J* [Hz]; ^{31}P-NMR: *Bruker AMX 300*, δ values in ppm (85% H_3PO_4 as external standard). ESI-MS: *VG Platform* single quadrupole ESI mass spectrometer. Abbreviation: HR-ESI-MS: high resolution ESI-MS.

Synthesis of Phenanthrene-derived Phosphoramidite Building Blocks

N-{5-[(N,N-diisopropylamino)(2-cyanoethyl)phosphinoxy]pentyl}-N'-{5-[(4,4'-dimethoxytrityl)oxy]pentyl}-phenanthrene-3,6-carboxamide (**1d**). Compound **1d** was prepared in analogy to the synthetic procedure reported previously.[14] Thus, starting from dimethyl phenanthrene-3,6-dicarboxylate[11], the intermediate mono- tritylated derivative (N-{5-[(4,4'-Dimethoxytrityl)oxy]pentyl}-N'-(5-hydroxypentyl)phenanthrene-3,6-carboxamide) was prepared in a 31% yield after CC (EtOAc/hexane 9:1, 2% Et_3N). TLC (AcOEt, 1%Et_3N): R_f. 0.26. ^{1}H-NMR (300 MHz, $CDCl_3$): 1.35-1.75 (m, 2 $CH_2CH_2CH_2CH_2CH_2$); 3.05 (t, J = 6.3, $DMTOCH_2$); 3.49 (m, CH_2N, CH_2N'); 3.67 (t, J = 5.9, CH_2OH); 3.74 (s, 2 MeO); 6.81 (d, J = 9.0, 4 arom. H); 7.15 – 7.95 (m, 15 arom. H, CONH, CON'H); 8.89, 8.93 (2s, 2 arom. H). ^{13}C-NMR (75 MHz, $CDCl_3$): 22.9, 23.8, 28.6, 29.5, 29.7, 31.4, 31.6 (6t, $NCH_2CH_2CH_2CH_2CH_2$, $N'CH_2CH_2CH_2CH_2$); 39.9, 40.3 (2t, NCH2, N'CH2); 55.1 (q, MeO); 62.2, 63.1 (2t, CH_2ODMT, CH_2OH); 85.6 (s, Ar_3C); 112.9, 121.5, 121.8, 124.8, 125.3, 126.5, 127.6, 127.8, 128.1, 128.58, 128.63, (11 d, arom. C); 129.5, 129.6 (2s, arom. C); 129.9 (d, arom. C); 132.4,

132.7, 133.6, 136.6, 145.3, 158.2, (6s, arom. C); 167.8, 168.0 (2s, *C*ONH, *C*ON'H). HR-ESI-MS (pos. mode): 761.3565 ($[M+Na]^+$; calc.761.3566).

The so obtained monotritylated intermediate was further transformed into the phosphoramidite **1d** following the procedure reported in the literature.[14] TLC (AcOEt/hexane 7:3, 1% Et_3N): R_f 0.51. ^{1}H-NMR (300 MHz, $CDCl_3$): 1.16, 1.17 (2d, J = 6.8, Me_2CH); 1.53 (m, $NCH_2CH_2CH_2$, $N'CH_2CH_2CH_2$); 1.70 (m, $NCH_2CH_2CH_2CH_2$, $N'CH_2CH_2CH_2CH_2$); 2.62 (t, J = 6.4, CH_2CN); 3.08 (t, J = 6.4, $DMTOCH_2$); 3.45-3.9 (m, $P(OCH_2)_2$, 2 $NCHMe_2$, NCH_2CH_2, $N'CH_2CH_2$); 3.76 (s, 6 H, 2 MeO); 6.59 (br. t, N*H*); 6.76 (br. t, N'*H*); 6.9-8.1 (m, 19 arom. H); 9.16 (s, 2 arom. H). ^{13}C-NMR (75 MHz, $CDCl_3$): 20.4 (t, CH_2CN); 23.5, 23.8 (2t, $NCH_2CH_2CH_2$, $NCH_2CH_2CH_2$); 24.5, 24.6 (2q, J(CP) = 4, Me_2CH); 29.3, 29.6, 29.8 (3t, $CH_2CH_2CH_2CH_2CH_2$); 30.7 (t, J(CP) = 7, $POCH_2CH_2CH_2$); 40.3 (t, NCH_2); 42.9 (d, J(CP) = 12, $PNCH$); 55.1 (q, MeO); 58.1 (t, , $POCH_2CH_2CN$); 63.1 (t, CH_2ODMT); 63.4 (t, J(CP) = 16, $POCH_2CH_2CH_2$); 85.7 (s, Ar_3C); 112.9 (d, arom.C); 118.5 (s, CN); 121.9, 122.0, 124.9, 125.6, 127.7, 128.0, 128.05, 128.1, 128.9, 129.0, 130.0, (11d, arom. C); 132.88, 132.9, 133.9, 136.6, 145.3, 158.3(6s, arom. C); 167.5 (s, CONH). ^{31}P-NMR (121 MHz, $CDCl_3$): 147.42. HR-ESI-MS (pos. Mode): 961.4657 ($[M+Na]^+$; calc.961.4645).

Synthesis and Analysis of Oligonucleotides

Standard phosphoramidites of the nucleosides and the abasic analogue were from *Chemgenes* (Ashland, MA). Oligonucleotides were synthesized on a 392 *DNA/RNA Synthesizer* (*Applied Biosystems*) according to the standard phosphoramidite chemistry[15,16] on a 1.0 µmol scale ('trityl-off' mode). The coupling time was extended to 1.5 min for the phenanthrene containing building blocks. Coupling efficiencies were > 98% for all building blocks. The oligomers were detached and deprotected under standard conditions (conc. aq. NH_3, 55°, 16 h). The crude oligomers were purified by anion-exchange HPLC: *MonoQ HR 5/5* (*Pharmacia*); flow 1 ml/min; eluent A: 20 mM sodium phosphate in H_2O (pH 11.5); eluent B: 20 mM sodium phosphate, 2 M NaCl in H_2O (pH 11.5); elution at r.t.; detection at 260, 280 and 320 nm and desalted over *Sep-Pak* cartridges (*Waters*, Milford, USA). All oligonucleotides were analysed by ESI-MS. The masses were found to be within 0.0005% of the expected mass. The extinction coefficients at 260 nm (ε_{260}) were calculated with "Biopolymer Calculator" (http://paris.chem.yale.edu/extinct.html). For the phenanthrene containing building blocks, an ε_{260} of 49300 was used [14].

Thermal denaturation experiments

UV Melting curves were determined at 260 nm on a *Varian Cary 3e* spectrophotometer equipped with a *Peltier block* and *Varian WinUV* software. Melting curves were measured at an oligomer concentration of 1.5 μM in 10 mM Tris-HCl, 100 mM NaCl pH 7.5. A heating/cooling/heating cycle in the temp. range of 20-95° was applied with a temp. gradient of 0.5°/min. All ramps were indicating equilibrium melting processes. Tm values were defined as the maximum of the first derivative of the melting curve.

Modelling

The conformation of DNA duplexes with phenanthrenes $\mathbf{P_2}$ and $\mathbf{P_4}$ opposite abasic sites (see *Figure 4.2.*) was minimized using the amber force field (*Hyperchem 7.0,* Hypercube, Waterloo, Ontario).

References

[1] T. Lindahl, B. Nyberg, *Biochemistry* **1972**, *11,* 3610-3618.

[2] B. Demple, L. Harrison, *Annual Review Of Biochemistry* **1994**, *63,* 915-948.

[3] O.D. Scharer, *Angewandte Chemie-International Edition* **2003**, *42,* 2946-2974.

[4] J. Lhomme, J.F. Constant, M. Demeunynck, *Biopolymers* **1999**, *52,* 65-83.

[5] N. Berthet, J.F. Constant, M. Demeunynck, P. Michon, J. Lhomme, *Journal Of Medicinal Chemistry* **1997**, *40,* 3346-3352.

[6] N. Berthet, J. Michon, J. Lhomme, M.P. Teulade-Fichou, J.P. Vigneron, J.M. Lehn, *Chemistry-A European Journal* **1999**, *5,* 3625-3630.

[7] K. Yoshimoto, S. Nishizawa, M. Minagawa, N. Teramae, *Journal Of The American Chemical Society* **2003**, *125,* 8982-8983.

[8] T.J. Matray, E.T. Kool, *Journal Of The American Chemical Society* **1998**, *120,* 6191-6192.

[9] S. Smirnov, T.J. Matray, E.T. Kool, C. Los Santos, *Nucleic Acids Research* **2002**, *30,* 5561-5569.

[10] E.T. Kool, J.C. Morales, K.M. Guckian, *Angewandte Chemie, International Edition* **2000** , *39,* 990-1009.

[11] S.M. Langenegger, R. Häner, *Helvetica Chimica Acta* **2002**, *85,* 3414-3421.

[12] U.B. Christensen, E.B. Pedersen, *Nucleic Acids Research* **2002**, *30,* 4918-4925.

[13] U.B. Christensen, E.B. Pedersen, *Helvetica Chimica Acta* **2003**, *86,* 2090-2097.

[14] A. Stutz, S.M. Langenegger, R. Häner, *Helvetica Chimica Acta* **2003**, *86,* 3156-3163.

[15] S.L. Beaucage, M.H. Caruthers, *Tetrahedron Letters* **1981**, *22,* 1859-1862.

[16] N.D. Sinha, J. Biernat, J. Mcmanus, H. Koster, *Nucleic Acids Res.* **1984**, *12,* 4539-4557.

[17] S.T. Hoehn, C.J. Turner, J. Stubbe, *Nucleic Acids Res.* **2001**, *29,* 3413-3423.

[18] R.D. Beger, P.H. Bolton, *J. Biol. Chem.* **1998**, *273,* 15565-15573.

[19] Y. Coppel, N. Berthet, C. Coulombeau, C. Coulombeau, J. Garcia, J. Lhomme, *Biochemistry* **1997**, *36,* 4817-4830.

5. Remarkable stabilization of duplex DNA containing an abasic site by non-nucleosidic phenanthroline and pyrene building blocks

Simon M. Langenegger, Robert Häner, *ChemBioChem*, **2005**, in press.

5.1. Introduction

Abasic sites represent a common type of lesion in DNA. Loss of a base can take place as a spontaneous process [1], it can happen as a result of base modification, or it can occur during an enzymatic repair process [2,3]. If not repaired, the resulting abasic site has a high potential for mutagenicity or may lead to cell death. Due to their biological importance, there is a strong interest in methods of recognizing abasic sites in DNA both, for diagnostic and pharmaceutical use. Intercalating ligands [4-6] have been evaluated as inhibitors of enzymatic repair processes to increase the efficacy of cytotoxic agents [7]. Stabilisation of abasic sites in duplex DNA has been achieved with complementary oligonucleotides carrying extended aromatic residues opposite to the abasic site. Thus, deoxyribofuranosides carrying pyrene and other polyaromatic hydrocarbons have been used as substitute for the missing nucleobase in order to maintain the aromatic stacking throughout the duplex [8-10]. We have recently reported that phenanthrene substituted with flexible aliphatic linkers can be used to stabilise abasic sites in a DNA duplex [11]. Such building blocks might present a considerable practical advantage over the synthetically more demanding sugar-derived analogues. From a structural point of view, an abasic site represents a discontinuity of the DNA base stack and, thus, leads to a deviation from the regular DNA duplex structure [7]. Model considerations suggest, that the aromatic building block replaces for the missing base by intercalation into the cavity resulting from loss of a nucleobase. Stacking interactions are influenced by factors, such as the dipole moment and the interaction surface of the aromatic compounds. Therefore, use of phenanthroline or pyrene instead of phenanthrene might have a further positive effect on the stability of abasic DNA. Here, we report on the effect of 2,9-disubstituted 1,10-phenanthrolines as well as 1,8-disubstituted pyrenes on the stability of double stranded DNA containing an abasic site.

5.2. Results and Discussion

The synthesis of the phenanthroline- and pyrene-derived phosphoramidite building blocks containing linkers of different lengths is shown in *Scheme 5.1.*. The preparation of the pyrene derivatives started from pyrene-1,8-dicarboxylic acid (**1**), which had been prepared according to the method described in the literature [12]. Derivatisation with the corresponding α,ω-aminoalcohols gave the amides **2a-d**. Subsequent phosphitylation provided the phosphoramidites **3a-d**. The synthesis of the respective phenanthroline building blocks followed the same synthetic scheme.

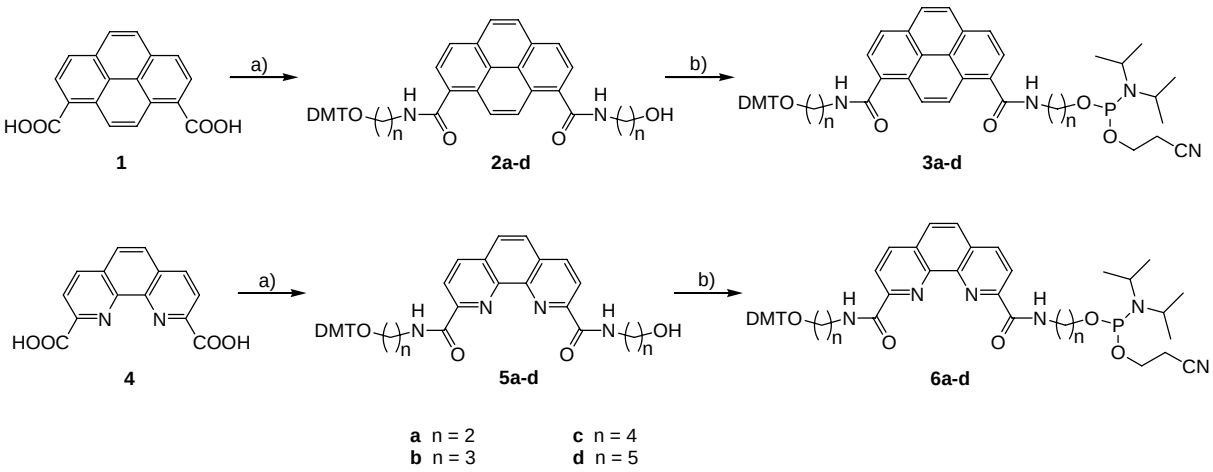

Scheme 5.1. Synthesis of the pyrene and phenanthroline phosphoramidites used in this study. Conditions: a) $HO(CH_2)_nNH_2$/$DMTO(CH_2)_nNH_2$ (1.0 eq. of each, in pyridine), BOP (2.2 eq.), Hünig's base (5 eq.), DMF; b) 2-cyanoethyl diisopropylamidochloridophosphite (1.0 eq.), Hünig's base (3 eq.), CH_2Cl_2.

Thus, the known 1,10-phenanthroline-2,9-dicarboxylic acid (**4**) [13] was transformed *via* the intermediates **5a-d** into the phosphoramidites **6a-d**. All compounds were characterised by standard analytical methods (see *Chapter 5.4.*).

The pyrene- and phenanthroline-derived phosphoramidite building blocks **3a-d** and **6a-d** were subsequently incorporated into oligonucleotides *via* standard oligonucleotide synthesis.[14;15] Coupling yields with the modified phosphoramidites were equal to the ones obtained with standard nucleoside building blocks. For synthesis of the abasic site (**ϕ**) [16] containing oligonucleotide (cf. *Table 5.1.*), a commercially available, tetrahydrofuran-derived phosphoramidite was used. After deprotection (*conc*. ammonia, 55°C), all oligonucleotides were purified by reverse phase HPLC and characterised by high-resolution mass spectrometry (see *Chapter 5.4.*).

The effect of the different phenanthroline and pyrene building blocks on the stability of an abasic site-containing DNA duplex was then analyzed by thermal denaturation experiments. The modified building blocks were positioned opposite to the abasic site. The melting temperature (Tm) data of the corresponding duplexes are summarized in *Table 5.1.*. In comparison to a duplex containing a natural nucleotide (adenosine) opposite to ϕ, all building blocks led to a significant increase of the melting temperature. ΔTm-values between 4°C up to 8°C were observed. A Tm-increase of this extent is comparable to the contribution of 1-2 base pairs to the stability of an oligonucleotide of this length. In the pyrene series, the Tm is rather independent from the linker length. Thus, going from two to five methylene groups in both linker arms, the Tm's varied within a narrow range of approximately 1°C. In the phenanthroline series, however, a stronger influence of the linker arms was observed.

Duplex	Tm (°C)	ΔTm (°C)[a]			
		n=2	n=3	n=4	n=5
5′ AGC TCG GTC A **T** C GAG AGT GCA 3′ TCG AGC CAG T **A** G CTC TCA CGT	67.7				
5′ AGC TCG GTC A ϕ C GAG AGT GCA 3′ TCG AGC CAG T **A** G CTC TCA CGT	**56.3**				
5′ AGC TCG GTC A ϕ C GAG AGT GCA 3′ TCG AGC CAG T**nAn**G CTC TCA CGT		**4.2**	**6.2**	**5.9**	**8.4**
5′ AGC TCG GTC A ϕ C GAG AGT GCA 3′ TCG AGC CAG T**nBn**G CTC TCA CGT		**5.9**	**6.2**	**6.9**	**5.5**

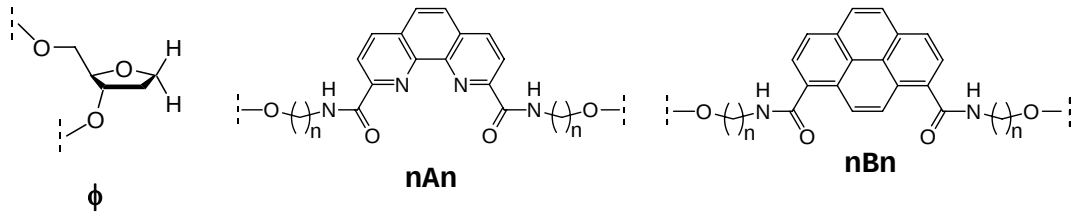

Table 5.1. Influence of phenanthroline- and pyrene-derived, non-nucleosidic building blocks on duplex DNA containing an abasic site. Conditions: oligomer concentration 1.0 μM, 10 mM Tris-HCl, 100 mM NaCl, pH 7.4. Experimental error: ±0.5°C. [a] Difference in Tm relative to the duplex containing an adenosine opposite to the abasic site (Tm = 56.3°C).

Thus, the Tm increased from 60.5°C with two methylene groups to approximately 62.5°C with three and four CH_2-groups and then to 64.7°C with the pentamethylene derivative. The latter Tm-value corresponds to an increase of more than 8°C, relative to the duplex with the adenosine opposite to the abasic site. Compared to the unmodified duplex containing an AT base pair, this is a destabilisation of 3.0°C. All the different phenanthroline and pyrene building blocks cause a considerably larger stabilisation than the corresponding phenanthrene analogs [11], except for the case of the tetramethylene linker. In this case, the phenanthrene leads to a stabilisation (ΔTm = 5.7°C) [11] which is equal to the one effected by the phenanthroline with the same linker (ΔTm = 5.9°C, Table 1, n=4). All melting curves showed a sigmoidal shape with a single transition (see *Chapter 5.4.*) indicating a cooperative melting process. The hyperchromicities of the denaturation processes ranged from 15 to 20%.

We have previously shown that non-nucleosidic phenanthrene building blocks are capable of stabilising a DNA duplex containing an abasic site. The degree of stabilisation was dependent on the length of the non-nucleosidic linker. A correlation between the linker and the structural stability of abasic site containing DNA was also found in the case of the present phenanthroline building blocks. The pyrene derivatives, on the other hand, are relatively insensitive to changes of the linker: with a given experimental error of ±0.5°C, no or only marginal differences are observed in the Tm values upon changing the number of methylene units in the linkers from two to five. NMR investigations of abasic DNA containing a *stacked-in* adenine [17,18] or thymine [19] show that the cavity arising from the missing nucleobase leads to a discontinuation of the stacking interactions within the helix. *Figure 5.1.* shows an *Amber*-minimized structure [20] of the abasic duplex containing the phenanthroline with the longest linkers.

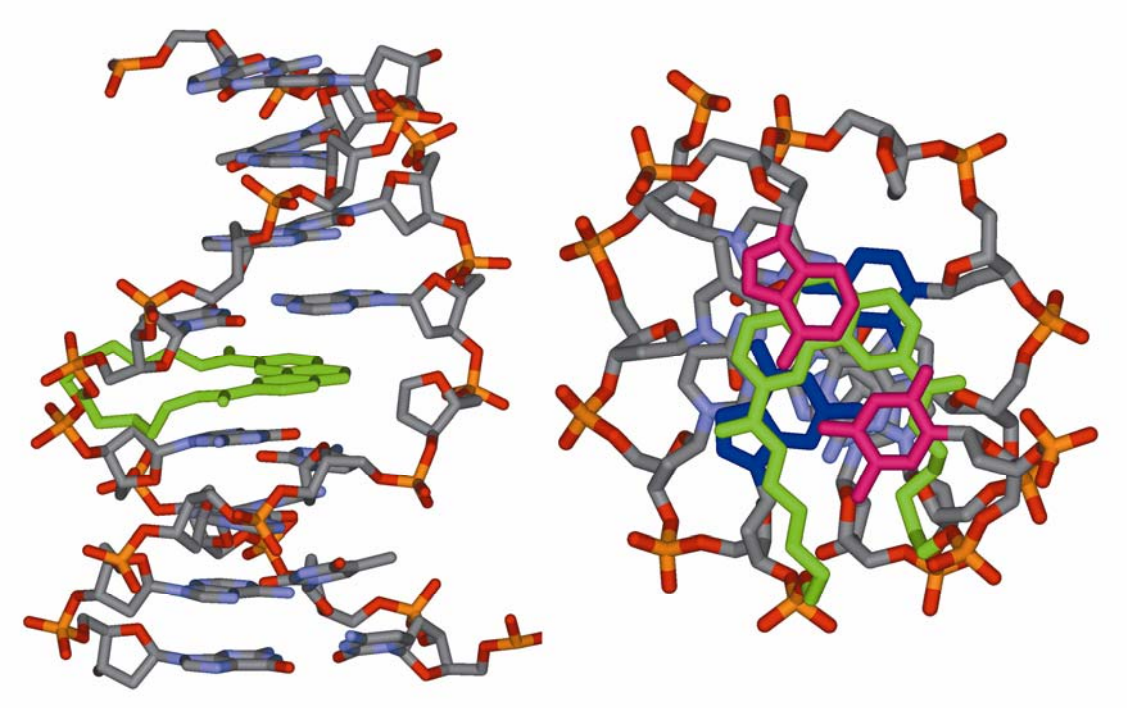

Figure 5.1. *Amber*-minimized structure of the duplex containing a phenanthroline building block containing pentamethylene linkers (highlighted in green) opposite to an abasic site. Left: view perpendicular to the helical axis; right: view along the helical axis. The base pairs adjacent to the phenanthroline are shown in blue and red.

In this model, the phenanthroline is positioned between the base pairs adjacent to the abasic site. This arrangement of the poly-aromatic residue allows for the continuation of stacking interactions in the absence of the nucleobase. The model agrees well with the NMR structure of a DNA duplex containing a sugar-derived pyrene opposite to an abasic site [9].

5.3. Conclusions

The influence of non-nucleosidic phenanthroline and pyrene dicarboxamide derivatives on the duplex stability of abasic DNA has been investigated. Different building blocks with flexible, aliphatic linkers have been incorporated opposite to an abasic site. Thermal denaturation experiments show that both types of polyaromatic hydrocarbons lead to a significant stabilization of the abasic DNA duplex. In comparison to the corresponding duplex an adenosine opposite to the abasic site, Tm's are increased by 4-8°C. Thus, a considerable stabilization is observed even in the absence of a pre-organised, continuous sugar phosphate backbone. The highest stabilisation is effected by the 1,10-phenanthroline-2,9-dicarboxamide bearing two pentamethylene linkers. Model considerations suggest that the stabilizing effect

arises from stacking interactions between the polyaromatic residues and the base pairs adjacent to the abasic site.

5.4. Experimental Section

General

Chemicals, solvents, and reagents for reactions were from *Acros*, *Aldrich*, or *Fluka*, and were of the highest quality available. Solvents for extraction and chromatography were of technical grade and distilled prior to use. Thin layer chromatography (TLC): silica-gel 60 F_{254} glass plates (*Merck*); visualisation by UV and/or A) by dipping in a soln. of anisaldehyde (10 ml), conc. H_2SO_4 (10 ml), and AcOH (2 ml) in EtOH (180 ml) or B) cerium (IV) sulfate (3mM)/ammonium molybdate (250mM in aq. H_2SO_4 (10%) followed by heating. Flash column chromatography (CC): silica gel 60 (40-63 μm, 230-400 mesh, *Fluka*) at low pressure. The chromatography of acid sensitive compounds was carried out with eluent containing 2% NEt_3. ^{1}H- and ^{13}C-NMR: *Bruker AC-300*, δ values in ppm (solvents signals as internal standards), *J* [Hz]; ^{31}P-NMR: *Bruker AC-300*, δ values in ppm (85% H_3PO_4 as external standard). ESI-MS: *VG Platform* single quadrupole ESI mass spectrometer. DMT: 4,4'-dimethoxytrityl; BOP: (Benzotriazol-1-yloxy)-tris-(dimthylamino)-phosphonium-hexafluorophosphate; AcOEt: ethyl acetate; r.t: room temperature; HR-ESI-MS: high resolution electrospray ionisation mass spectrometry.

General Procedures (see *Scheme 5.1.*)

Preparation of the intermediates 2a-d

1 eq. pyrene-1,8-dicarboxylic(**1**) acid and 5 eq. *Hünig's* base were solved in dry DMF (concentration of the acid 0.2M), then a solution of 1 eq. $HO(CH_2)_nNH_2$ and 1 eq. $DMTO(CH_2)_nNH_2$ in dry pyridine (concentration of the DMT protected linker 0.5M) was added at r.t.. After this 2.2 eq of BOP was added and stirred under N_2 atmosphere for 1h.

The mixture was diluted with AcOEt washed with 10% *aq.* citric acid and *sat. aq* $NaHCO_3$ *soln.* The org. layer was dried (K_2CO_3) and evaporated under reduced pressure. Purification of the resulting oil bye CC (silica gel; $CH_2Cl_2 \rightarrow CH_2Cl_2$: MeOH (98: 2) (+2% Et_3N)) furnished as yellow foam.

Preparation of phosphoramidites 3a-d

1 eq. of the DMT protected pyrene was dissolved under a nitrogen atmosphere in dry CH_2Cl_2 and 3 eq. *Hünig's* base. Then 1 eq. of 2-cyanoethyl diisopropylamidochloridophosphite was added and the mixture was stirred for 1 h at r.t.. The reaction mixture was directly applied onto silica gel and purified by CC (silica gel; $CH_2Cl_2 \rightarrow CH_2Cl_2$: MeOH (98:2)(+ 2% Et_3N)). Compounds **3a-d** were obtained as yellow foams.

Pyrene-1,8-dicarboxylic acid 1-({2-[(4,4'dimethoxytrityl)-oxy]-ethyl}-amide) 8-[(2-hydroxy-ethyl)-amide] (**2a**). Yield: 28%, yellow foam. TLC (AcOEt): R_f 0.25
^{1}H-NMR(300MHz,$CDCl_3$): 3.47 (*t*, *J* = 4.7, $ROCH_2$); 3.7-3.85 (*m*, CH_2N, CH_2N'); 3.72 (*s*, 2MeO); 3.97 (m, CH_2OH); 6.79 (*d*, 4 arom. H); 7.15-8.1 (*m*, 15 arom. H); 8.25 (*m*, 2H). ESI-MS (*pos. mode*): 701[*M*+Na]$^+$

Pyrene-1,8-dicarboxylic acid 1-({3-[(4,4'dimethoxytrityl)-oxy]-propyl}-amide) 8-[(2-hydroxy-propyl)-amide] (**2b**). Yield: 22%, yellow foam. TLC (AcOEt): R_f 0.25
^{1}H-NMR(300MHz,$CDCl_3$): 1.95 (*m*, 2 $CH_2CH_2CH_2$); 3.33 (*t*, *J* = 5.4, $ROCH_2$); 3.55 (*s*, 2MeO); 3.7-3.9 (*m,* CH_2N, CH_2N', CH_2OH); 6.59 (*d*, 4 arom. H); 7.0-7.8 (*m*, 15 arom. H); 8.25 (*m*, 2H). ESI-MS (*pos. mode*): 729[*M*+Na]$^+$

Pyrene-1,8-dicarboxylic acid 1-({4-[(4,4'dimethoxytrityl)-oxy]-butyl}-amide) 8-[(2-hydroxy-butyl)-amide] (**2c**). Yield: 20%, yellow foam. TLC (AcOEt): R_f 0.27
^{1}H-NMR(300MHz,$CDCl_3$): 1.81 (*m*, 2 $CH_2CH_2CH_2CH_2$); 3.14 (*m*, $ROCH_2$); 3.70 (*s*, 2MeO); 3.5-3.8 (*m,* CH_2N, CH_2N', CH_2OH); 6.70 (*d*, 4 arom. H); 7.1-8.0 (*m*, 15 arom. H); 8.29 (*m*, 2H). ESI-MS (*pos. mode*): 757[*M*+Na]$^+$

Pyrene-1,8-dicarboxylic acid 1-({5-[(4,4'dimethoxytrityl)-oxy]-pentyl}-amide) 8-[(2-hydroxy-pentyl)-amide] (**2d**). Yield: 17%, yellow foam. TLC (AcOEt): R_f 0.36
^{1}H-NMR(300MHz,$CDCl_3$): 1.69 (*m*, 2 $CH_2CH_2CH_2CH_2CH_2$); 3.11 (*m*, $ROCH_2$); 3.73 (*s*, 2MeO); 3.5-3.8 (*m,* CH_2N, CH_2N', CH_2OH); 6.79 (*d*, 4 arom. H); 7.1-8.0 (*m*, 15 arom. H); 8.23 (*m*, 2H). ESI-MS (*pos. mode*): 785[*M*+Na]$^+$

Preparation of phosphoramidites 3a-d

1 eq. of the DMT protected pyrene was dissolved under a nitrogen atmosphere in dry CH_2Cl_2 and 3 eq. *Hünig's* base. Then 1 eq. of 2-cyanoethyl diisopropylamidochloridophosphite was

added and the mixture was stirred for 1 h at r.t.. The reaction mixture was directly applied onto silica gel and purified by CC (silica gel; $CH_2Cl_2 \rightarrow CH_2Cl_2$: MeOH (98:2)(+ 2% Et_3N)). Compounds **3a-d** were obtained as yellow foams.

Diisopropyl-phosphoramidous acid 2-[(8-{2-[bis-(4,4'dimethoxytrityl)-oxy]-ethylcarbamoyl}-pyrene-1-carbonyl)-amino]-ethyl ester 2-cyano-ethyl ester (**3a**). Yield: 81%, yellow foam. TLC (AcOEt:hexane 6:4 + 2% Et_3N): R_f 0.22

^{1}H-NMR(300MHz,$CDCl_3$): 1.17 (*d*, J = 6.9, 2 *Me*CHN); 2.46 (*t*, J = 6.2, CH_2CN); 3.4-4.0 (*m*, CH_2CH_2N, CH_2CH_2N', OCH_2CH_2CN, 2 Me_2CHN); 3.73 (*s*, 2MeO); 6.79 (*d*, 4 arom. H); 7.1-7.5 (*m*, 9 arom. H); 8.0-8.3(*m*, 6 arom. H); 8.64 (*m*, 2H). ^{31}P-NMR(162MHz, $CDCl_3$): 148.79. HR-ESI-MS (*pos. mode*): 901.3701 ([*M*+Na]$^+$; calc. 901.3706)

Diisopropyl-phosphoramidous acid 2-[(8-{3-[bis-(4,4'dimethoxytrityl)-oxy]-propylcarbamoyl}-pyrene-1-carbonyl)-amino]-propyl ester 2-cyano-ethyl ester (**3b**). Yield: 43%, yellow foam. TLC (AcOEt:hexane 6:4 + 2% Et_3N): R_f 0.24

^{1}H-NMR(300MHz,$CDCl_3$): 1.03, 1.04 (2*d*, J = 6.8, 2 *Me*CHN); 2.03 (*m*, 2 $CH_2CH_2CH_2$); 2.35 (*m*, CH_2CN); 3.3-3.9 (*m*, $CH_2CH_2CH_2N$, $CH_2CH_2CH_2N$', OCH_2CH_2CN, 2 Me_2CHN); 3.58 (*s*, 2MeO); 6.59 (*d*, 4 arom. H); 7.0-7.4 (*m*, 9 arom. H); 7.9-8.25(*m*, 6 arom. H); 8.59 (*m*, 2H). ^{31}P-NMR(162MHz, $CDCl_3$): 148.24. HR-ESI-MS (*pos. mode*): 925.4536 ([*M*+Na]$^+$; calc. 925.4543)

Diisopropyl-phosphoramidous acid 2-[(8-{4-[bis-(4,4'dimethoxytrityl)-oxy]-butylcarbamoyl}-pyrene-1-carbonyl)-amino]-butyl ester 2-cyano-ethyl ester (**3c**). Yield: 61%, yellow foam. TLC (AcOEt:hexane 6:4 + 2% Et_3N): R_f 0.42

^{1}H-NMR(300MHz,$CDCl_3$): 1.04, 1.05 (2*d*, J = 6.6, 2 *Me*CHN); 1.82 (*m*, 2 $CH_2CH_2CH_2CH_2$); 2.50 (*t*, J = 6.3, CH_2CN); 3.1-3.8 (*m*, $CH_2CH_2CH_2CH_2N$, $CH_2CH_2CH_2CH_2N$', OCH_2CH_2CN, 2 Me_2CHN); 3.70 (*s*, 2MeO); 6.71 (*d*, 4 arom. H); 7.1-7.5 (*m*, 9 arom. H); 7.9-8.25(*m*, 6 arom. H); 8.57 (*m*, 2H). ^{31}P-NMR(162MHz, $CDCl_3$): 147.71. ESI-MS (*pos. mode*): 952 [*M*+NH_4]$^+$

Diisopropyl-phosphoramidous acid 2-[(8-{5-[bis-(4,4'dimethoxytrityl)-oxy]-pentylcarbamoyl}-pyrene-1-carbonyl)-amino]-pentyl ester 2-cyano-ethyl ester (**3d**). Yield: 68%, yellow foam. TLC (AcOEt:hexane 6:4 + 2% Et_3N): R_f 0.94.

^{1}H-NMR(300MHz,$CDCl_3$): 1.17, 1.18 (2*d*, J = 6.7, 2 *Me*CHN); 1.72 (*m*, 2 $CH_2CH_2CH_2CH_2CH_2$); 2.63 (*m*, CH_2CN); 3.0-3.9 (*m*, $CH_2CH_2CH_2CH_2CH_2N$, $CH_2CH_2CH_2CH_2CH_2N$', OCH_2CH_2CN, 2 Me_2CHN); 3.77 (*s*, 2MeO); 6.81 (*d*, 4 arom. H);

7.1-7.5 (*m*, 9 arom. H); 7.9-8.25(*m*, 6 arom. H); 8.55 (*m*, 2H). ^{31}P-NMR(162MHz, $CDCl_3$): 147.35. HR-ESI-MS (*pos. mode*): 963.4828 ([*M*+Na]$^+$; calc. 963.4825)

Preparation of the intermediates 5a-d

1 eq. [1,10]Phenanthroline-2,9-dicarboxylic acid (**4)** and 5 eq. *Hünig's* base were dissolved in dry DMF (concentration of the acid was 0.2M); then a solution of 1 eq. $HO(CH_2)_nNH_2$ and 1 eq. $DMTO(CH_2)_nNH_2$ in dry pyridine(concentration of the DMT protected linker 0.5M) was added at r.t.. After this, 2.2 eq of BOP was added and the mixture was stirred under a nitrogen atmosphere for 1h.

The mixture was diluted with AcOEt, washed with 10% *aq.* citric acid and *sat. aq* $NaHCO_3$ *soln.* The org. layer was dried (K_2CO_3) and evaporated under reduced pressure. Purification of the resulting oil bye CC (silica gel; AcOEt→ AcOEt: MeOH (95: 5) (+2% Et_3N)) furnished **5a-d** as light yellow foams.

[1,10]Phenanthroline-2,9-dicarboxylic acid 2-({2-[bis-(4-methoxy-phenyl)-phenyl-methoxy]-ethyl}-amide) 9-[(2-hydroxy-ethyl)-amide] (**5a**). Yield: 28%. TLC (AcOEt): R_f 0.2

^{1}H-NMR(300MHz,$CDCl_3$): 3.29 (*m*, $ROCH_2$); 3.45 (*m,* CH_2N, CH_2N'); 3.65 (*s*, 2MeO); 3.84 (m, C*H*$_2$OH); 6.72 (*d*, 4 arom. H); 7.1-7.5 (*m*, 9 arom. H); 7.94 (*s*, 2 arom H); 8.46 (*m*, 2 arom. H); 8.56 (*m*, 2 arom. H); 9.09 (*t*, *J* = 6.6, NH); 9.30 (*t*, *J* = 5.4, N'H). ESI-MS (*pos. mode*): 679[*M*+Na]$^+$

[1,10]Phenanthroline-2,9-dicarboxylic acid 2-({3-[bis-(4-methoxy-phenyl)-phenyl-methoxy]-propyl}-amide) 9-[(3-hydroxy-propyl)-amide] (**5b**). Yield: 27%. TLC (AcOEt): R_f 0.2

^{1}H-NMR(300MHz,$CDCl_3$): 1.81 (*m*, $CH_2CH_2CH_2OR$); 2.07 (*m*, $CH_2CH_2CH_2OH$); 3.25 (*t*, *J* = 5.9, $ROCH_2$); 3.34 (*m*, OH); 3.66 (*s*, 2MeO); 3.65-3.85 (*m,* CH_2N, CH_2N', C*H*$_2$OH); 6.73 (*d*, 4 arom. H); 7.1-7.5 (*m*, 9 arom. H); 7.80 (*m*, 2 arom. H); 8.29 (*m*, 1 arom. H); 8.38 (*m*, 1 arom. H); 8.54 (*m*, 2 arom. H); 8.87 (*t*, *J* = 5.8, NH); 9.27 (*t*, *J* = 5.7, N'H). ESI-MS (*pos. mode*): 707[*M*+Na]$^+$

[1,10]Phenanthroline-2,9-dicarboxylic acid 2-({4-[bis-(4-methoxy-phenyl)-phenyl-methoxy]-butyl}-amide) 9-[(4-hydroxy-butyl)-amide] (**5c**). Yield: 26%. TLC (AcOEt): R_f 0.23

^{1}H-NMR(300MHz,$CDCl_3$): 1.7 (*m*, 2 $CH_2CH_2CH_2CH_2$); 3.14 (*m*, $ROCH_2$); 3.61 (m, 3.70, CH_2N, CH_2N') 3.76 (*s*, 2MeO); 3.7-3.8 (*m,* , C*H*$_2$OH); 6.79 (*d*, 4 arom. H); 7.15-7.45 (*m*, 9

arom. H); 7.90 (*s*, 2 arom. H); 8.45 (*m*, 2 arom. H); 8.58 (*m*, 1 arom. H); 8.65 (*m*, 1 arom. H); 9.19 (*t*, *J* = 5.7, NH); 9.34 (*t*, *J* = 5.7, N'H). ESI-MS (*pos. mode*): 735[*M*+Na]$^+$

[1,10]Phenanthroline-2,9-dicarboxylic acid 2-({5-[bis-(4-methoxy-phenyl)-phenyl-methoxy]-pentyl}-amide) 9-[(5-hydroxy-pentyl)-amide] (**5d**). Yield: 23%. TLC (AcOEt): R_f 0.24
^{1}H-NMR(300MHz,$CDCl_3$): 1.65 (*m*, 2 $CH_2CH_2CH_2CH_2CH_2$); 3.08 (*m*, $ROCH_2$); 3.5-3.7 (*m,* CH_2N, CH_2N', CH_2OH); 3.75 (*s*, 2MeO); 6.79 (*d*, 4 arom. H); 7.1-7.45 (*m*, 9 arom. H); 7.93 (*s*, 2 arom. H); 8.44 (*m*, 2 arom. H); 8.62 (*m*, 2 arom. H); 8.99 (*t*, NH); 9.06 (*t*, N'H). ESI-MS (*pos. mode*): 763[*M*+Na]$^+$

Preparation of phosphoramidites 6a-d

1 eq. of the DMT protected phenanthroline was dissolved in dry CH_2Cl_2 containing 3 eq. of *Hünig's* base. Then 1 eq. of 2-cyanoethyl diisopropylamidochloridophosphite was added under a nitrogen atmosphere and the mixture was stirred for 1 h at r.t.. The reaction mixture was directly applied onto silica gel and purified by CC (silica gel; AcOEt:hexane (3:7)→ AcOEt:hexane (7:3)(+ 2% Et_3N)). Compounds **6a-d** were obtained as light yellow foams.

Diisopropyl-phosphoramidous acid 2-[(9-{2-[bis-(4-methoxy-phenyl)-phenyl-methoxy]-ethylcarbamoyl}-[1,10]phenanthroline-2-carbonyl)-amino]-ethyl ester 2-cyano-ethyl ester (**6a**). Yield: 70%. TLC (AcOEt:hexane 2:1 + 2% Et_3N): R_f 0.27
^{1}H-NMR(300MHz,$CDCl_3$): 1.10, 1.12 (2*d*, J = 6.8, 2 *Me*CHN); 2.47 (*t*, J = 6.2, CH_2CN); 3.35-3.9 (*m,* CH_2CH_2N, CH_2CH_2N', OCH_2CH_2CN, 2 Me_2CHN); 3.70 (*s*, 2MeO); 6.73 (*d*, 4 arom. H); 7.1-7.5 (*m*, 9 arom. H); 7.94 (*s*, 2 arom. H); 8.45 (*m*, 2 arom. H); 8.59 (*m*, 2 arom. H); 8.78 (*t*, *J* = 6.0, NH); 9.00 (*t*, *J* = 6.3, N'H). ^{31}P-NMR(162MHz, $CDCl_3$): 148.23. HR-ESI-MS (*pos. mode*): 857.3813 ([*M*+H]$^+$; calc. 857.3791)

Diisopropyl-phosphoramidous acid 3-[(9-{3-[bis-(4-methoxy-phenyl)-phenyl-methoxy]-propylcarbamoyl}-[1,10]phenanthroline-2-carbonyl)-amino]-propyl ester 2-cyano-ethyl ester (**6b**). Yield: 76%. TLC (AcOEt:hexane 7:3 + 2% Et_3N): R_f 0.28
^{1}H-NMR(300MHz,$CDCl_3$): 1.11, 1.13 (2*d*, J = 6.7, 2 *Me*CHN); 2.03 (*m*, 2 $CH_2CH_2CH_2$); 2.49 (*t*, J = 6.4, CH_2CN); 3.25 (*m*, CH_2ODMT) 3.3-3.9 (*m,* $CH_2CH_2CH_2N$, $CH_2CH_2CH_2N'$, OCH_2CH_2CN, 2 Me_2CHN); 3.65 (*s*, 2MeO); 6.74 (*d*, 4 arom. H); 7.1-7.5 (*m*, 9 arom. H); 7.93 (*s*, 2 arom. H); 8.44 (*m*, 2 arom. H); 8.59 (*m*, 2 arom. H, NH, N'H). ^{31}P-NMR(162MHz, $CDCl_3$): 147.78. HR-ESI-MS (*pos. mode*): 925.3943 ([*M*+Na]$^+$; calc. 907.3924)

Diisopropyl-phosphoramidous acid 4-[(9-{4-[bis-(4-methoxy-phenyl)-phenyl-methoxy]-butylcarbamoyl}-[1,10]phenanthroline-2-carbonyl)-amino]-butyl ester 2-cyano-ethyl ester (**6c**). Yield: 63%. TLC (AcOEt:hexane 7:3 + 2% Et_3N): R_f 0.31
^{1}H-NMR(300MHz,$CDCl_3$): 1.14, 1.15 (2*d*, J = 6.8, 2 *Me*CHN); 1.79 (*m*, 2 $CH_2CH_2CH_2CH_2$); 2.56 (*t*, J = 6.4, CH_2CN); 3.14 (*m*, CH_2ODMT); 3.5-3.9 (*m,* $CH_2CH_2CH_2CH_2N$, $CH_2CH_2CH_2CH_2N'$, OCH_2CH_2CN, 2 Me_2CHN); 3.76 (*s*, 2MeO); 6.79 (*d*, 4 arom. H); 7.15-7.45 (*m*, 9 arom. H); 7.93 (*s*, 2 arom. H); 8.44 (*m*, 2 arom. H); 8.61 (*m*, 2 arom. H, NH, N'H). ^{31}P-NMR(162MHz, $CDCl_3$): 147.59. HR-ESI-MS (*pos. mode*): 913.4430 ($[M+H]^+$; calc. 913.4417).

Diisopropyl-phosphoramidous acid 5-[(9-{5-[bis-(4-methoxy-phenyl)-phenyl-methoxy]-pentylcarbamoyl}-[1,10]phenanthroline-2-carbonyl)-amino]-pentyl ester 2-cyano-ethyl ester (**6d**). Yield: 67%. TLC (AcOEt:hexane 8:2 + 2% Et_3N): R_f 0.35.
^{1}H-NMR(300MHz,$CDCl_3$): 1.12, 1.13 (2*d*, J = 6.7, 2 *Me*CHN); 1.7 (*m*, 2 $CH_2CH_2CH_2CH_2CH_2$); 2.54 (*t*, J = 6.4 CH_2CN); 3.07 (*t*, J = 6.4, CH_2DMT); 3.4-3.9 (*m,* $CH_2CH_2CH_2CH_2CH_2N$, $CH_2CH_2CH_2CH_2CH_2N'$, OCH_2CH_2CN, 2 Me_2CHN); 3.75 (*s*, 2MeO); 6.78 (*d*, 4 arom. H); 7.1-7.45 (*m*, 9 arom. H); 7.93(*m*, 2 arom. H); 8.44 (*m*, 2 arom. H); 8.59 (*m*, 2 arom. H, NH, N'H). ^{31}P-NMR(162MHz, $CDCl_3$): 147.54. ESI-MS (*pos. mode*): 958 $[M+NH_4]^+$.

Oligonucleotide Synthesis

Phenanthroline- and pyrene-derived phosphoramidite building blocks **6a-d**, **3a-d** were incorporated into oligonucleotides *via* standard automated oligonucleotide synthesis using I_2/pyridine/water in the oxidation step. Coupling yields with **6a-d** and **3a-d** were equal to the ones obtained with standard phosphoramidite building blocks. All oligonucleotides were purified by reverse phase HPLC and characterised by MS (*Table 5.2.*).

#	oligonucleotide	calculated for $(M-H)^-$	found
I	5‘ AGC TCG GTC A ϕ C GAG AGT GCA	6346.0	6346.2
II	3‘ TCG AGC CAG T**2A2**G CTC TCA CGT	6484.5	6484.5
III	3‘ TCG AGC CAG T**3A3**G CTC TCA CGT	6512.5	6512.5
IV	3‘ TCG AGC CAG T**4A4**G CTC TCA CGT	6540.5	6540.6
V	3‘ TCG AGC CAG T**5A5**G CTC TCA CGT	6568.5	6568.7
VI	3‘ TCG AGC CAG T**2B2**G CTC TCA CGT	6506.5	6506.5
VII	3‘ TCG AGC CAG T**3B3**G CTC TCA CGT	6534.5	6534.4
VIII	3‘ TCG AGC CAG T**4B4**G CTC TCA CGT	6562.5	6562.4
IX	3‘ TCG AGC CAG T**5B5**G CTC TCA CGT	6590.5	6590.3

Table 5.2. Molecular weights of oligonucleotides used in this study (*electrospray ionisation time-of-flight*, *ESI-TOF*).

Figure 5.2.A-H. Melting curves of different hybrids. Conditions: oligomer concentration 1.0 µM, 10 mM Tris-HCl, 100 mM NaCl, pH 7.4; temp. gradient: 0.5°C/min. Exptl. error: ± 0.5°C. Absorbance was measured at 260nm. **A**) duplex **I*II**, **B**) duplex **I*III**; **C**) duplex **I*IV**; **D**) duplex **I*V**; **E**) duplex **I*VI**; **F**) duplex **I*VII**; **G**) duplex **I*VIII**; **H**) duplex **I*iX.**

A)

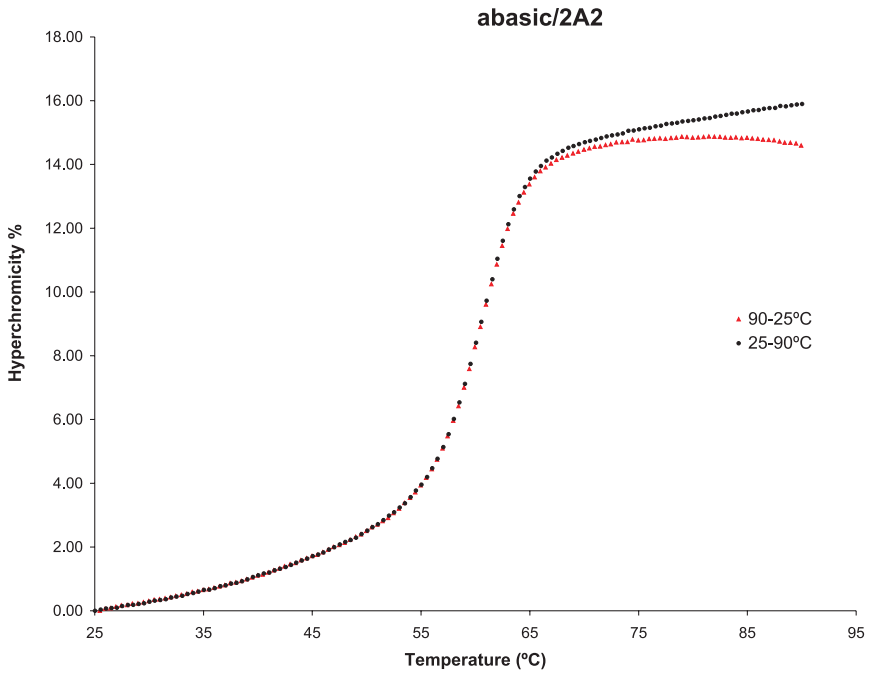

B)

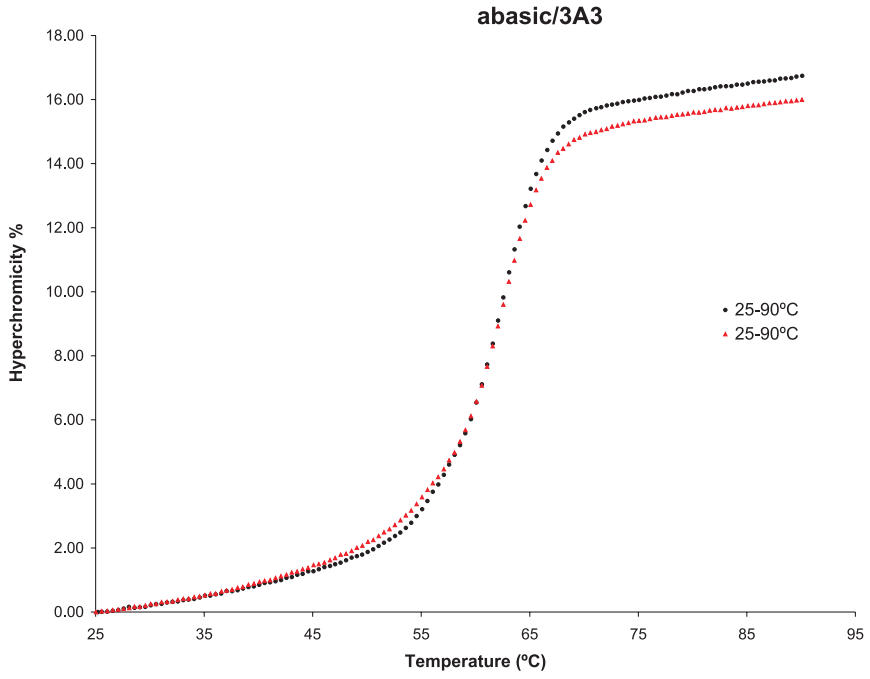

C)

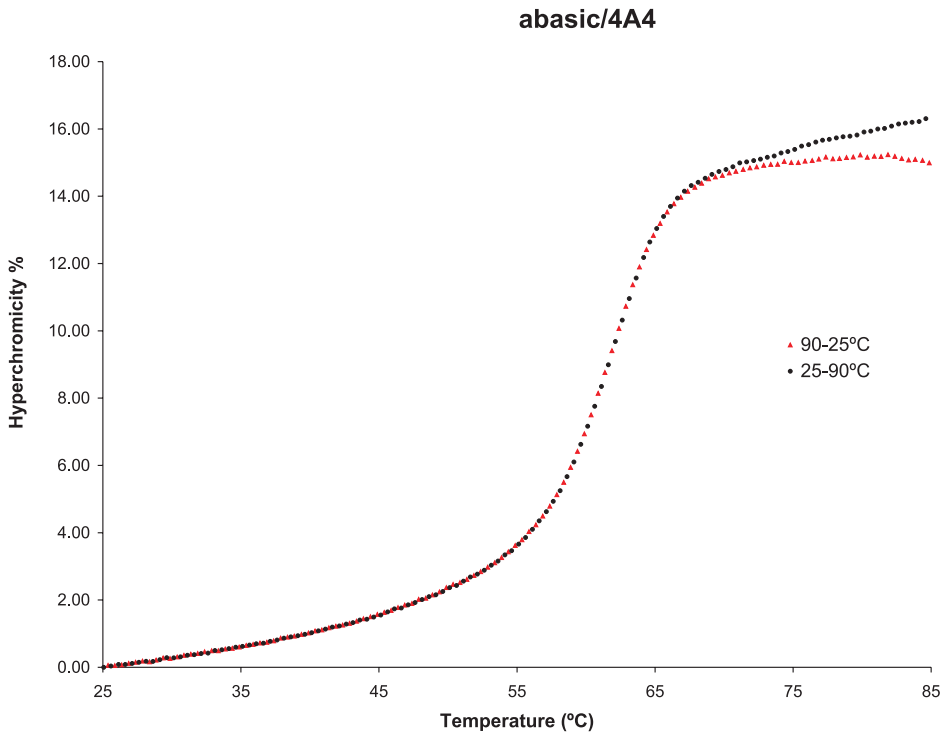
abasic/4A4
Hyperchromicity %
18.00
16.00
14.00
12.00
10.00
8.00
6.00
4.00
2.00
0.00
25
35
45
55
65
75
85
Temperature (°C)
90-25°C
25-90°C

D)

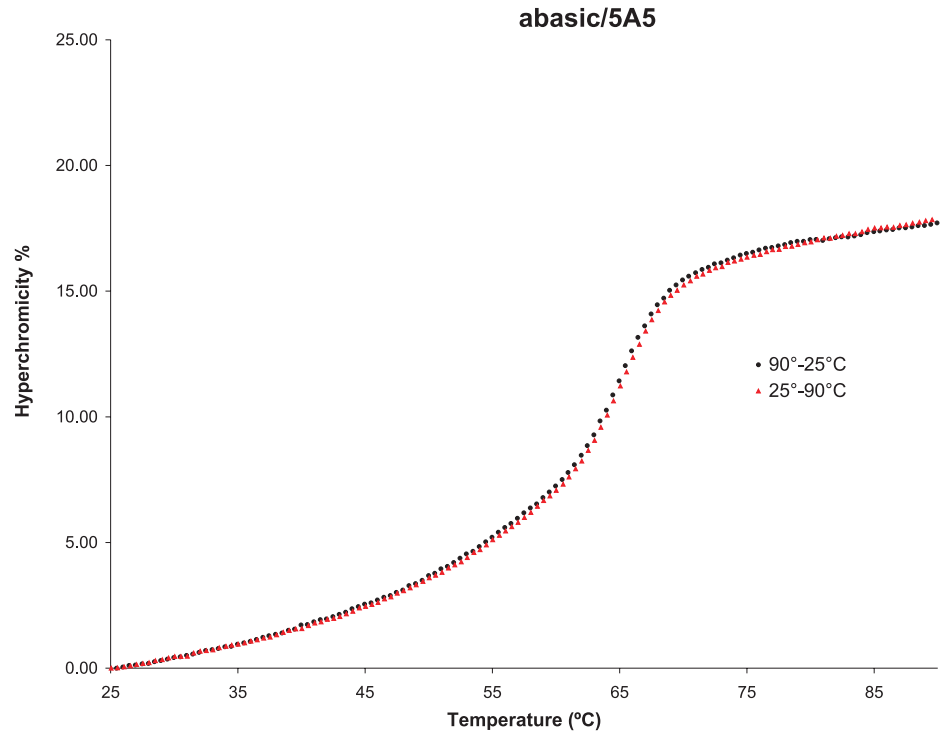
abasic/5A5
Hyperchromicity %
25.00
20.00
15.00
10.00
5.00
0.00
25
35
45
55
65
75
85
Temperature (°C)
90°-25°C
25°-90°C

E)

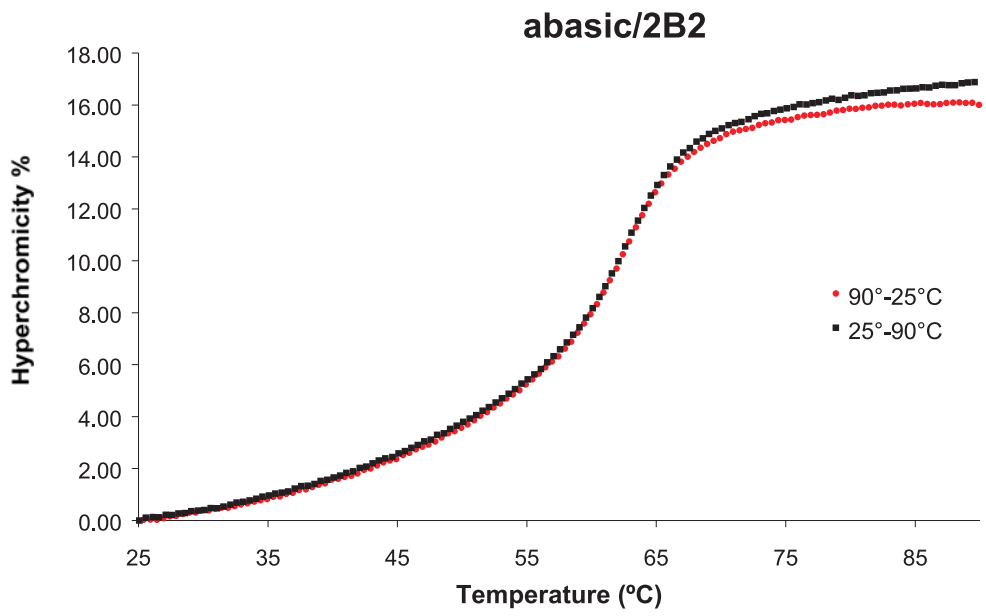
abasic/2B2
Hyperchromicity %
18.00
16.00
14.00
12.00
10.00
8.00
6.00
4.00
2.00
0.00
25
35
45
55
65
75
85
Temperature (°C)
90°-25°C
25°-90°C

F)

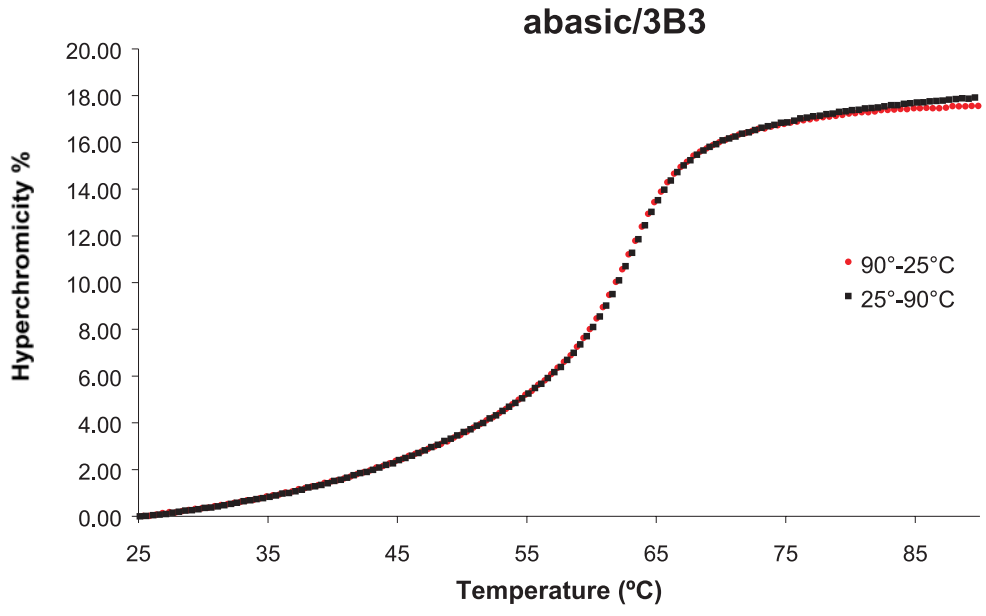
abasic/3B3
Hyperchromicity %
20.00
18.00
16.00
14.00
12.00
10.00
8.00
6.00
4.00
2.00
0.00
25
35
45
55
65
75
85
Temperature (°C)
90°-25°C
25°-90°C

G)

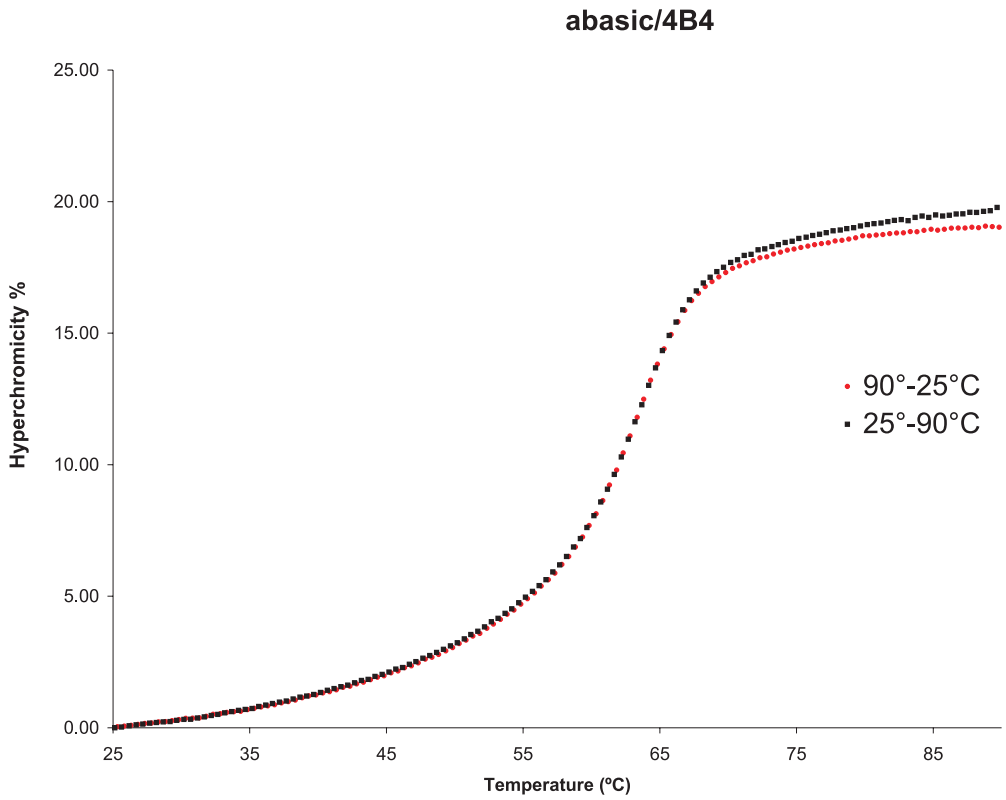
abasic/4B4
25.00
20.00
15.00
10.00
5.00
0.00
Hyperchromicity %
25
35
45
55
65
75
85
Temperature (ºC)
90°-25°C
25°-90°C

H)

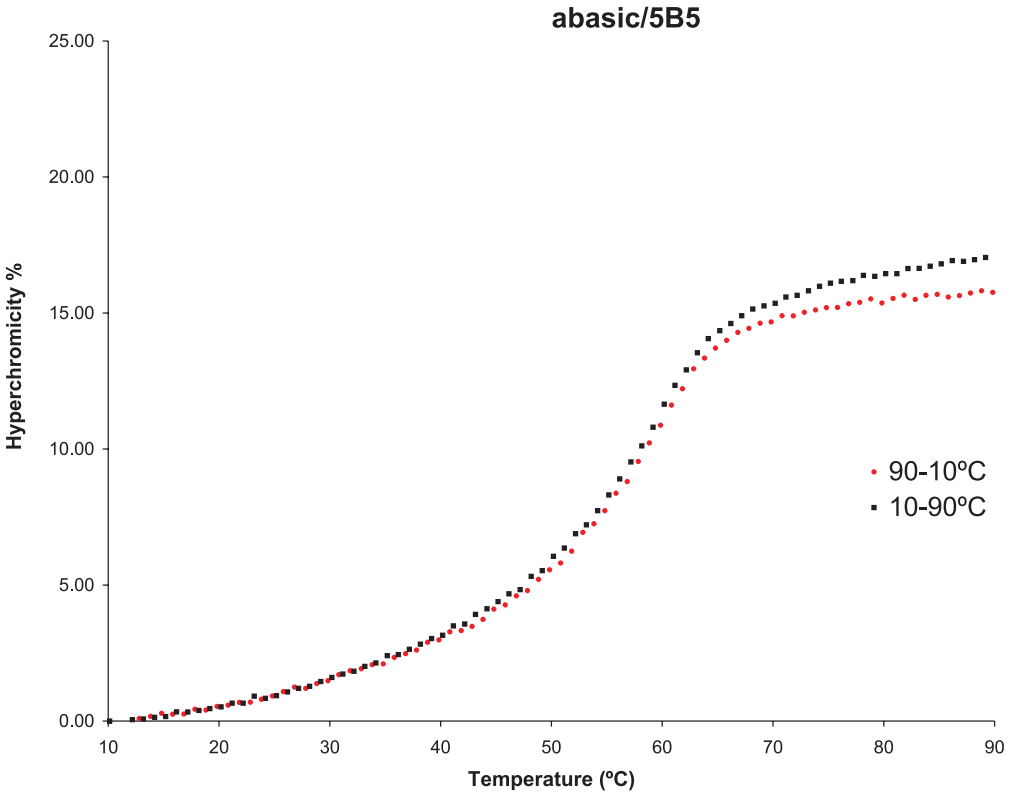
abasic/5B5
25.00
20.00
15.00
10.00
5.00
0.00
Hyperchromicity %
10
20
30
40
50
60
70
80
90
Temperature (ºC)
90-10ºC
10-90ºC

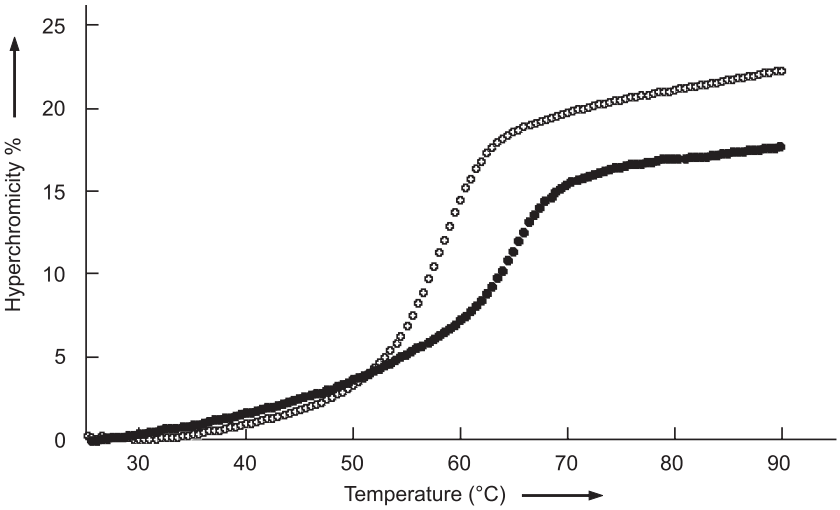

Figure 5.3. Comparison of thermal denaturation curves of the duplex containing the phenanthroline building block with pentamethylene linkers (closed circles) or an adenosine (open circles) opposite to the abasic site. (Conditions: see *Fig. 7.2*)

Refrences

[1] T. Lindahl, B. Nyberg, *Biochemistry* **1972,** *11*, 3610-3618.

[2] B. Demple, L. Harrison, *Annu.Rev.Biochem.* **1994,** *63*, 915-948.

[3] O. D. Scharer, *Angew.Chem., Int.Ed.Engl.* **2003,** *42*, 2946-2974.

[4] N. Berthet, J. F. Constant, M. Demeunynck, P. Michon, J. Lhomme, *J.Med.Chem* **1997,** *40*, 3346-3352.

[5] N. Berthet, J. Michon, J. Lhomme, M. P. Teulade-Fichou, J. P. Vigneron, J. M. Lehn, *Chem.Eur.J.* **1999,** *5*, 3625-3630.

[6] K. Yoshimoto, S. Nishizawa, M. Minagawa, N. Teramae, *J.Am.Chem.Soc.* **2003,** *125*, 8982-8983.

[7] J. Lhomme, J. F. Constant, M. Demeunynck, *Biopolymers* **1999,** *52*, 65-83.

[8] T. J. Matray, E. T. Kool, *J.Am.Chem.Soc.* **1998,** *120*, 6191-6192.

[9] S. Smirnov, T. J. Matray, E. T. Kool, C. los Santos, *Nucleic Acids Res.* **2002,** *30*, 5561-5569.

[10] E. T. Kool, J. C. Morales, K. M. Guckian, *Angew.Chem.Int.Ed Engl.* **2000,** *39*, 990-1009.

[11] S. M. Langenegger, R. Häner, *Chem.Biodiv.* **2004,** *1*, 259-264.

[12] H. Vollmann, H. Becker, M. Corell, H. Streeck, G. Langbein, *Ann.* **1937,** *531*, 1-159.

[13] C. J. Chandler, L. W. Deady, J. A. Reiss, *J.Heterocyclic Chem.* **1981,** *18*, 599-601.

[14] S. L. Beaucage, M. H. Caruthers, *Tetrahedron Lett.* **1981,** *22*, 1859-1862.

[15] N. D. Sinha, J. Biernat, J. McManus, H. Koster, *Nucleic Acids Res.* **1984,** *12*, 4539-4557.

[16] The building block ϕ is commonly used as a chemically stable analog of an abasic site. We refer to this building block as an abasic site' although it is not an abasic site in the strict sense.

[17] S. T. Hoehn, C. J. Turner, J. Stubbe, *Nucleic Acids Res.* **2001,** *29*, 3413-3423.

[18] R. D. Beger, P. H. Bolton, *J.Biol.Chem.* **1998,** *273*, 15565-15573.

[19] Y. Coppel, N. Berthet, C. Coulombeau, C. Coulombeau, J. Garcia, J. Lhomme, *Biochemistry* **1997,** *36*, 4817-4830.

[20] HyperChem(TM), Hypercube, Inc., 1115 NW 4th Street, Gainesville, Florida 32601, USA.

6. Stretches of Interstrand Stacked Phenanthrenes in DNA

6.1. Introduction

As shown before, non-nucleosidic, polyaromatic building blocks can well be incorporated into DNA. Complementary strands form stable hybrid duplexes, in which opposite phenanthrene or other building blocks interact in an interstrand stacking mode (see *Chapters 2.,3.*). These building blocks can serve as base surrogates without destabilizing the DNA duplex. Since the replacement of two base pairs by phenanthrene-derived building blocks had no negative influence on duplex stability, we subsequently investigated the synthesis and properties of oligomers containing extended stretches of non-nucleosidic phenanthrenes.

6.2. Results and Discussion

We decided to use the building block with the three carbon linker (*Table 6.1.*). This linker had been found previously to be well hybridizing and optimal with regard to its synthesis. The synthesis of the phenanthrene phosphoramidite was as described previously (*Chapter 2.*). Assembly of the oligomers involved standard automated oligonucleotide synthesis. The crude oligomers were purified by reverse phase HPLC and their identity was verified by *electrospray ionisation time-of-flight* (*ESI-TOF*) mass spectrometry (*Chapter 6.4.*). The influence of the base substitutions by the phenanthrene building blocks on the DNA duplex stability was analyzed by thermal denaturation experiments (*Table 6.1.*). All oligomers investigated in this study showed a single, cooperative transition. As described before (*Chapter 2*), the replacement of one or two phenenathrene ‘pairs’ had either no or a slight stabilizing effect (entries 2 and 3). Replacement of a third and even a fourth base pair is still well tolerated. Only in the case where seven pairs of phenanthrenes were introduced, a decrease of 8.3°C was observed. This translates into a ΔTm of 1.2°C per modification.

Entry	Duplex	Tm (°C)[a,b]	ΔTm[c]	ΔTm/mod[d]
1	(5') AGC TCG GTC ATC GAG AGT GCA (3') TCG AGC CAG TAG CTC TCA CGT	68.0	**-**	-
2	(5') AGC TCG GTC A**P**C GAG AGT GCA (3') TCG AGC CAG T**P**G CTC TCA CGT	68.3	**0.3**	0.3
3	(5') AGC TCG GTC **PP**C GAG AGT GCA (3') TCG AGC CAG **PP**G CTC TCA CGT	69.3	**1.3**	0.6
4	(5') AGC TCG GT**P PP**C GAG AGT GCA (3') TCG AGC CA**P PP**G CTC TCA CGT	67.7	**-0.3**	-0.1
5	(5') AGC TCG G**PP PP**C GAG AGT GCA (3') TCG AGC C**PP PP**G CTC TCA CGT	66.0	**-2.0**	-0.5
6	(5') AGC TC**P PPP PPP** GAG AGT GCA (3') TCG AG**P PPP PPP** CTC TCA CGT	59.7	**-8.3**	-1.2

P =

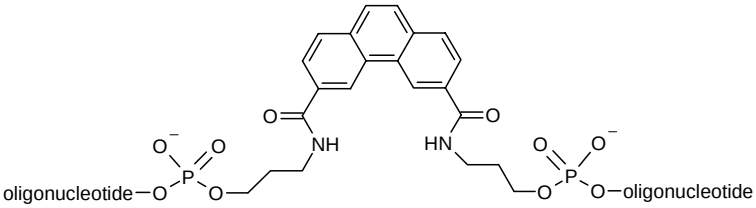

Table 6.1. Influence of natural base pair substitution by non-nucleosidic phenanthrene moieties on the thermal stability of duplex DNA. [a] Conditions: oligomer concentration 1.0µM, 10 mM Tris-HCl, 100 mM NaCl, pH 7.4; temp. gradient: 0.5°C/min. [b] Melting temperatures were determined from the maximum of the first derivative of the melting curve (A_{260} against temperature); each Tm is the average of three independent experiments; exptl. error: ± 0.5°C. [c] Difference in Tm relative to the control duplex (entry 1). [d] Difference in Tm relative to the control duplex (entry 1) divided by the number of modifications per single strand.

The circular dichroism (CD) spectra are in good overall agreement with a typical B-DNA structure (*Figure 6.3.).* While the minima and maxima of the modified duplexes correlate very well with the ones of the unmodified DNA duplex, an additional shoulder is apparent in the spectra of the modified duplexes in the range of 230nm to 250nm.

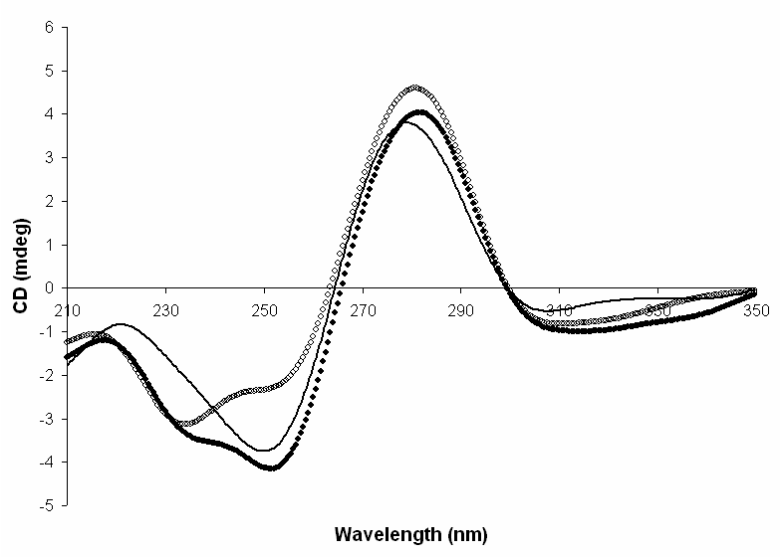

Figure 6.3. Circular dichroism spectra. Unmodified DNA duplex (straight line), duplex containing three phenanthrene "pairs" (filled diamonds), and seven phenanthrene "pairs" containing duplex (open diamonds).

An illustration of the hybrids showing the planes of the bases and the interstrand stacked phenanthrenes is presented in *Figure 6.1.* The part of the phenanthrene stretches is somewhat slimmer than the DNA parts on both sides. It is well possible, that the stability can be further influenced by choosing a different linker in the part where we have no transition between DNA and interstrand stacked phenanthrenes. Nevertheless, exchange of seven natural base pairs by the same number of flexible phenanthrene residues of this type results in a mere destabilization of about 8°C.

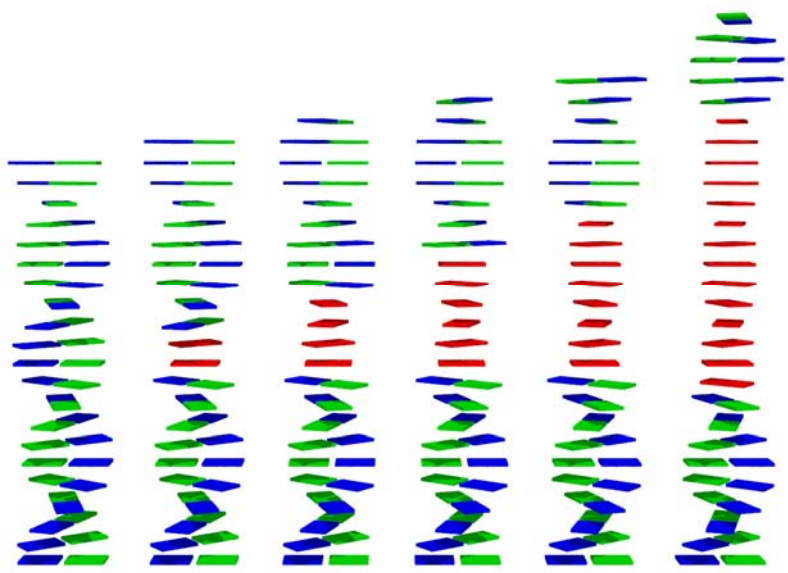

Figure 6.2. Illustration of the phenanthrene-modified duplex. Only the base pairs (but not the backbone) are shown; natural base pairs are in green and blue, phenanthrene residues in red. From left to right: unmodified duplex, then the modified duplexes with increasing numbers of phenanthrenes (cf. entries 1-6 in *Table 6.1.*).

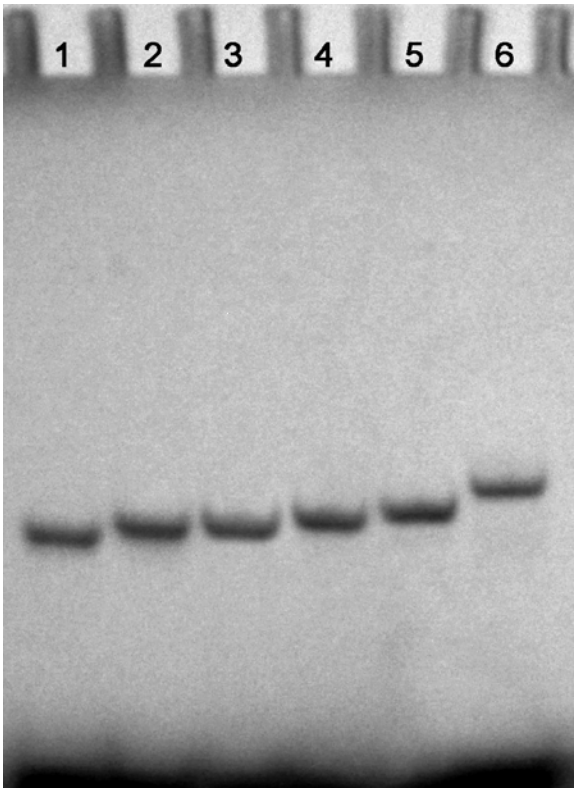

Figure 6.4. Non-denaturing 20% polyacrylamide gel of phenanthrene-containing hybrids. The line numbers correspond to the entry numbers in *Table 6.1.*, i.e. the number of phenanthrenes increases from left (zero) to right (seven). Bands were visualized by UV-light (260nm).

The model of interstrand stacked phenanthrenes predicts a lengthening of the duplex by about 3.4 Å with each substitution of a natural base by a phenanthrene derived building block. The charge of the hybrids, on the other hand, stays the same (*Figure 6.1.*, *Figure 6.2.*). To further investigate this property, we performed native gel mobility experiments. *Figure 6.4.* shows a gradual reduction in the gel mobility with an increasing number of phenanthrenes. The largest effect (*lane 6*) is a result of the replacement of seven natural base pairs by seven interstrand stacking phenanthrene pairs. According to the interstrand stacked model, this should give a duplex, the length of which is comparable to an unmodified, 14 base pair-duplex (*Figure 6.2.*). The middle part, which corresponds to approximately half of the length of this duplex, is stabilized only by interstrand stacking interactions. A similar structure was also proposed by *Leumann et al.* [1] In that work, up to four biphenyl C-nucleoside residues per each strand were incorporated in DNA. Furthermore, *Iverson et al.* showed that interstrand stacking forces could stabilize also duplexes with flexible backbones. In this latter case, the investigated oligomers were not in a DNA context [2].

6.3. Conclusions

We have shown that complementary DNA strands containing up to seven non-nucleosidic phenanthrene building blocks in opposite positions form stable hybrids. The phenanthrene residues contribute to the overall stability of the duplex trough interstrand stacking interactions. Replacement of the bases by the phenanthrene moieties results in a lengthening of the duplex, which is a consequence of the interstrand stacking.

6.4. Experimental Section

Synthesis of the Phenanthrene Building Block

The synthesis of the phenanthrene phosphoramidite followed the procedure described previously (*Chapter 2.*) [3].

Oligonucleotide Synthesis

Phenanthrene-derived phosphoramidite building blocks were incorporated into oligonucleotides *via* standard automated oligonucleotide synthesis using I_2/pyridine/water in the oxidation step. Coupling yields were equal to the ones obtained with standard phosphoramidite building blocks. Oligonucleotides were purified by reverse phase HPLC and characterised by MS (*Table 6.2*).

oligonucleotide	calculated for $(M-H)^-$	found
(5') AGC TCG GTC A**P**C GAG AGT GCA	6608.0	6608.4
(3') TCG AGC CAG T**P**G CTC TCA CGT	6510.1	6510.6
(5') AGC TCG GTC **PP**C GAG AGT GCA	6737.7	6737.5
(3') TCG AGC CAG **PP**G CTC TCA CGT	6648.6	6648.8
(5') AGC TCG GT**P** **PP**C GAG AGT GCA	6890.9	6891.0
(3') TCG AGC CA**P** **PP**G CTC TCA CGT	6761.9	6762.3
(5') AGC TCG G**PP** **PP**C GAG AGT GCA	7029.1	7029.4
(3') TCG AGC C**PP** **PP**G CTC TCA CGT	6891.1	6891.9
(5') AGC TC**P** **PPP** **PPP** GAG AGT GCA	7408.7	7409.1
(3') TCG AG**P** **PPP** **PPP** CTC TCA CGT	7310.7	7311.2

Table 6.2. Molecular weights of oligonucleotides used in this study (*electrospray ionisation time-of-flight, ESI-TOF*)

Gel-electrophoresis

20% non-denaturing polyacrylamide gels (19:1 mono-/bis-acrylamide) were prepared according to standard procedures [4]. DNA-samples (~350 pmol) were dried in a Speedvac at room temperature. After dissolution in the loading buffer (90 mM Tris-borat, 5% glycerol) the samples were heated to 90 °C and slowly allowed to cool to room temperature prior to the loading onto the gel. The gels were run at room temperature [max. 250 V, max.3 W, 1 h in a TBE buffer (90mM Tris-borat, pH 7.2)]. Bands were visualized by UV light.

Refrences

[1] C. Brotschi, C.J. Leumann, *Angew. Chem. Int. Ed.* **2003**, 42, 1655-1658.

[2] G.J. Gabriel, B.L. Iverson, *J. Am. Chem. Soc.* **2002**, 124, 15174-15175.

[3] S. M. Langenegger, R. Häner, *Helv.Chim.Acta* **2002,** *85*, 3414-3421.

[4] J. Sambrook, E.F. Fritsch, T. Maniatis *in Molecular Cloning, A Laboratory Manual, Vol. 1*, Cold Spring Harbor Laboratory Press, New York **1989**.

7. Excimer Formation by Interstrand Stacked Pyrenes

Simon M. Langenegger, Robert Häner, *Chem. Commun*. **2004**, 2792-2793.

7.1. Introduction

Besides their importance as genetic material, nucleic acids are increasingly gaining interest as nanometer-sized, functional matter [1-4]. Due to the repetitive, well-defined arrangement of their building blocks, nucleic acids and related types of oligomers [5-7] are ideal objects for the designed construction of larger assemblies and architectures [8-10]. Furthermore, the combination of nucleotides with non-natural building blocks greatly enhances the number of possible constructs and their potential applications. Recently, we reported the synthesis of a non-nucleosidic, phenanthrene-derived building block and its incorporation into double stranded DNA [11,12]. This simple building block serves as a base surrogate without destabilizing the DNA duplex nor altering its overall B-DNA structure. Based on the data obtained, a model of interstrand-stacked phenanthrenes was proposed [11]. Consequently, replacement of the non-nucleosidic phenanthrenes by analogous pyrenes should then give rise to excimer formation [13]. Here, we report the synthesis, the hybridisation behaviour as well as the spectroscopic properties of duplex DNA containing non-nucleosidic pyrene building blocks.

7.2. Results and Discussion

The synthesis of the required pyrene building blocks is shown in *Scheme 7.1*.. Thus, pyrene 1,8-dicarboxylic acid (**1**) was obtained according to a procedure reported in the literature [14]. Subsequent derivatisation with the corresponding linkers, followed by phosphitylation under standard conditions gave the desired pyrene phosphoramidites **2a-d**.

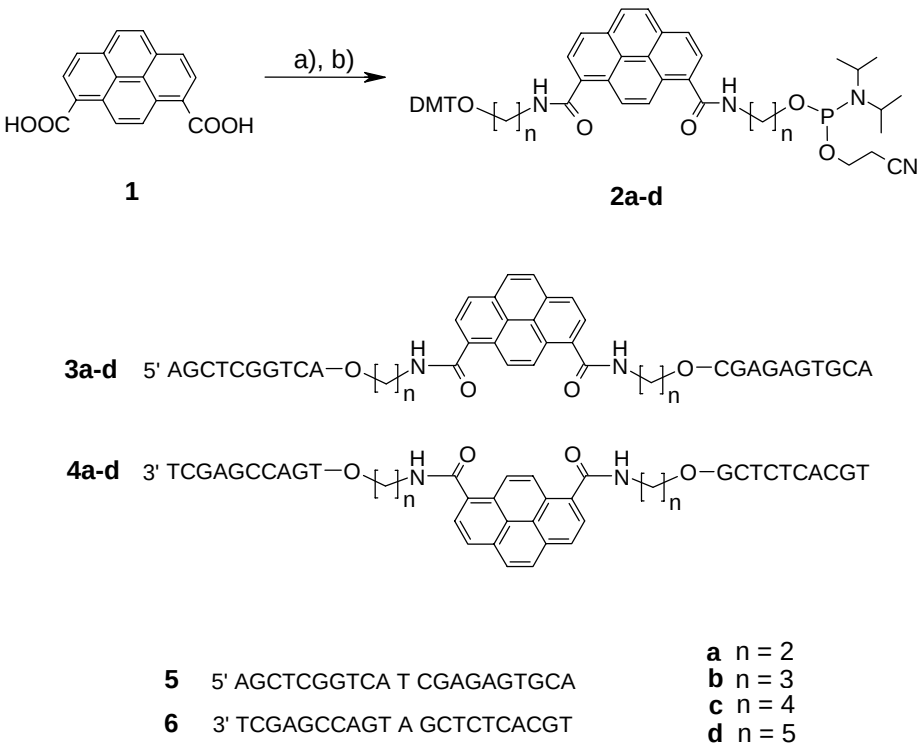

Scheme 7.1. Phosphoramidite building blocks and pyrene-modified oligonucleotides used in this study. Reagents and conditions: a) $H_2N(CH_2)_nOH/H_2N(CH_2)_nODMT$ (1:1), *Hünig's* base, BOP; b) 2-cyanoethyl diisopropylamidochloridophosphite, *Hünig's* base**.**

These building blocks were further used for the preparation of the oligomers **3a-d** and **4a-d** by automated oligonucleotide synthesis. Incorporation of the pyrene phosphoramidites proceeded without any difficulties, coupling yields being equal to those of unmodified nucleotide bases. In addition to the pyrene-containing oligomers, oligonucleotides **5** and **6** were prepared for control purposes. All oligomers were purified by reverse phase HPLC and characterized by *electrospray ionisation time-of-flight* (*ESI-TOF*) mass spectrometry (see *chapter 7.4.*).

Thermal denaturation experiments revealed a slight, but distinct, influence by the length of the non-nucleosidic linkers on the thermal stability of pyrene-modified duplexes (*Table 7.1.*). The highest thermal stability was observed with pyrene building blocks having four methylene units in the linkers (duplex **3c*4c**). This hybrid is equally stable as the control duplex **5*6**, in which an AT-base pair substitutes for the two pyrenes. The building blocks with shorter (i.e. duplexes **3a*4a** and **3b*4b**) or longer (duplex **3d*4d**) linkers led to a decrease in the Tm-value in the range of 2-3°C. Furthermore, circular dichroism (CD) spectra were typical for a B-DNA structure (see *chapter 7.4.*).

Duplex	**5*6**	**3a*4a**	**3b*4b**	**3c*4c**	**3d*4d**
Tm [°C][b]	68.0	65.0	65.7	67.8	64.7
ΔTm [°C][c]	-	-3.0	-2.3	-0.2	-3.3
excimer/monomer ratio[d]	-	1.68	2.58	3.24	0.48

Table 7.1. Tm-values and fluorescence ratios of pyrene-modified double stranded DNAs. Conditions: oligomer concentration 1.0 μM, 10 mM Tris-HCl, 100 mM NaCl, pH 7.4; temp. gradient: 0.5°C/min. [b] Melting temperatures were determined from the maximum of the first derivative of the melting curve (A_{260} against temperature); exptl. error: ± 0.5°C. [c] Difference in Tm relative to **5*6**. [d] Emission wavelengths: excimer: 493nm; monomer: 398nm.

We next investigated the fluorescence properties of the different pyrene-containing oligomers (see *Fig. 7.1.*). Upon irradiation at a wavelength of 354nm, all hybrids showed emission at 398nm, which is characteristic for pyrene monomer fluorescence. For the single stranded oligomer **3c**, emission was observed only at this wavelength. In contrast, all pyrene-containing duplexes showed a second fluorescence emission with a maximum value at 493nm, typical for pyrene eximers. The degree of excimer formation is parallel to the thermal stability observed for the respective duplexes. Thus, the most stable duplex **3c*4c** showed the strongest excimer fluorescence. For the less stable duplex **3d*4d**, the monomer emission is dominant and only weak eximer fluorescence was observed. The other two hybrids, **3a*4a** and **3b*4b**, showed an intermediate behaviour. This trend is also illustrated by the excimer/monomer fluorescence ratio given in *Table 7.1.*, which is highest for the most stable duplex **3c*4c** and least for **3d*4d**.

Like the structurally similar 3,6-disubstituted phenanthrene derivatives (*Chapter 2.*)[11], the non-nucleosidic pyrene derivatives described herein form stable DNA hybrids. With an optimal linker length, two pyrene building blocks contribute to duplex stability approximately as much as a natural AT-base pair. The observation of strong excimer fluorescence is clear evidence for interstand-stacking interactions of the two pyrenes arranged in opposite positions within the DNA duplex. Furthermore, duplex stability and excimer formation are both influenced by the linker in the same way. This observation is well in agreement with a model

of interstrand stacked pyrenes, since stacking interactions should favour the formation of the excimer [13] and, at the same time, also the interaction between the two strands.

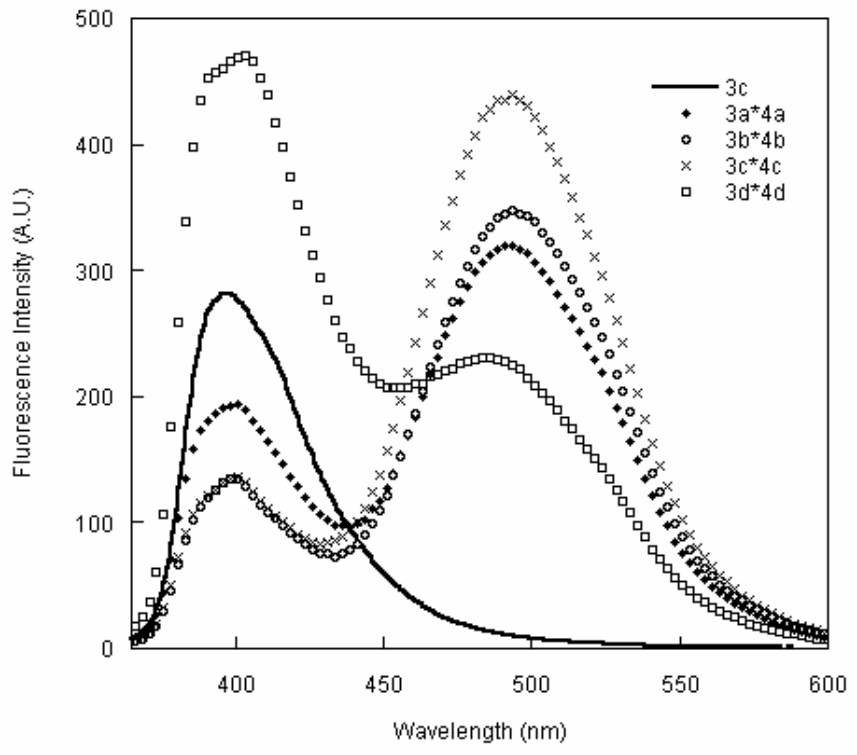

Figure 7.1. Fluorescence spectra of pyrene-containing duplexes **3a-d*4a-d**, as well as of the single stranded oligonucleotide **3c**. Conditions: oligomer concentration 1.0 μM, 10 mM Tris-HCl, 100 mM NaCl, pH 7.4, room temperature. Excitation wavelength: 354nm; excitation slit: 5nm; emission slit: 7nm.

Formation of excimers has been observed in pyrene-modified, single as well as double stranded DNAs [16-23]. Due to the many potential diagnostic applications, hybridisation-induced excimer formation is of particular interest. Thus, attachment of pyrene derivatives to the backbone[20,21,23] as well as to terminal positions [18,19] of oligonucleotides have been reported in this context. Hybridisation-induced pyrene excimer formation was observed by Korshun and coworkers [20] in the major groove of double stranded DNA and, very recently, also in the minor groove of DNA containing pyrene-LNA residues by Wengel and coworkers [21]. The results described here show, for the first time, that excimer formation can also take place through interstrand stacking interactions. This observation is different to the findings of Malakov et al., who reported that two pyrenes placed in opposite positions in double stranded DNA did not form an excimer[24]. *Fig. 7.2.* shows a molecular model of the hybrid **3c*4c** with the two pyrenes embedded within the aromatic core of the duplex. A similar arrangement of two intercalating pyrenes in a DNA duplex was recently reported by Nielsen and

colleagues [25]. Furthermore, the model shows that the non-nucleosidic linkers do not disturb the overall continuity of the helical backbone.

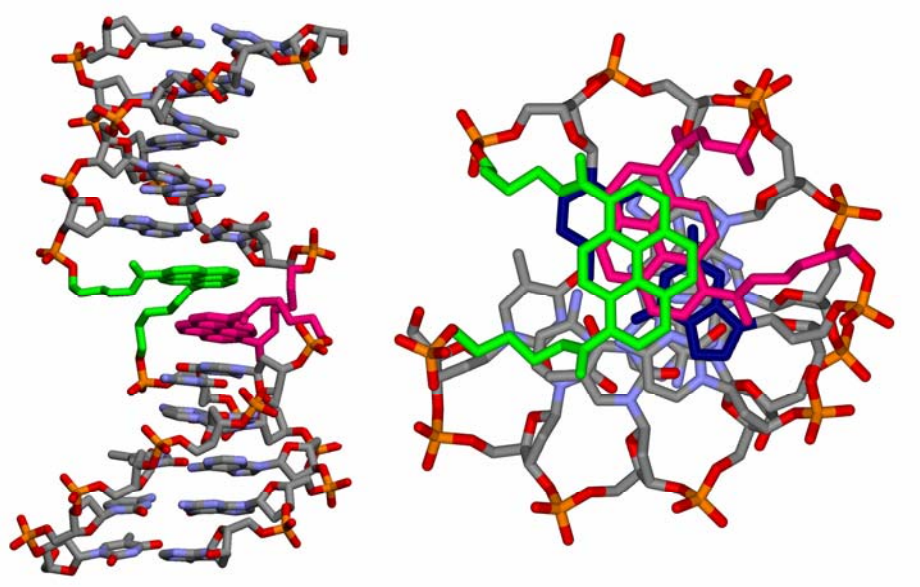

Figure 7.2. Molecular model of the duplex **3c*4c** with two interstrand stacked pyrenes (HyperChem™ 7.0, minimised with *amber* force field).[15] The non-nucleosidic building blocks are highlighted in red and green. Left: view perpendicular to the helical axis. Right: view along the helical axis. showing the pyrenes stacked on the nucleotide bases; nucleotides on the viewers side have been omitted for clarity; the GC-base pair adjacent to the pyrenes is shown in yellow.

7.3. Conclusions

In conclusion, we have shown that complementary DNA strands containing simple, non-nucleosidic pyrene building blocks in opposite positions form stable hybrids. The pyrene residues contribute to the overall stability of the duplex through interstrand stacking interactions. Strong excimer fluorescence is observed upon hybridisation of two modified strands.

7.4. Experimental Section

Oligonucleotide Synthesis

Pyrene-derived phosphoramidite building blocks **2a-d** were incorporated into oligonucleotides *via* standard automated oligonucleotide synthesis using I_2/pyridine/water in the oxidation step. Coupling yields with **2a-d** were equal to the ones obtained with standard phosphoramidite building blocks. Oligonucleotides were purified by reverse phase HPLC and characterised by MS (*Table 7.2.*).

oligonucleotide	calculated for $(M-H)^-$	found
3a	6604.5	6604.4
3b	6632.5	6632.6
3c	6660.5	6660.5
3d	6688.5	6688.6
4a	6506.5	6506.5
4b	6534.5	6534.4
4c	6562.5	6562.4
4d	6590.5	6590.3

Table 7.2. Molecular weights of oligonucleotides used in this study (*electrospray ionisation time-of-flight*, *ESI-TOF*)

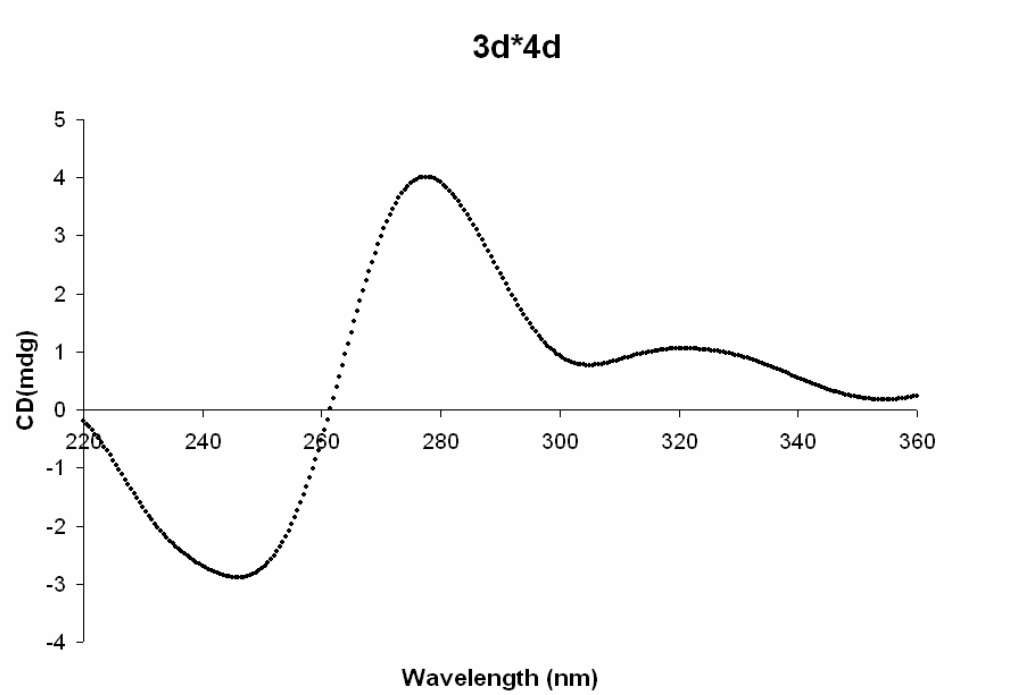

Figure 7.3. Circular dichroism curve of hybrid **3d*4d**. Conditions: 1.0 µM oligomers (each strand); 100mM NaCl; 10mM Tris.HCl, pH 7.4, 20°C.

Figures 7.4. A-E: Melting curves of different hybrids. Conditions: Oligomer concentration 1.0 µM, 10 mM Tris-HCl, 100 mM NaCl, pH 7.4; temp. gradient: 0.5°C/min. Exptl. error: ± 0.5°C. Absorbance was measured at 260nm. **A**) duplex **5*6**, **B**) duplex **3a*4a**; **C**) duplex **3b*4b**; **D**) duplex **3c*4c**; **E**) duplex **3d*4d**.

A)

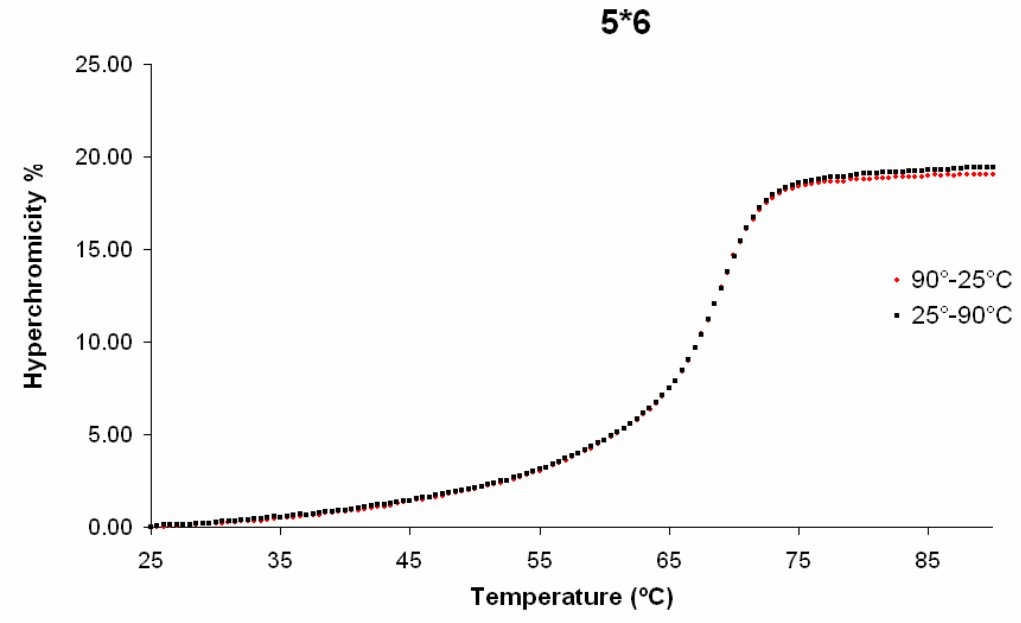

B)

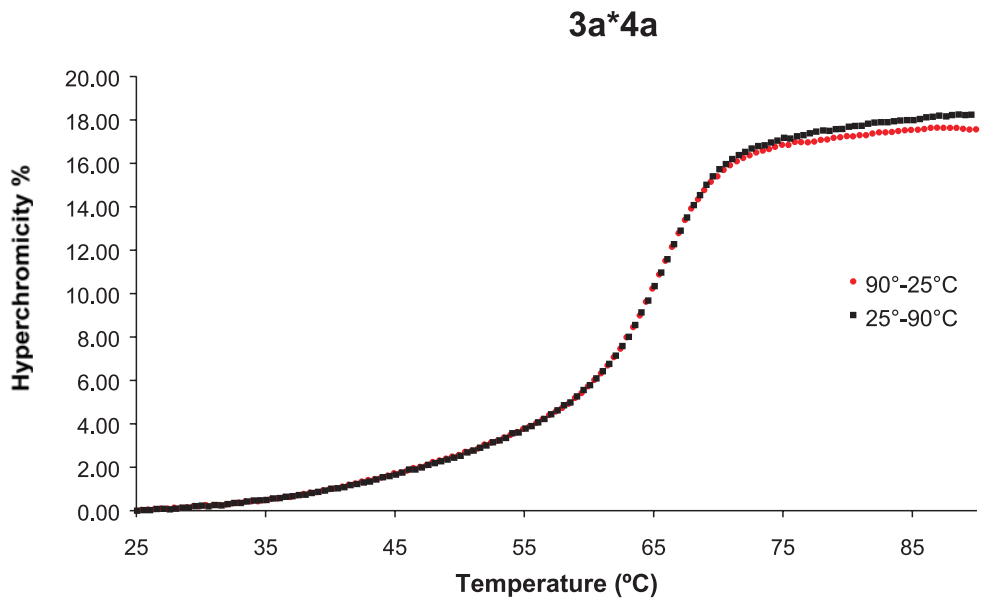
3a*4a
Hyperchromicity %
20.00
18.00
16.00
14.00
12.00
10.00
8.00
6.00
4.00
2.00
0.00
25
35
45
55
65
75
85
Temperature (ºC)
90°-25°C
25°-90°C

C)

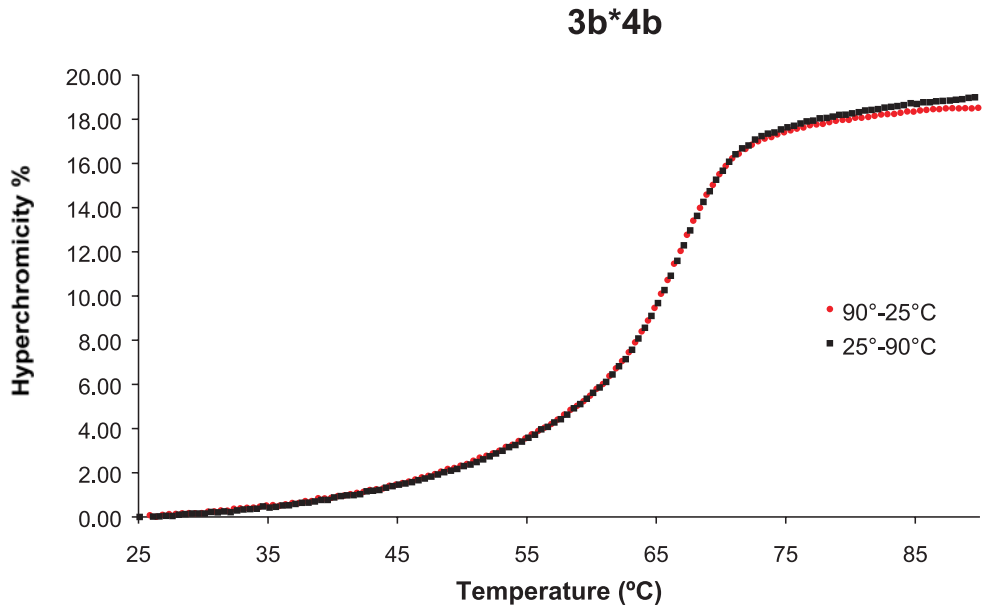
3b*4b
Hyperchromicity %
20.00
18.00
16.00
14.00
12.00
10.00
8.00
6.00
4.00
2.00
0.00
25
35
45
55
65
75
85
Temperature (ºC)
90°-25°C
25°-90°C

D)

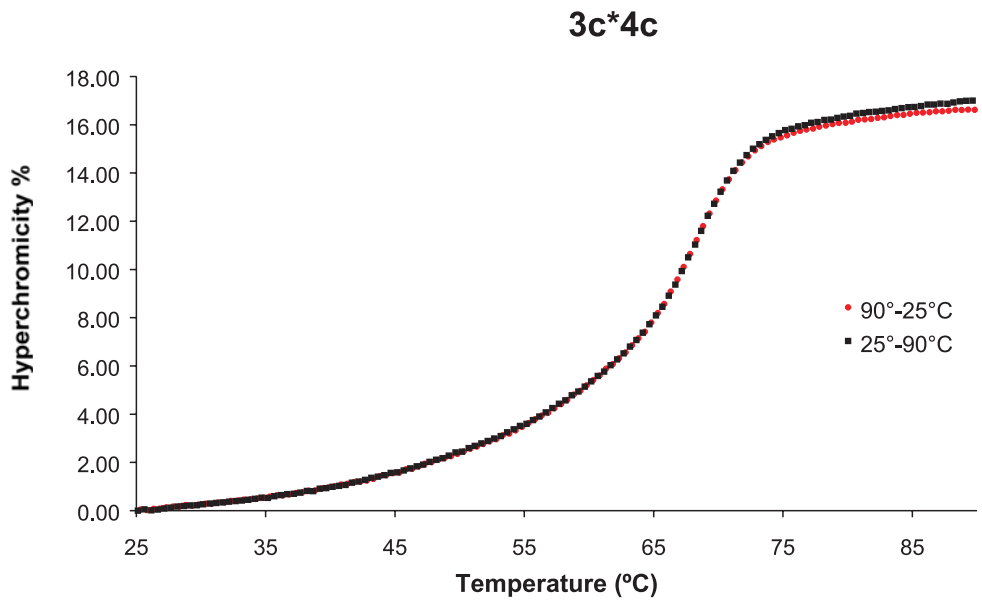
3c*4c
Hyperchromicity %
18.00
16.00
14.00
12.00
10.00
8.00
6.00
4.00
2.00
0.00
25
35
45
55
65
75
85
Temperature (ºC)
90°-25°C
25°-90°C

E)

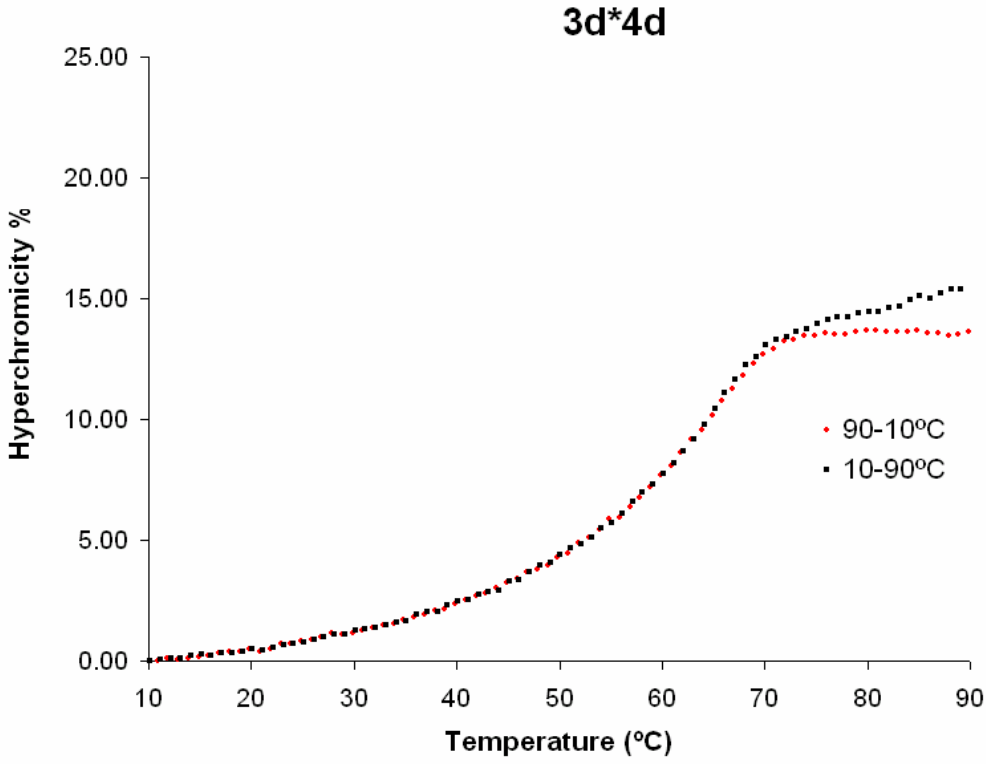
3d*4d
Hyperchromicity %
25.00
20.00
15.00
10.00
5.00
0.00
10
20
30
40
50
60
70
80
90
Temperature (ºC)
90-10ºC
10-90ºC

References and Notes

[1] N. C. Seeman, *Acc.Chem.Res.* **1997,** *30*, 357-363.

[2] N. C. Seeman, *Nature* **2003,** *421*, 427-431.

[3] J. Wengel, *Org.Biomol.Chem.* **2004,** *2*, 277-280.

[4] R. Bashir, *Superlattices and Microstructures* **2001,** *29*, 1-16.

[5] E. Uhlmann, A. Peymann, *Chem.Rev.* **1990,** *90*, 543-584.

[6] A. Eschenmoser, *Science* **1999,** *284*, 2118-2124.

[7] E. T. Kool, *Acc. Chem. Res.* **2002,** *35*, 936-943.

[8] J. F. Shi, D. E. Bergstrom, *Angew.Chem., Int.Ed.Engl.* **1997,** *36*, 111-113.

[9] W. M. Shih, J. D. Quispe, G. F. Joyce, *Nature* **2004,** *427*, 618-621.

[10] E. Winfree, F. Liu, L. A. Wenzler, N. C. Seeman, *Nature* **1998,** *394*, 539-544.

[11] S. M. Langenegger, R. Häner, *Helv.Chim.Acta* **2002,** *85*, 3414-3421.

[12] S. M. Langenegger, R. Häner, *Chem.Biodiv.* **2004,** *1*, 259-264.

[13] F. M. Winnik, *Chem. Rev.* **1993,** *93*, 587-614.

[14] H. Vollmann, H. Becker, M. Corell, H. Streeck, G. Langbein, *Ann.* **1937,** *531*, 1-159.

[15] HyperChem(TM), Hypercube, Inc., 1115 NW 4th Street, Gainesville, Florida 32601, USA.

[16] G. Tong, J. M. Lawlor, G. W. Tregear, J. Haralambidis, *J.Am.Chem.Soc.* **1995,** *117*, 12151-12158.

[17] K. Yamana, M. Takei, H. Nakano, *Tetrahedron Lett.* **1997,** *38*, 6051-6054.

[18] M. Masuko, H. Ohtani, K. Ebata, A. Shimadzu, *Nucl.Acids.Res.* **1998,** *26*, 5409-5416.

[19] P. L. Paris, J. M. Langenhan, E. T. Kool, *Nucl.Acids.Res.* **1998,** *26*, 3789-3793.

[20] M. N. Dioubankova, A. D. Malakhov, D. A. Stetsenko, M. J. Gait, P. E. Volynsky, R. G. Efremov, V. A. Korshun, *ChemBioChem* **2003,** *4*, 841-847.

[21] P. J. Hrdlicka, B. R. Babu, M. D. Sorensen, J. Wengel, *Chem. Commun.* **2004,** 1478-1479.

[22] U. B. Christensen, E. B. Pedersen, *Nucleic Acids Res.* **2002,** *30*, 4918-4925.

[23] U. B. Christensen, E. B. Pedersen, *Helv.Chim.Acta* **2003,** *86*, 2090-2097.

[24] A. D. Malakhov, M. V. Skorobogatyi, I. A. Prokhorenko, S. V. Gontarev, D. T. Kozhich, D. A. Stetsenko, I. A. Stepanova, Z. O. Shenkarev, Y. A. Berlin, V. A. Korshun, *Eur. J. Org. Chem.* **2004,** 1298-1307.

[25] C. B. Nielsen, M. Petersen, E. B. Pedersen, P. E. Hansen, U. B. Christensen, *Bioconjug.Chem.* **2004,** *15*, 260-269.

8. Control of Excimer Formation by Interstrand Stacking

8.1. Introduction

Due to the many potential diagnostic applications, hybridization-induced excimer formation is of particular interest [1-10]. As shown in the previous chapter, hybridization of single strands containing non-nucleosidic pyrene residues leads to strong excimer fluorescence. Based on these data, we explored the possibility of controlling excimer formation by using the pyrenes in combination with other types of building blocks, which are also interacting via interstrand stacking but do not lead to eximer or exciplex formation. One possibility consists in the use of the phenanthrene derivative **P**, which was already described in the previous chapters (*Chapter 2.)*. Thus, the use of phenanthrenes might allow the specific formation or preventing of pyrene eximers. This approach is illustrated in *Figure 8.1*.

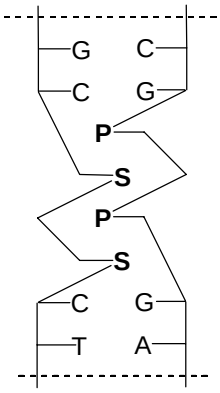

Figure 8.1. Schematic illustration of excimer preventing by interstrand stacking phenanthrene residues (**S** = pyrene, **P** = phenanthrene).

8.2. Results and Discussion

Assembly of the required oligomers was carried out as described before. Purification involved reverse phase HPLC and the identities were verified by *electrospray ionisation time-of-flight* (*ESI-TOF*) mass spectrometry (see *chapter 8.4.*). The influence of the different pyrene and phenanthrene substitutions on DNA duplex stability is summarized in *Table 8.1.*. As with all the modified oligomers described previously, the denaturation curves showed for all the duplexes in this study a single, cooperative transition. The duplexes **3*4** and **9*10** are destabilized by 3 and 2°C, respectively, in comparison with the unmodified duplex (**1*2**). In

contrast, duplex **7*8** is as stable and **5*6** is more stable by 2°C than the reference duplex. These differences seem to be mostly sequence dependent and there is no obvious general rule visible, which would allow predicting these changes in stability.

Oligo	Duplex	Tm (°C)[a,b]	ΔTm[c]
1	(5') AGC TCG GTC ATC GAG AGT GCA	69.0	**-**
2	(3') TCG AGC CAG TAG CTC TCA CGT		
3	(5') AGC TCG GTC **SS**C GAG AGT GCA	66.0	**-3.0**
4	(3') TCG AGC CAG **PP**G CTC TCA CGT		
5	(5') AGC TCG GTC **PP**C GAG AGT GCA	70.9	**1.9**
6	(3') TCG AGC CAG **SS**G CTC TCA CGT		
7	(5') AGC TCG GTC **SP**C GAG AGT GCA	68.7	**-0.3**
8	(3') TCG AGC CAG **PS**G CTC TCA CGT		
9	(5') AGC TCG GTC **PS**C GAG AGT GCA	66.9	**-2.1**
10	(3') TCG AGC CAG **SP**G CTC TCA CGT		

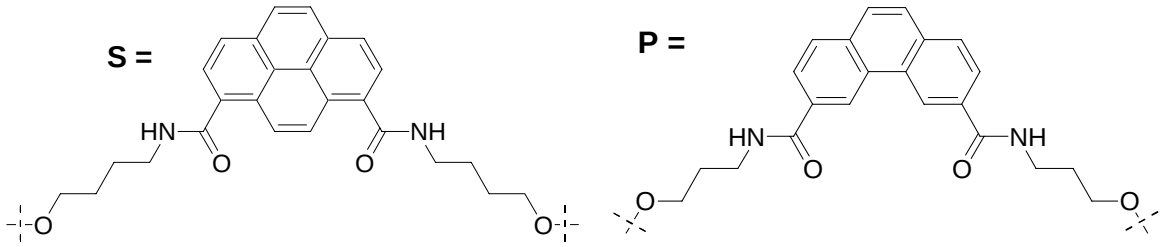

Table 8.1. Influence of substitution natural base pair by non-nucleosidic phenanthrene and pyrene moieties on the thermal stability of duplex DNA. [a] Conditions: oligomer concentration 1.0µM, 10 mM Tris-HCl, 100 mM NaCl, pH 7.4; temp. gradient: 0.5°C/min. [b] Melting temperatures were determined from the maximum of the first derivative of the melting curve (A_{260} against temperature); each Tm is the average of three independent experiments; exptl. error: ± 0.5°C. [c] Difference in Tm relative to the control duplex (entry 1).

We next investigated the fluorescence properties of the different pyrene containing oligomers (*Figure 8.2.*). Upon irradiation at 354 nm, the single strands **3** and **6** showed a high intensity fluorescence signal at 495 nm, which is typical for the pyrene excimer; the monomer fluorescence of the pyrene, at about 400 nm, is practically inexistent. This result shows that the two pyrenes are forming an excimer in the single strand. The fluorescence signal in **6** is somewhat lower than in **3**, which can be explained by the presence of two guanosines adjacent to the pyrenes, an interaction which is known to have a quenching effect on the fluorescence [11]. Upon hybridization with complementary oligomers containing

phenanthrenes, the two duplexes **3*4** and **5*6** are formed. In both duplexes, the fluorescence is substantially decreased compared to the single strand, in the duplex **3*4** by a factor of 3.3 and in the duplex **5*6** by a factor of 2.7 (at 495 nm). This observation is in agreement with a model of interstrand stacked phenanthrenes and pyrenes (*Figure 8.3.*). In the single strand, which contains two pyrenes (**S**) in juxtaposed positions, the excimer can form. Upon formation of the duplex, the two pyrenes (**S**) and the two phenanthrenes (**P**) interact in an interstrand stacking mode. As a consequence the pyrenes are separated by a phenanthrene moiety and, thus, formation of the excimer is prevented. The shoulder at about 450nm in the fluorescence spectra of the duplexes **3*4** and **5*6** could be due to existence of an exciplex between the pyrene and the phenanthrene building blocks. Further studies are, however, required to clarify this point further.

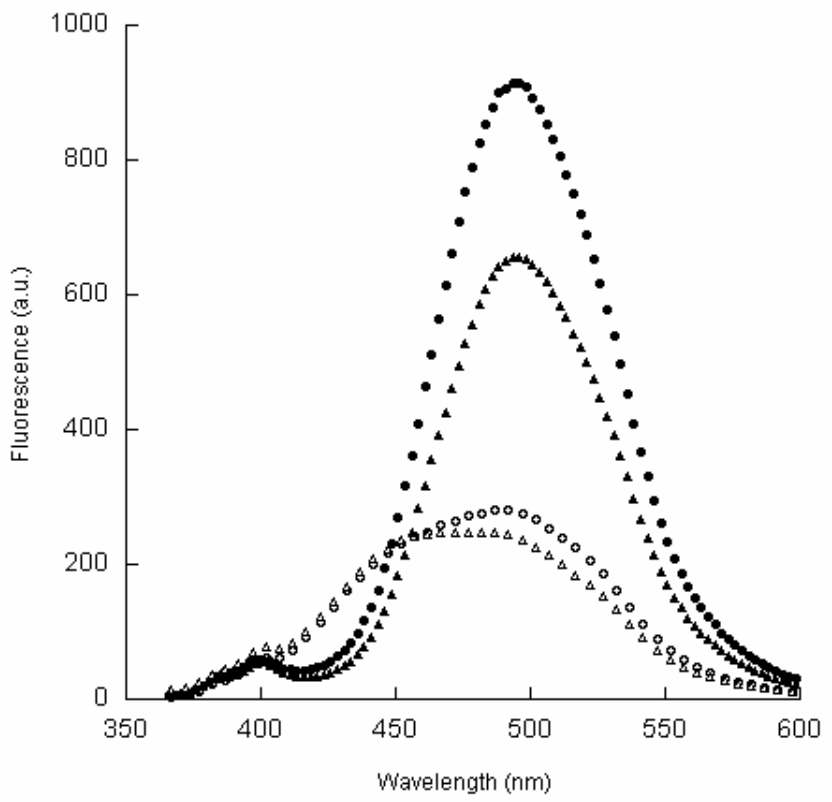

Figure 8.2. Fluorescence spectra of pyrene-containing single strands and duplexes: **3** single strand (filled circle), **6** single strand (filled triangle), **3*4** duplex (open circle), **5*6** duplex (open triangle). Conditions: oligomer concentration 1.0 µM, 10 mM Tris-HCl, 100 mM NaCl, pH 7.4, room temperature. Excitation wavelength: 354nm; excitation slit: 5nm; emission slit: 7nm.

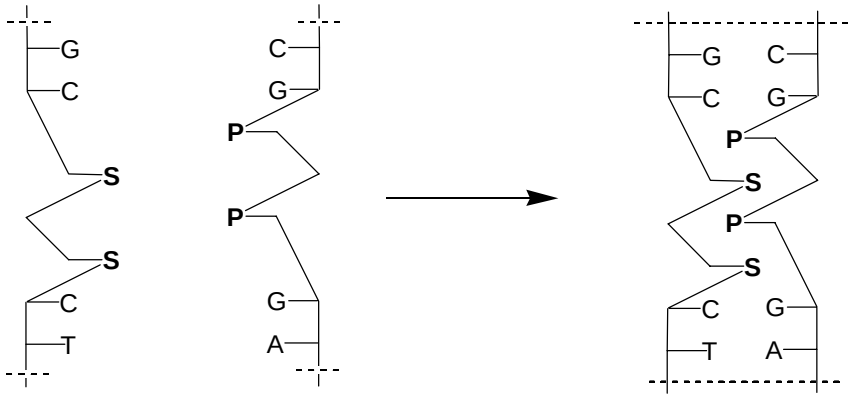

Figure 8.3. Two single strands containing two juxtaposed pyrene moieties (**S**) or phenanthrenes (**P**) form a duplex, in which the pyrene and phenanthrene building blocks are arranged in an alternating fashion.

To further understand the stacking interactions in this duplex, an additional set of oligomers (**7-10**, shown in *Figure 8.5.*) was synthesized and their fluorescence properties were analysed. Both duplexes (**7*8**, **9*10**) show a strong excimer fluorescence signal (495 nm) but only a small signal due to the pyrene monomer fluorescence (400 nm). No other signal or shoulders are apparent. The fluorescence in the duplex **7*8** is slightly stronger than in the duplex **9*10**. The single strands **9** and **10** show a decreased fluorescence at about 435 nm, which may again be due to a pyrene(**S**)/phenanthrene(**P**) exciplex. Furthermore, there is some residual pyrene monomer fluorescence at 400 nm. Again, these results can be interpreted as illustrated in *Figure 8.5.*, showing a schematic representation of the middle part of the oligonucleotides **9** and **10**. The two single strands (middle of the *Figure 8.5.*) have principally two different possibilities to form a hybrid with interstrand stacked aromatic residues. In one case, the two pyrenes are close to each other (left side) to give an excimer. In the second possibility, formation of the excimer is excluded, since the pyrenes are separated by the phenanthrenes. Since with both duplexes (**7*8**, **9*10**) high excimer fluorescence was observed, the arrangement must be as shown in the situation on the left. Again, it must be noted that these data were obtained with a given set of linkers. Changing the linkers might lead to different results.

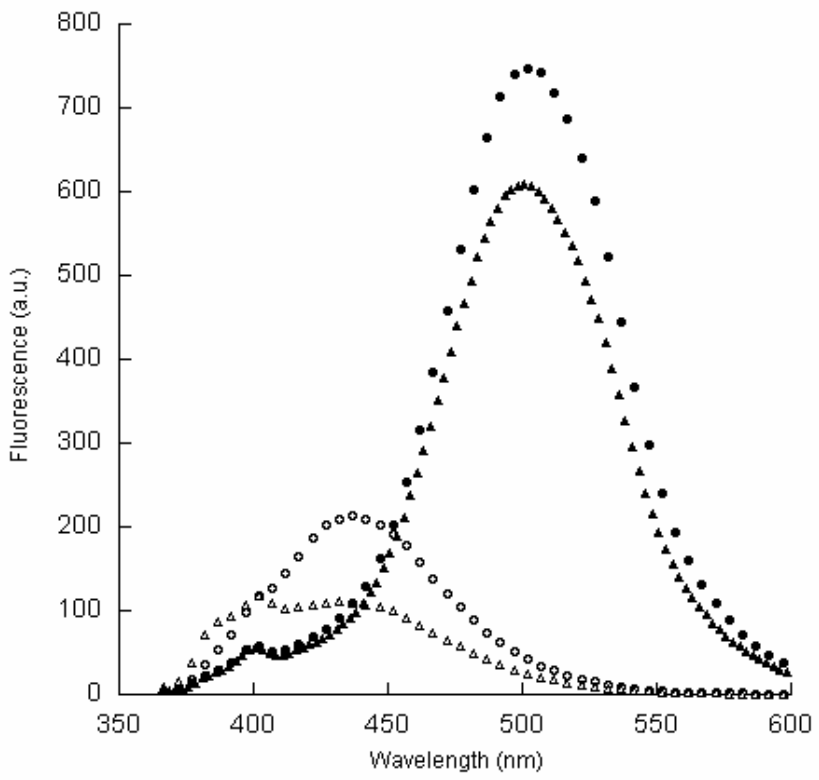

Figure 8.4. Fluorescence spectra of pyrene-and phenanthrene containing single strands and duplexes: duplexes **7*8** (filled circle), **9*10** (filled triangle) and single strands **9** (open circle) and **10** (open triangle). Conditions: oligomer concentration 1.0 µM, 10 mM Tris-HCl, 100 mM NaCl, pH 7.4, room temperature. Excitation wavelength: 354nm; excitation slit: 5nm; emission slit: 7nm.

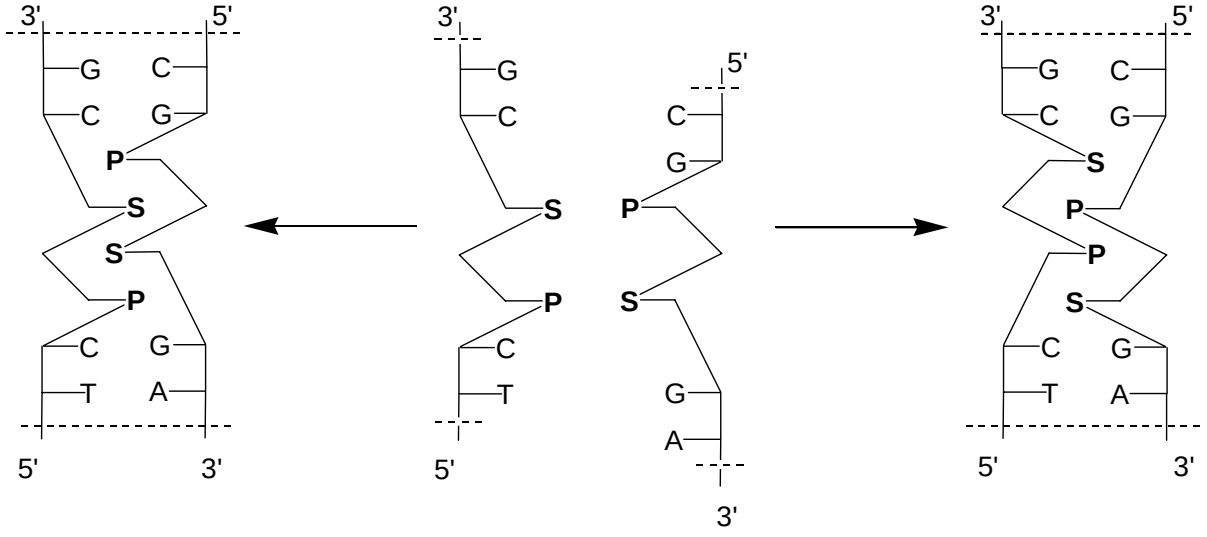

Figure 8.5. Schematic representation of the two possible geometric different hybridization. In the middle the unhybridized single strands. On the left side, the duplex where the pyrene building blocks (**S**) are juxtaposed, flanked by the phenanthrene building blocks (**P**). On the right, the pyrene building blocks (**S**) are separated by the phenanthrene building blocks (**P**).

8.3. Conclusions

The data presented in this chapter show that the formation of excimers can be controlled through interstrand stacking interactions with other aromatic residues, which do not form excimers or exciplexes. Furthermore, the analysis of different combinations of pyrenes and phenanthrenes revealed that interstrand stacking interactions between pyrenes are preferred over those of phenanthrenes.

8.4. Experimental Section

Oligonucleotide Synthesis

Phenanthrene- and pyrene-derived phosphoramidite building blocks were incorporated into oligonucleotides *via* standard automated oligonucleotide synthesis using I_2/pyridine/water in the oxidation step. Coupling yields were equal to the ones obtained with standard phosphoramidite building blocks. Oligonucleotides were purified by reverse phase HPLC and characterised by MS (*Table 8.2.*).

	oligonucleotide	calculated for $(M-H)^-$	found
3	(5') AGC TCG GTC **SS**C GAG AGT GCA	6841.9	6841.7
4	(3') TCG AGC CAG **PP**G CTC TCA CGT	6648.6	6648.8
5	(5') AGC TCG GTC **PP**C GAG AGT GCA	6737.7	6737.5
6	(3') TCG AGC CAG **SS**G CTC TCA CGT	6752.9	6752.4
7	(5') AGC TCG GTC **SP**C GAG AGT GCA	6789.9	6789.6
8	(3') TCG AGC CAG **PS**G CTC TCA CGT	6700.9	6700.8
9	(5') AGC TCG GTC **PS**C GAG AGT GCA	6789.9	6789.8
10	(3') TCG AGC CAG **SP**G CTC TCA CGT	6700.9	6700.6

Table 8.2. Molecular weights of oligonucleotides used in this study (*electrospray ionisation time-of-flight, ESI-TOF*)

References

[1] G. Tong, J. M. Lawlor, G. W. Tregear, J. Haralambidis, *J.Am.Chem.Soc.* **1995,** *117*, 12151-12158.

[2] K. Yamana, M. Takei, H. Nakano, *Tetrahedron Lett.* **1997,** *38*, 6051-6054.

[3] M. Masuko, H. Ohtani, K. Ebata, A. Shimadzu, *Nucl.Acids.Res.* **1998,** *26*, 5409-5416.

[4] P. L. Paris, J. M. Langenhan, E. T. Kool, *Nucl.Acids.Res.* **1998,** *26*, 3789-3793.

[5] M. N. Dioubankova, A. D. Malakhov, D. A. Stetsenko, M. J. Gait, P. E. Volynsky, R. G. Efremov, V. A. Korshun, *ChemBioChem* **2003,** *4*, 841-847.

[6] P. J. Hrdlicka, B. R. Babu, M. D. Sorensen, J. Wengel, *Chem. Commun.* **2004,** 1478-1479.

[7] U. B. Christensen, E. B. Pedersen, *Nucleic Acids Res.* **2002,** *30*, 4918-4925.

[8] U. B. Christensen, E. B. Pedersen, *Helv.Chim.Acta* **2003,** *86*, 2090-2097.

[9] R. L. Letsinger, T. Wu, *J.Am.Chem.Soc.* **1994,** *116*, 811-812.

[10] F. D. Lewis, T. F. Wu, E. L. Burch, D. M. Bassani, J. S. Yang, S. Schneider, W. Jäger, R. L. Letsinger, *J.Am.Chem.Soc.* **1995,** *117*, 8785-8792.

[11] S. A. E. Marras, F. R. Kramer, S. Tyagi, *Nucleic Acids Res.* **2002** ,30, e122

9. Towards A New Type of Molecular Beacon

9.1. Introduction

Molecular beacons are single-stranded oligonucleotide hybridization probes that form a stem-and-loop structure. The loop contains a probe sequence that is complementary to a target sequence, and the stem is formed by the annealing of complementary arm sequences that are located on either side of the probe sequence. A fluorophore is covalently linked to the end of one arm and a quencher is covalently linked to the end of the other arm. Molecular beacons do not fluoresce when they are free in solution. However, when they hybridize to a nucleic acid strand containing a target sequence they undergo a conformational change that enables them to fluoresce brightly (*Figure 9.1.*).

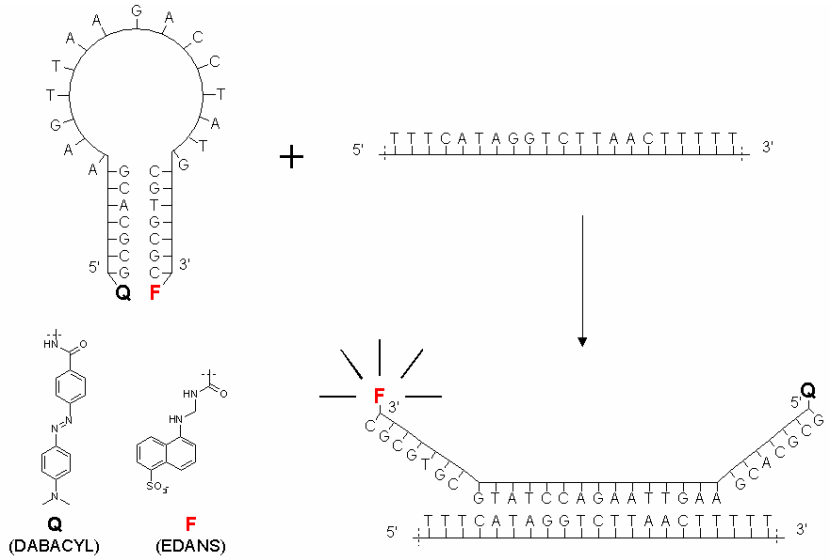

Figure 9.1. Principle of a molecular beacon.

In the absence of targets, the probe is dark, because the stem places the fluorophore so close to the non-fluorescent quencher that the energy from the fluorophore is transferred by the *Förster* mechanism to the non-fluorescent quencher, eliminating the ability of the fluorophore to fluoresce. When the probe encounters a target molecule, it forms a probe-target hybrid that is longer and more stable than the stem hybrid. The rigidity and length of the probe-target hybrid precludes the simultaneous existence of the stem hybrid. Consequently, the molecular beacon undergoes a spontaneous conformational reorganization that forces the stem hybrid to

dissociate and the fluorophore and the quencher to move away from each other, restoring fluorescence [1-5].

There is only one contribution in the literature, which uses the absence/presence of excimer in connection with a molecular beacon. *Fujimoto et al.* have presented the approach shown in *Figure 9.2.* [6]. In this beacon, the excimer disappears upon hybridization to the target and the positive signal depends on detection of the monomer fluorescence.

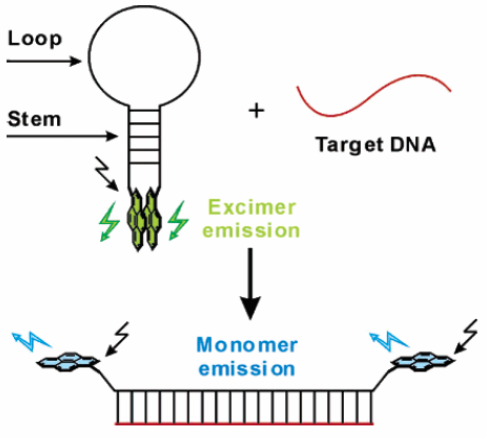

Figure 9.2. Molecular beacon based on excimer and monomer fluorescence emission.

Since our non-nucleosidic pyrene building blocks provide the possibility of efficient excimer formation in the single strand (*Chapter 8.*), it should be possible to detect the excimer when it is hybridised to its target.

9.2. Results and Discussion

Two molecular beacons (**1**, **2**) with different stem length and a target oligonucleotide (**3**) were prepared (*Table 9.1.*). The presumed secondary structure is schematically shown in *Figure 9.3.* In the absence of the target, the molecular beacon adopts a stem-loop structure, in which the alternately interstrand stacked pyrene and phenanthrene residues prevent the formation of pyrene excimer. After addition of the target, the molecular beacon should hybridize and form a duplex with it. Now, the pyrene residues will be juxtaposed in the single strand and can form the excimer.

Oligo	Sequence
1	(5') gcg c**SS** AAG TTA AGA CCT ATG **PP**g cgc
2	(5') cg c**SS** AAG TTA AGA CCT ATG **PP**g cg
3	(5') ttt CAT AGG TCT TAA CTT ttt

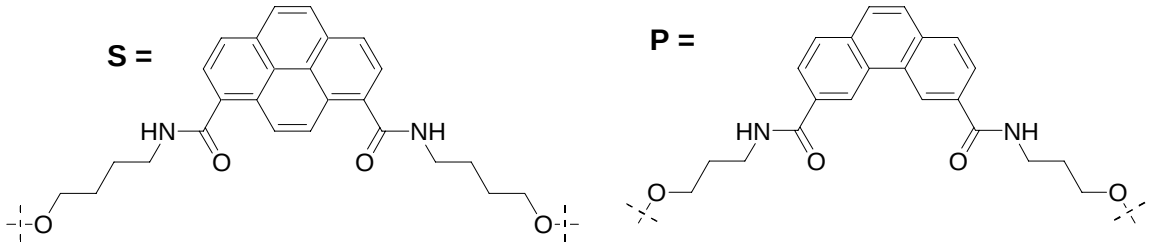

Table 9.1. Molecular beacons **1**,**2**. Target oligonucleotide **3**.

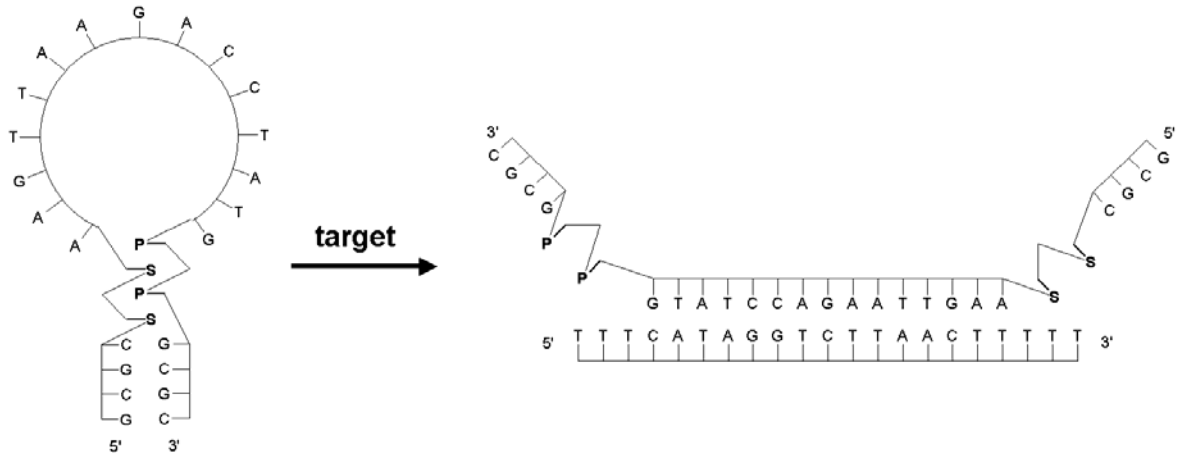

Figure 9.3. Schematic representation of molecular beacon **1**. **P** phenanthren residues. **S** pyrene residues.

Figure 9.4. shows the fluorescence emission spectra of the molecular beacon **1** in absence and presence of the target **3**. The fluorescence of **1** in absence of the target shows a broad band with a maximum at around 495 nm, typical for the pyrene excimer, with a shoulder in the range of 450 nm, which might again be due to a pyrene/phenanthrene exciplex. Thus, the pyrene excimer is not completely prevented in the absence of the target. The reason for that could be that the phenanthrene and pyrene residues are placed between a paired DNA duplex and an unpaired loop and so the building blocks have more flexibility. After adding the target **3** to **1** at room temperature, the pyrene excimer fluorescence at 495 nm increases immediately by about a factor of 2.8 and the shoulder at about 450 nm disappears. This increase was somewhat surprising since it is almost as large as the in the previous examples (increase by a

factor of 2.7 and 3.3, see chapter 9), in which the 'prevented' excimer was located in the middle of a stem, whereas here it is at the junction of a stem and a loop. We had anticipated that this factor would be smaller because the pyrene/phenanthrene stack in the molecular beacon is less well ordered.

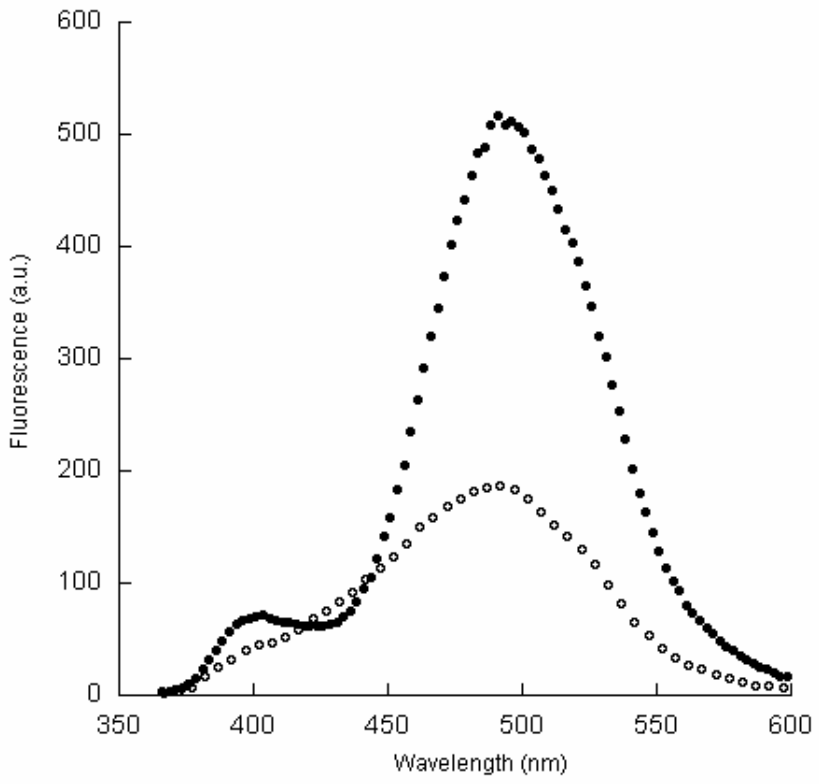

Figure 9.4. Fluorescence spectra of the molecular beacon **1**: **1** and 5eq. of target **3** (filled circle); **1** without target (open circle). Conditions: molecular beacon concentration 1.0 µM, 100 mM Tris-HCl, 2 mM $MgCl_2$, pH 7.4, room temperature. Excitation wavelength: 354 nm; excitation slit: 5 nm; emission slit: 4 nm.

The molecular beacon **3**, in which the stem is composed of just three natural base pairs, behaves very similarly. Here, a factor of 2.4 between the fluorescence intensities of the molecular beacon **2** without the target and with the target **3** was observed (*Figure 9.5.*). Also in this beacon, the excimer is not completely prevented in the absence of the target. For a useful molecular beacon, this aspect needs to be improved. Further improvements, such as changing the length and type of the linker of both, the pyrene and phenanthrene moieties are currently ongoing.

A further interesting aspect is the fact that the molecular beacon has unnatural building blocks in the stem, which are orthogonal to the natural base pairs [7]. This might lead to a more

specific probe, since it should lead to a minimization of cross-hybridization between the stem region and the target [8].

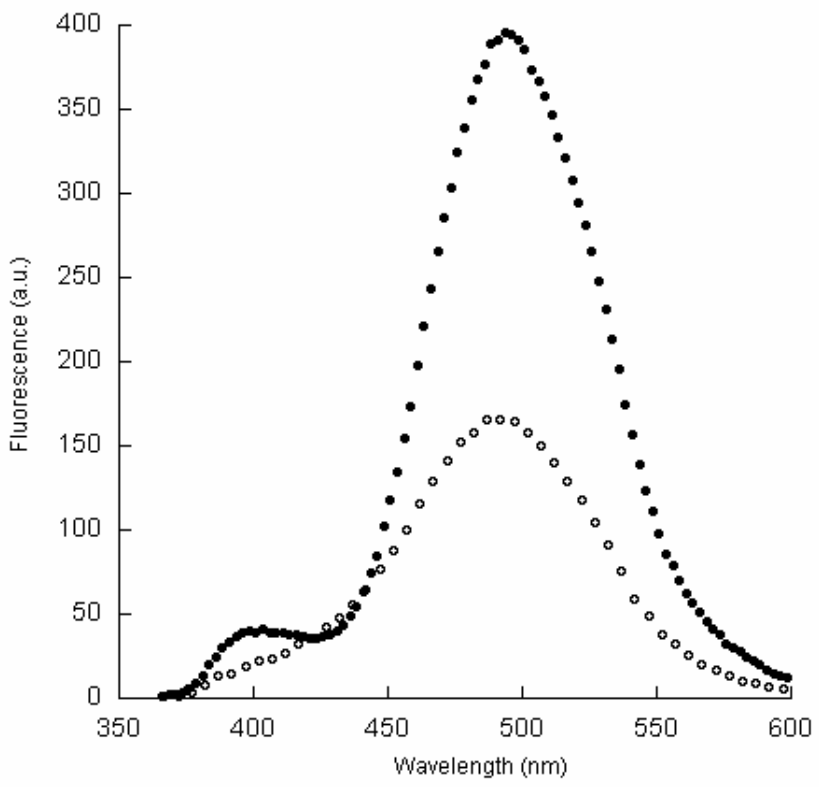

Figure 9.5. Fluorescence spectra of the molecular beacon **2**: **2** and 5eq. of target **3** (filled circle); **2** without target (open circle). Conditions: molecular beacon concentration 1.0 µM, 100 mM Tris-HCl, 2 mM $MgCl_2$, pH 7.4, room temperature. Excitation wavelength: 354 nm; excitation slit: 5 nm; emission slit: 3 nm.

9.3. Conclusions

In this part, we could show that the principle of interstrand stacked alternately pyrene and phenanthrene residues as excimer control may be used for the development of a new type of molecular beacon. In this approach, excimer formation in the beacon is prevented by interstrand stacked phenanthrenes and enabled through hybridization with the target. So far, however, some pyrene excimer fluorescence still occurs in the stem-loop form. Optimisation of this aspect may be achieved by altering the linkers of the non-nucleosidic building blocks. Replacement of the natural bases in the stem region with the polyaromatic building blocks might turn out to be an additional advantage, since this should prevent unwanted hybridization between non-target sequences and stem nucleotides.

9.4. Experimental Section

Oligonucleotide Synthesis

Phenanthrene- and pyrene-derived phosphoramidite building blocks were incorporated into oligonucleotides *via* standard automated oligonucleotide synthesis using I_2/pyridine/water in the oxidation step. Coupling yields were equal to the ones obtained with standard phosphoramidite building blocks. Oligonucleotides were purified by reverse phase HPLC and characterized by MS (*Table 9.2*).

	oligonucleotide	calc. $(M-H)^-$	found
1	(5') gcg c**SS** AAG TTA AGA CCT ATG **PP**g cgc	8946.4	8945.8
2	(5') cg c**SS** AAG TTA AGA CCT ATG **PP**g cg	8328.0	8327.3
3	(5') ttt CAT AGG TCT TAA CTT ttt	6366.2	6366.0

Table 9.2. Molecular weights of oligonucleotides used in this study (*electrospray ionisation time-of-flight, ESI-TOF*)

References

[1] S. Tyagi, F. R. Kramer, *Nature Biotechnology* **1996,** 14, 303-308.

[2] www.molecular-beacons.org

[3] S. A. E. Marras, F. R. Kramer, S. Tyagi, *Genet. Anal.* **1999**,14, 151-156.

[4] S. A. E. Marras, F. R. Kramer, S. Tyagi, *Nucleic Acids Res.* **2002**,30, e122.

[5] N. E. Broude, *Trends Biotechnol.* **2002**, 20, 249-256.

[6] K. Fujimoto, H. Shimizu, M. Inouye, *J.Org.Chem.* **2004,** 69, 3271-3275.

[7] S. M. Langenegger, R. Häner, *Helv.Chim.Acta* **2002,** 85, 3414-3421.

[8] W. T. Monroe, F. R. Haselton, *Biotechniques* **2003**, 34, 68-73.

10. Phenanthrene-derived DNA Hairpin Mimics

Alfred Stutz, Simon M. Langenegger, Robert Häner, *Helv. Chim. Acta* **2003**, 86,3156-3163.

10.1. Abstract

Self-complementary oligodeoxynucleotides containing 3,6-disubstituted phenanthrenes adopt highly stable, hairpin-like structures. The thermodynamic stability of the hairpin mimics depends on the overall length of the phenanthrene building block. Hairpin loops composed of a 3,6-phenanthrene dicarboxamide and ethylene linkers were found to be optimal. The hairpin mimics are more stable than the analogous hairpins containing either a dT_4 or dA_4 tetraloop. Model studies suggest that the thermodynamic stability of the hairpin mimics is primarily due to aromatic stacking of the phenanthrene-3,6-dicarboxamide onto the adjoining base pair of the DNA duplex.

10.2. Introduction

Hairpins belong to the most common and most important secondary structural motives found in nucleic acids [1]. In functional RNA they are essential elements for the formation of the correct three-dimensional structure [2-5]. In particular, hairpins containing a four base loop (tetraloop) are emerging as a class of highly stable and structurally well-defined components of ribonucleic acids. [1,6] Hairpin formation is, although to a lesser extent, also observed in DNA. The requirements for the formation of DNA hairpins [7] and cruciform structures [8] in palindromic DNA sequences have been investigated in detail and the involvement of such structures in the regulation of gene expression has been discussed [9,10].

Due to the importance of the hairpin motif the replacement of the nucleotide loop by synthetic, non-nucleosidic linkers has been a topic of thorough investigation. Thus, the hairpin loop has been replaced with flexible, oligo ethylene glycol linkers in DNA [11] and RNA [12,13] as well as with more rigid aromatic derivatives [14-17]. In particular, *trans*-stilbene derived linkers led to a strong stabilization of the hairpin. [15] Structural analysis revealed a favourable stacking interaction between the stilbene and the adjacent base pair of the stem [18].

We have previously shown that phenanthrene-3,6-carboxamide modified oligonucleotides form stable duplexes. Phenanthrene residues positioned in opposite sites can significantly

enhance duplex stability, most likely *via* interstrand aromatic stacking [19]. In the course of this work, we found that self-complementary oligonucleotides connected through a phenanthrene-3,6-carboxamide derived linker form stable, hairpin-like structures. We report here the synthesis of phenanthrene-3,6-dicarboxamide derivatives and their use as hairpin loop mimics.

10.3. Results and Discussion

Preparation of Phenanthrene-derived Building Blocks and Incorporation into Oligonucleotides

Synthesis of the different phenanthrene 3,6-dicarboxamide phosphoramidite building blocks was carried out in analogy to a previously reported procedure (*Chapter 2.*) [19]. Thus, dimethyl phenanthrene-3,6-dicarboxylate (**1**) was converted into the corresponding bis-hydroxyethyl and bis-hydroxypropyl phenanthrene-3,6-carboxamides by reaction with the corresponding amino alcohols (see *Scheme 10.1.*). Subsequent treatment of the crude intermediates with DMT-Cl in pyridine resulted in a mixture of mono- and bis-protected derivatives. The desired mono-4,4'-dimethoxytritylated compounds **2** and **3** were isolated by column chromatography and converted to the corresponding phosphoramidite building blocks **4** and **5**. Attempts to prepare the corresponding butyl-linked phosphoramidite in an analogous way failed. Reaction of dimethyl-phenanthrene-3,6-dicarboxylate with 4-aminobutanol even under forced conditions (180°C, 24 h) did not afford the desired 4-hydroxybutylphenanthrene-3,6-dicarboxamide. Therefore, diester **1** was hydrolysed with aqueous NaOH. The crude sodium phenanthrene-3,6-dicarboxylate was activated with BOP and further reacted with a 1:1-mixture of 4-(4,4'-dimethoxytrityloxy)butylamine (**6**) and 4-amino-1-butanol in DMF. This procedure yielded, albeit in a modest yield (22%), the desired 4,4'-monomethoxytritylated product **7**, which was converted into the phosphoramidite **8**. The three different phenanthrene-derived building blocks **4**, **5** and **8** were incorporated into self-complementary oligonucleotides using the standard phosphoramidite procedure [20,21]. To ensure a high incorporation yield of the modified building blocks, the coupling time was prolonged to 1.5 min in the respective cycles (see *Experimental Section*). Deprotection (*conc.* ammonia, 55°C), followed by standard HPLC purification yielded oligodeoxynucleotides **9**-**11** and **14** (*Table 10.1.*), along with the corresponding control oligodeoxynucleotides **12**, **13**, **15** and **16**, containing dT_4 and dA_4 sequences instead of the phenanthrenes.

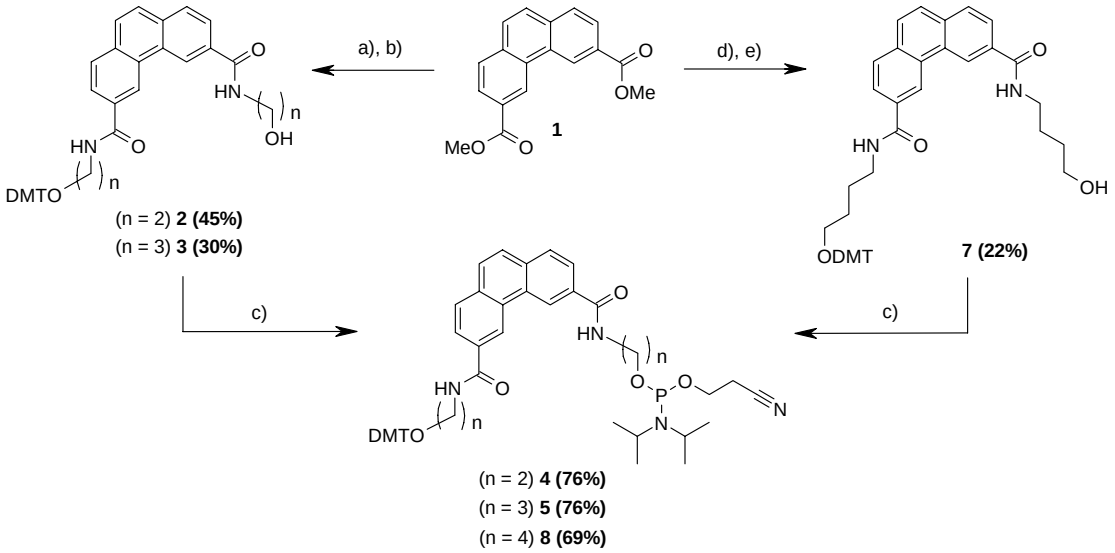

Scheme 10.1. a) 2-Aminoethanol (n = 2) or 3-amino-1-propanol (n = 3), 175°C, 30min. b) DMT-Cl, Py, r.t. c) $(^{i}Pr_2N)_2P(OCH_2CH_2CN)$, *N*,*N*-Diisopropylammonium 1*H*-tetrazolide, CH_2Cl_2, rt 3 h d) NaOH (2 eq.), THF/EtOH/H_2O 1:1:1, reflux, 2 h. e) 4-(4,4'-dimethoxytrityloxy) butane-1-amine (6) / 4-amino-1-butanol (1:1), $^{i}Pr_2NEt$, BOP, DMF, rt, 1 h.

Investigation of Phenanthrene-derived Hairpins

In their pioneering work, *Letsinger, Lewis and coworkers* have demonstrated that *cis*-and *trans*-stilbene linkers can give rise to stable hairpin analogue [15]. In a series of papers, they show that *trans*-stilbene derivatives form more stable hairpin structures than the corresponding *cis*-isomers. The higher stability of the *trans*-isomers was attributed to the difference of the spacer lengths between the *cis*- and the *trans*-derivative [15] [22]. This finding can, however, also be explained by the fact that *cis*-stilbene derivatives are considerably deviating from planarity and, thus, do not allow perfect stacking onto the duplex stem [23,24]. Phenanthrene represents a planar analogue of *cis*-stilbene, and should, therefore, result in more favourable stacking effects.

To investigate the suitability of phenanthrene-3,6-dicarboxamide linkers as hairpin mimics, the self complementary oligonucleotides bearing ethyl-, propyl- and butyl- spacers (**9**, **10**, and **11**, respectively, see *Table 10.1.*) were prepared, along with the corresponding control oligonucleotides containing either a dT_4- or dA_4-loop (**12** or **13**). Thermal denaturation experiments were carried out at 100mM NaCl, pH 7.5 (10mM Tris-HCl) using a 2.5μM oligonucleotide concentration. As can be seen from the Tm data in *Table 10.1.*, all phenanthrene-linked oligonucleotides form a more stable structure than the control oligonucleotides. Thermal denaturation curves revealed a single, sharp transition for all

oligonucleotides under the given experimental conditions (see *Figure 10.1.*). Several observations support the conclusion that the observed transitions correspond to the melting of the respective hairpins. First, the experimental Tm values correspond well with the calculated transition temperatures [25] for the hairpins **12** (Tm calc: 70.1°C, found: 73.4°C) and **13** (Tm calc: 66.6°C, found: 72.5°C).

Hairpin		Tm [°C]
9	5′-GCA ATT GC -**P2**- GC AAT TGC-3′	79.2
10	5′-GCA ATT GC -**P3**- GC AAT TGC-3′	77.5
11	5′-GCA ATT GC -**P4**- GC AAT TGC-3′	76.7
12	5′-GCA ATT GC **TTTT** GC AAT TGC-3′	73.4
13	5′-GCA ATT GC **AAAA** GC AAT TGC-3′	72.5
14	5′-ATT GC -**P2**- GC AAT-3′	65.7
15	5′-ATT GC **TTTT** GC AAT-3′	60.0
16	5′-ATT GC **AAAA** GC AAT-3′	57.6

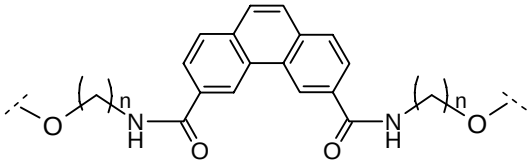

P2: n = 2
P3: n = 3
P4: n = 4

Table 10.1. Tm-values of hairpin sequences containing a phenanthrene linker in comparison with their counterparts containing either a T_4- or A_4-hairpin loop. Conditions: oligonucleotides 2.5μM, 100mM NaCl, 10mM Tris-HCl pH 7.5.

Second, the Tm values were independent from the concentration of the oligonucleotides over a range from 1 to 5 μM (see *Table 10.2.*), indicating a mono-molecular process. The hairpin mimic **9** containing the ethyl linked phenanthrene derivative P2 showed the highest Tm (79.2°C). The analogues **10** and **11** containing longer spacers had slightly lower Tm's (77.5 and 76.7°C for P3 and P4, respectively). A similar dependence of the stability of hairpin mimics on the linker length has been reported for stilbene-derived linkers [18]. The optimal phenanthrene building block (P2) was further incorporated into a shorter, self-complementary

oligonucleotide (*Table 10.1.*, oligonucleotide **14**) and compared to its dT_4 and dA_4 analogues (oligodeoxynucleotides **15** and **16**).

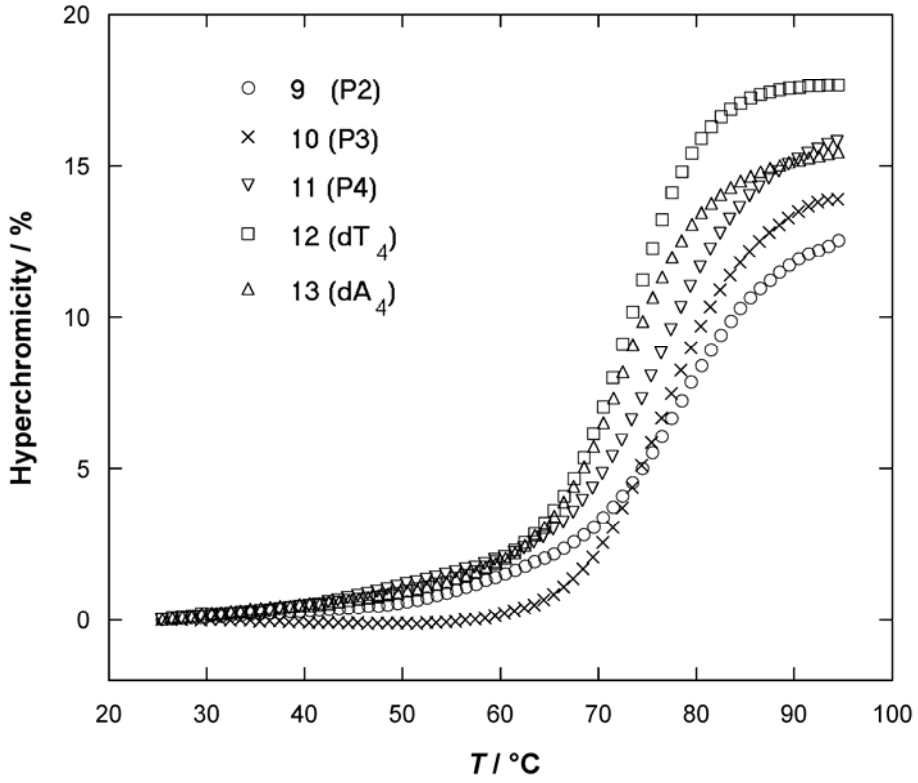

Figure 10.1. Melting curves of the hairpin mimics **9-11** in comparison to the control hairpins **12** and **13**. Conditions: oligonucleotides 2.5μM, 100mM NaCl, 10mM Tris-HCl, pH 7.5.

Hairpin	Tm [°C]		
	1 μM	2.5 μM	5 μM
9 (P2)	78.8	79.3	79.4
10 (P3)	77.6	77.2	77.0
11 (P4)	76.1	77.2	76.7
12 (dT_4)	73.0	73.2	73.8
13 (dA_4)	72.4	72.6	72.6

Table 10.2. Tm-values of 9-13 measured at different oligomer concentrations. Conditions: 100mM NaCl, 10mM Tris-HCl pH 7.5.

Again, the phenanthrene derived hairpin mimic showed a significantly higher thermodynamic stability (ΔTm = 5.7 and 8.1°C, respectively). Circular dichroism (CD) spectral analysis of the hairpin mimic **14** is in full agreement with an overall B-conformation (data not shown).

Structural Model of the Phenanthrene Hairpin Mimic

A model of the P2-containing hairpin **9** is shown in *Figure 10.2.*. The conformation represents a local minimum structure obtained with *Hyperchem* starting from B-form DNA using the amber force-field. According to this model, the concave side of the phenanthrene moiety is directed towards the minor groove of the B-form helix. The distance between the phenanthrene and the adjacent GC base pair is approximately 3.3-3.4Å, i.e. well within the distance normally observed for base stacking in B-DNA. The increase of the transition temperature of the phenanthrene modified hairpin analogues compared to their natural dA_4- or dT_4-containing counterparts can, therefore, be attributed to the optimal stacking interaction with the first base pair of the stem. The distance between the two phenanthrene-linked phosphates in the modelled structure of hairpin **9** is approximately 16.0Å. This distance is shorter than the 17.8Å found in a trans-stilbene derived hairpin structure [18], but lies well within the range of diametrical P-P distances (15.0 to 16.9Å) observed in other, reported DNA hairpin structures [26,27]. This relatively large range of P-P distances can also serve as an explanation for the observation that the steady increase in the linker length from oligomers **9**-**11** (*Table 10.1.*) does not affect the stability in a dramatic way. All these factors point towards the stacking effects as the major contribution to the stability of the hairpin-like structures.

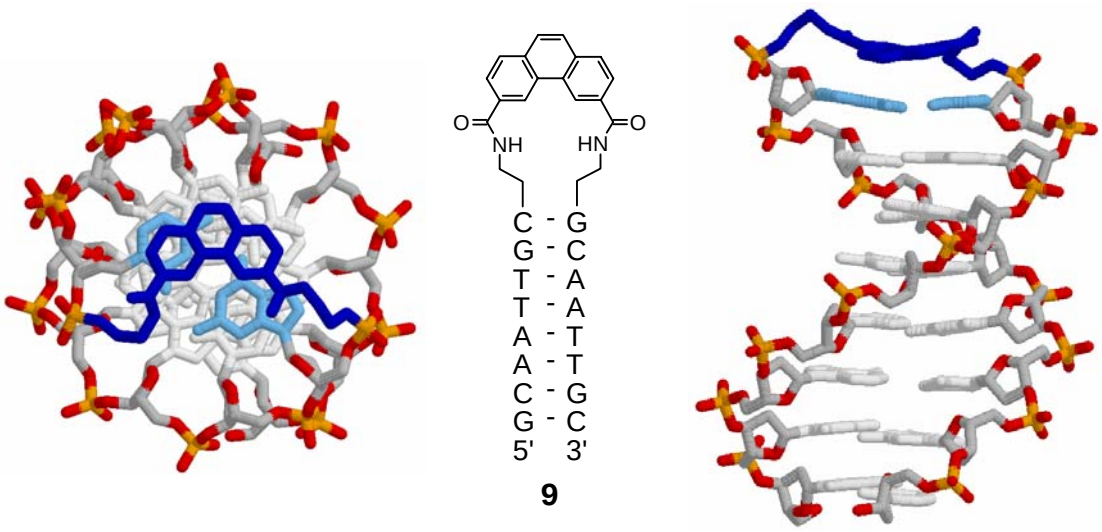

Figure 10.2. *Amber*-minimized structure of the hairpin 9 containing P2 (dark blue). Left: view along the helical axis; right: view perpendicular to the helical axis. The GC base pair adjacent to the phenanthrene is shown in light blue.

10.4. Conclusions

Self-complementary oligodeoxynucleotides containing 3,6-disubstituted phenanthrenes adopt highly stable, hairpin-like structures. The thermodynamic stability of these hairpin mimics is higher than the one of comparable hairpins with a dT_4 or dA_4 tetraloop. Spectroscopic analysis of the phenanthrene-modified hairpins shows no structural deviation from canonical B-form DNA. Model studies as well as the relative insensitivity of the structural stability towards the linker length suggest that the thermodynamic stability of the hairpin mimics is primarily due to aromatic stacking of the phenanthrene-3,6-dicarboxamide onto the adjoining base pair of the DNA duplex.

10.5. Experimental Section

General

Chemicals, solvents, and reagents for reactions were from *Acros*, *Aldrich*, or *Fluka*, and were of the highest quality available. Compound **1**, **3** and **5** were prepared as described [19]. (Cyanoethoxy)bis(*N*,*N*-dimethylamino)phosphine was prepared according to [28]. Solvents for extraction and chromatography were of technical grade and distilled prior to use. Thin layer chromatography (TLC): silica-gel 60 F_{254} glass plates (*Merck*); visualisation by UV and/or A) by dipping in a soln. of anisaldehyde (10 ml), conc. H_2SO_4 (10 ml), and AcOH (2 ml) in EtOH (180 ml) or B) cerium (IV) sulfate (3mM)/ammonium molybdate (250mM in aq. H_2SO_4 (10%) followed by heating. Flash column chromatography (CC): silica gel 60 (40-63 μm, 230-400 mesh, *Fluka*) at low pressure. The chromatography of acid sensitive compounds was carried out with eluent containing 2% NEt_3. ^{1}H- and ^{13}C-NMR: *Bruker AC-300* or *Bruker AMX 400*, δ values in ppm (solvents signals as internal standards), *J* [Hz]; ^{31}P-NMR: *Bruker AMX 400*, δ values in ppm (85% H_3PO_4 as external standard). ESI-MS: *VG Platform* single quadrupole ESI mass spectrometer. HR-MALDI-MS: *IonSpec Ultima* FTMS mass spectrometer, 3,5-dihydroxybenzoic acid as matrix, pos. mode; Abbreviation: DMT: 4,4'-dimethoxytrityl; BOP: Benzotriazol-1-yloxy)-tris-(dimthylamino)-phosphonium-hexafluorophosphate; MeCN: acetonitrile; AcOEt: ethyl acetate; rt: room temperature; HR-MALDI-MS: high resolution MALDI-MS; HR-ESI-MS: high resolution ESI-MS.

Synthesis of Phenanthrene-derived Phosphoramidite Building Blocks

N-{2-[(4,4'-Dimethoxytrityl)oxy]ethyl}-N'-(2-hydroxyethyl)phenanthrene-3,6-carboxamid (2). Dimethyl phenanthrene-3,6-dicarboxylate **1** (1.38 g, 4.69 mmol) was dissolved in 2-aminoethanol (6.9 ml, 0.11 mol) and heated to 175°C for 30 min. Then the excess of 2-aminoethanol was removed under reduced pressure to give the crude *N*,*N*'-bis(2-hydroxyethyl) phenanthrene-3,6-dicarboxylate as a yellow solid (TLC(AcOEt/MeOH 9:1): R_f 0.24). At rt this intermediate was dissolved in dry pyridine (12 ml). Then, a solution of DMT-Cl (1.52 g, 4.5 mmol) in pyridine (6 ml) was added over 1 h. The reaction was stirred for another 2 h and then the solvent was removed under reduced pressure. The residue was taken up in CH_2Cl_2 and washed first with 10% citric acid and second with $NaHCO_3$ sat., dried ($MgSO_4$) and evaporated to give a highly viscous oil. The purification by CC (silica gel; AcOEt/hexane 8:2 $\rightarrow$ AcOEt (+1% NEt_3)) furnished **2** (1.391 g, 2.12 mmol, 45%) as colourless foam.

TLC (AcOEt/hexane): R_f 0.29. ^{1}H-NMR (400 MHz, $CDCl_3$): 2.43 (br. s, 1 H, OH); 3.42 (t, 2 H, *J* = 5.3, $ROCH_2$); 3.68 (m, 2 H, C*H*$_2$OH); 3.73 (s, 6 H, 2 MeO) 3.74 (t, 2 H, *J* = 4.8, (partially hidden), NCH_2); 3.91 (t, 2 H, *J* = 4.9, N'CH_2); 6.80 (d, *J* = 8.8, 4 arom. H); 7.12 – 7.82 (m, 17 arom. H); 8.80, 8.85 (2s, 2 H, CONH). ^{13}C-NMR (100 MHz, $CDCl_3$): 41.0, 43.7 (2t, NCH_2, N'CH_2); 55.6 (q, MeO); 62.5 (t, CH_2OH); 67.3 (t, CH_2OCAr_2Phe); 86.7 (s, CAr_2Phe); 113.6, 122.0, 122.7, 124.8, 125.8, 127.3, 128.1, 128.2, 128.3, 128.5, 128.9, 129.0 (12 d, arom. C); 129.7, 130.0 (2s, arom. C); 130.4 (d, arom. C); 132.65, 132.71, 134.01, 134.02 136.4, 145.2, 158.9 (7s, arom. C); 168.4, 169.2 (2s, CONH). HR-MALDI-MS: m/z found: 677.2630 (calc. 677.2622) $[M+Na]^+$. UV (MeCN): 315 (15900), 309 (13800), 303 (16400), 288 (10100), 278 (sh, 13600), 258 (54500), 254 (52900), 251 (53800), 242 (49800), 237 (50000), 220 (36200).

N-{2-[(4,4'-Dimethoxytrityl)oxy]ethyl}-N'-{2-[(N,N-diisopropylamino)(2-cyanoethyl)-phosphinoxy]ethyl}phenanthrene-3,6-carboxamide (4). At rt a solution of **2** (1.29 g, 1.97 mmol) in CH_2Cl_2 (4 ml) was added slowly (over 30 min) to a suspension of *N*,*N*-diisopropylammonium *1H*-tetrazolide (472 mg, 2.76 mmol) and (2-cyanoethyl)bis(diisopropylamino)phosphine (713 mg, 2.36 mmol) in CH_2Cl_2 (6 ml). After 4 h at rt CH_2Cl_2 the reaction was diluted with CH_2Cl_2, washed with sat. $NaHCO_3$. The organic layer was dried over K_2CO_3 and evaporated under reduced pressure. Purifying of the resulting oil by CC (silica gel; AcOEt/hexane 2:3 $\rightarrow$ 3:2 (+ 2% NEt_3)) furnished **4** (1.284 g, 1.502

mmol, 76%) as colourless foam. TLC (AcOEt/hexane/NEt_3 5:4:1) R_f 0.36. ^{1}H-NMR (400 MHz, $CDCl_3$): 1.19 (d, 12 H,*J* = 6.5, NCH*Me*$_2$); 2.62 (t, 2 H, *J* = 6.0, CH_2CN); 3.4-4.0 (m, 12 H, O*CH*$_2$$CH_2CN$, N*CH*$Me_2$, NCH_2CH_2, N'CH_2CH_2); 3.75 (s, 6 H, 2 MeO); 6.91 (d, *J* = 8.3, 4 arom. H); 6.9-8.1 (m, 17 arom. H); 9.23 (s, 2 H, NH, N'H); ^{13}C-NMR (100 MHz, $CDCl_3$): 21.0 (t, *J*(CP) = 5, CH_2CN);

25.0, 25.1 (2q, *J*(CP) = 4, $CHMe_2$); 40.9 (t, NCH_2);

41.6 (t, *J*(CP) = 7.0, $POCH_2$*CH*$_2$N'); 43.5 (d, *J*(CP) = 12, *C*HMe_2); 55.6 (q, MeO); 58.9 (t, *J*(CP) = 20, $POCH_2$); 62.7 (t, J(CP) = 15, $POCH_2$); 62.9 (t, DMTO*C*H_2); 86.6 (s, Ar_2*C*Phe); 113.6 (d, arom. C); 118.8 (s, CN); 122.5, 122.7, 125.3, 125.7, 127.2, 127.3, 128.3, 128.5, 128.6, 129.4, 129.5, 130.4 (12 d, arom. C); 133.2, 133.3, 134.38, 134.43, 136.4, 145.3, 158.9 (7s, arom. C); 167.88, 168.00 (2s, CONH). ^{31}P-NMR (216 MHz, $CDCl_3$): 149.53. UV (MeCN): 316 (15800), 310 (13600), 303 (16500), 288 (10000), 279 (sh, 13600), 258 (54600), 255 (52800), 251 (53700), 242 (49500), 237 (49900), 220 (36800). HR-ESI-MS (pos. Mode): m/z found: 873.4220 (calc. 873.4230) $[M + NH_4]^+$.

4-[(4,4'-dimethoxytrityl)oxy]butane-1-amine (6). A mixture of 4-aminobutan-1-ol (1 g, 11.22 mmol) and phthalic anhydride (1.662 g, 11.22 mmol) was kept at 145°C for 2 h. After cooling to rt the resulting yellow oil was dissolved in pyridine (20 ml), then DMT-Cl (4.06 g, 12 mmol) was added. After 2 h at rt the reaction solution was diluted with AcOEt/hexane 1:1 (100 ml), washed twice with $NaHCO_3$ sat., dried over $MgSO_4$ and evaporated. The remaining solid was dissolved in MeOH (40 ml) together with NH_2NH_2*H_2O (2.5 g, 50 mmol). This solution was stirred at 40°C for 4 h. Then the precipitate was filtered off and the filtrate reduce to about 10 ml. This solution was diluted with CH_2CH_2 (150 ml), washed with 2 M Na_2CO_3, dried over $MgSO_4$ and evaporated to give the crude product as a yellow oil. After purification by CC (20 g silica gel; CH_2Cl_2 → CH_2Cl_2 + 3% MeOH,(+ 5% NEt_3)) **6** (2.89 g, 7.4 mmol, 66%) was obtained as highly viscous, colorless oil.

TLC (CH_2Cl_2/MeOH/NEt_3 8:1:1): R_f 0.6. ^{1}H-NMR (300 MHz, $CDCl_3$): 1.46 (br. s, 2 H, NH_2); 1.55, 1.64 (2 m, 4 H, NCH_2*CH*$_2$*CH*$_2$$CH_2O$); 2.68 (t, 2 H, *J* = 6.6, CH_2N); 3.07 (t, 2 H, *J* = 6.5 CH_2O); 3.80 (s, 6 H, 2 MeO); 6.83 (d, *J* = 8.8, 4 arom. H); 7.1-7.5 (m, 9 arom. H). ^{13}C-NMR (100 MHz, $CDCl_3$): 26.5, 27.7 (2t, CH_2*C*H_2*C*H_2CH_2); 40.4 (t, NCH_2); 54.3 (q, MeO); 62.1 (t, *C*H_2ODMT); 84.9 (s, Ar_2*C*Phe); 112.1, 125.8, 126.9, 127.3, 127.5, 129.1 (6d, arom. C); 135.7, 144.4, 157.5 (3s, arom. C). UV (MeOH): 272 (8300), 256 (6700); 235 (17100), 221 (13900). HR-ESI-MS (pos. Mode): m/z found: 783.4390 (calc. 783.4373) $[2 M + H]^+$.

N-{4-[(4,4'-Dimethoxytrityl)oxy]butyl}-N'-(4-hydroxybutyl))phenanthrene-3,6-carboxamid (7). At rt a suspension of **1** (0.5 g, 1.7 mmol) in EtOH/THF 1:1 (10 ml) was treated with 1 M aq. NaOH (3.4 ml) and heated to reflux for 2 h. The solvent was then removed under reduced pressure and the remaining solid dried under high vacuum. The crude intermediate was suspended in DMF (8.5 ml) / $^{i}Pr_2NEt$ (0.6 ml) and stirred for 30 min after the addition of BOP (827 mg, 1.87 mmol). Then a solution of **6** (800 mg, 2.04 mmol) and 4-aminobutanol (182 mg, 2.04 mmol)in CH_2Cl_2 (3 ml) was added and the suspension stirred for another hour. The reaction mixture was then diluted with AcOEt/hexane 1:1 (100 ml), washed with sat. aq. $NaHCO_3$, dried ($MgSO_4$) and evaporated. The purification by CC (AcOEt) afforded **7** (269 mg, 0.378 mmol, 22%) as colourless foam.

TLC (AcOEt/MeOH 95:5): R_f 0.54. ^{1}H-NMR (300 MHz, $CDCl_3$):

1.75 (m, 8 H, $CH_2CH_2CH_2CH_2$); 3.13 (t, 2 H, J = 5.5, $DMTOCH_2$); 3.52 (m, 5 H, NCH_2, $N'CH_2$, OH); 3.75 (s, 6 H, 2 MeO); 3.76 (m, CH_2OH); 6.80 (d, J = 8.8, 4 arom. H); 7.00-7.92 (m, 17 arom. H); 8.87, 8.88 (2s, 2 H, NH, N'H). ^{13}C-NMR(100 MHz, $CDCl_3$): 26.2, 26.7, 27.8, 30.1 (4t, $NCH_2CH_2CH_2$, $N'CH_2CH_2CH_2$); 40.3, 40.4 (2t, NCH_2, $N'CH_2$); 55.2 (q, 2 MeO); 62.5, 63.1 (2t, CH_2ODMT, CH_2OH); 85.9 (s, Ar_2CPhe); 113.0, 121.4, 121.8, 124.7, 125.3, 126.6, 126.7, 127.5, 127.8, 128.1, 128.2, 128.5 (12d, arom. C); 129.4, 129.5 (2s, arom. C); 130.0 (d, arom. C); 132.3, 132.5, 133.4, 133.5, 136.5, 145.2, 158.3 (7s, arom. C); 167.9, 168.0 (2s, 2 CONH). UV (MeCN): 315 (14900), 309 (12700), 302 (15400), 292 (9600), 258 (51200), 254 (49900), 250 (51100), 241 (47800), 237(48400) 220 (35900), 205 (58000). HR-MALDI-MS: m/z found: 733.3256 (calc. 733.3248) $[M+Na]^+$.

N-{4-[(4,4'-Dimethoxytriyl)oxy]butyl}-N'-{4-[(diisopropylamino)(2-cyanoethyl)-phosphinoxy]butyl} phenanthrene-3,6-carboxamide (8). A solution of **7** (370 mg, 0.52 mmol) in CH_2Cl_2 (2.5 ml) was added at rt over 30 min to a suspension of diisopropylammonium tetrazolide (125 mg, 0.73 mmol) and (2-cyanoethyl)bis(diisopropylamino)phosphine (188 mg, 0.63 mmol) in CH_2Cl_2 (3 ml). The reaction was stirred at rt for 4 h, then diluted with CH_2Cl_2 and washed with sat. aq. $NaHCO_3$ solution. The organic layer was dried over K_2CO_3 and the solvent removed under reduced pressure. After CC [silica gel; AcOEt/hexane 2:3 → 3:2 (+ 2% NEt_3)] the phosphoramidite **8** (1.284 g, 1.502 mmol, 76%) was obtained as colourless foam.

TLC (AcOEt/hexane/NEt_3 5:4:1): R_f 0.32.

^{1}H-NMR (400 MHz, $CDCl_3$): 1.08, 1.09 (2d, 12 H, J = 6.8, $CHMe_2$); 1.6-1.8 (m, 8 H, $CH_2CH_2CH_2CH_2$); 2.54 (t, 2 H, J = 6.3, CH_2CN); 3.06 (t, 2 H, J = 6.0, CH_2ODMT); 3.4-3.8

(m, 10 H, $P(OCH_2)_2$, NCH_2, $N'CH_2$, $NCHMe_2$); 3.67 (s, 6 H, 2 MeO); 6.6-8.0 (m, 21 arom. H); 5.05 (s, 2 H, NH, N'H).

^{13}C-NMR (100 MHz, $CDCl_3$): 20.9 (t, *J*(CP) = 8, CH_2CN); 25.0, 25.1 (2q, *J*(CP) = 4, $CHMe_2$); 26.7, 27.2, 28.2 (3t, $CH_2CH_2CH_2CH_2$); 29.1 (t, *J*(CP) = 7, $POCH_2CH_2$); 40.4, 40.7 (2t, NCH_2, $N'CH_2$); 43.4 (d, *J*(CP) = 12, PNCH); 55.6 (q, MeO); 58.6 (t, *J*(CP) = 20, $POCH_2CH_2CN$); 63.5 (t, CH_2ODMT); 63.6 (t, J(CP) = 17, $POCH_2CH_2CH_2$); 86.3 (s, Ar_2CPhe); 113.4 (d, arom. C); 118.5 (s, CN); 122.4, 122.5, 125.4, 125.6, 127.0, 128.2, 128.4, 128.5, 129.3, 130.4 (10d, arom. C); 133.3, 133.4, 134.2, 134.3, 136.9, 145.6, 158.7 (7s, arom. C); 167.96, 167.99 (2s, CONH). ^{31}P-NMR (216 MHz, $CDCl_3$): 148.68. HR-MALDI-MS: m/z found: 933.4338 (calc. 933.4327) $[M+Na]^+$. UV (MeCN): 315 (15700), 309 (13300), 303 (16200), 286 (10400), 278 (sh, 13600), 259 (55400), 255 (53500), 250 (54500), 241 (49500), 237(49800) 220 (37100).

Synthesis and Analysis of Oligonucleotides

Standard nucleoside phosphoramidites were from *Chemgenes* (Ashland, MA). Oligonucleotides were synthesized on a 392 *DNA/RNA Synthesizer* (*Applied Biosystems*) according to the standard phosphoramidite chemistry [20,21] on a 1.0 μmol scale ('trityl-off' mode). The coupling time was extended to 1.5 min for **4**, **5** and **8**. Coupling efficiencies were > 98% for all building blocks, including **4**, **5** and **8**. The oligomers were detached and deprotected under standard conditions (conc. aq. NH_3, 55°, 16 h). The crude oligomers were purified by anion-exchange HPLC: *MonoQ HR 5/5* (*Pharmacia*); flow 1 ml/min; eluent A: 20 mM sodium phosphate in H_2O (pH 11.5); eluent B: 20 mM sodium phosphate, 2 M NaCl in H_2O (pH 11.5); elution at r.t.; detection at 260, 280 and 320 nm and desalted over *Sep-Pak* cartridges (*Waters*, Milford, USA). All oligonucleotides were analysed by ESI-MS. The masses were found to be within 0.0005% of the expected mass. The extinction coefficients at 260 nm (ε_{260}) were calculated with "Biopolymer Calculator" (http://paris.chem.yale.edu/extinct.html). For the analogues P2, P3 and P4, respectively an ε_{260} of 49300 was estimated, according to the UV-spectra of bis-(2-hydroxyethyl)phenanthrene-3,6-carboxamide (data not shown, measured in H_2O, 0.1 M NaCl, 10 mM Tris-HCl pH 7.5.

Thermal Denaturation Experiments

UV Melting curves were determined at 260 nm on a *Varian Cary 3e* spectrophotometer equipped with a *Peltier block* and *Varian WinUV* software. Unless otherwise indicated, the

melting curves were measured at an oligomer concentration of 2.5 μM in 10 mM Tris-HCl, 100 mM NaCl pH 7.5. A heating/cooling cycle in the temp. range of 0-95° or 20-95° was applied with a temp. gradient of 0.5°/min. All ramps were indicating equilibrium melting processes. Tm values were defined as the maximum of the first derivative of the melting curve.

RNA folding Prediction and Modelling

Secondary structure predictions and Tm calculations of **12** and **13** were obtained using RNA *mfold* ([25] http://www.bioinfo.rpi.edu/applications/mfold/.) The conformation of hairpin **9** (see *Figure 10.2.*) was optimised using the amber force field (*Hyperchem 7.0*, Hypercube, Waterloo, Ontario).

References

[1] R.T. Batey, R.P. Rambo, J.A. Doudna, *Angew. Chem. Int. Ed Engl.* **1999**, *38,* 2326-2343.

[2] H.W. Pley, K.M. Flaherty, D.B. Mckay, *Nature* **1994**, *372,* 111-113.

[3] J.H. Gate, A.R. Gooding, E. Podell, K.H. Zhou, B.L. Golden, A.A. Szewczak, C.E. Kundrot, T.R. Cech, J.A. Doudna, *Science* **1996**, *273,* 1696-1699.

[4] J.H. Cate, A.R. Gooding, E. Podell, K.H. Zhou, B.L. Golden, C.E. Kundrot, T.R. Cech, J.A. Doudna, *Science* **1996**, *273,* 1678-1685.

[5] M. Perbandt, A. Nolte, S. Lorenz, R. Bald, C. Betzel, V.A. Erdmann, *Febs Letters* **1998**, *429,* 211-215.

[6] P.B. Moore, *Annu. Rev. Biochem.* **1999**, *68,* 287-300.

[7] C.W. Hilbers, C.A.G. Haasnoot, S.H. Debruin, J.J.M. Joordens, G.A. Vandermarel, J.H. Vanboom, *Biochimie* **1985**, *67,* 685-695.

[8] A.I.H. Murchie, D.M.J. Lilley, *Methods In Enzymology* **1992**, *211,* 158-180.

[9] D.T. Weaver, M.L. Depamphilis, *Journal Of Molecular Biology* **1984**, *180,* 961-986.

[10] U.R. Muller, W.M. Fitch, *Nature* **1982**, *298,* 582-585.

[11] M. Durand, K. Chevrie, M. Chassignol, N.T. Thuong, J.C. Maurizot, *Nucleic Acids Research* **1990**, *18,* 6353-6359.

[12] M.Y.X. Ma, L.S. Reid, S.C. Climie, W.C. Lin, R. Kuperman, M. Sumnersmith, R.W. Barnett, *Biochemistry* **1993**, *32,* 1751-1758.

[13] W. Pils, R. Micura, *Nucleic Acids Research* **2000**, *28,* 1859-1863.

[14] M. Salunkhe, T.F. Wu, R.L. Letsinger, *Journal Of The American Chemical Society* **1992**, *114,* 8768-8772.

[15] R.L. Letsinger, T.F. Wu, *Journal Of The American Chemical Society* **1995**, *117,* 7323-7328.

[16] F.D. Lewis, R.S. Kalgutkar, Y.S. Wu, X.Y. Liu, J.Q. Liu, R.T. Hayes, S.E. Miller, M.R. Wasielewski, *Journal Of The American Chemical Society* **2000**, *122,* 12346-12351.

[17] K. Yamana, A. Yoshikawa, H. Nakano, *Tetrahedron Letters* **1996** , *37,* 637-640.

[18] F.D. Lewis, X. Liu, Y. Wu, S.E. Miller, M.R. Wasielewski, R.L. Letsinger, R. Sanishvili, A. Joachimiak, V. Tereshko, M. Egli, *J. Am. Chem. Soc.* **1999**, *121,* 9905-9906.

[19] S.M. Langenegger, R. Häner, *Helvetica Chimica Acta* **2002**, *85,* 3414-3421.

[20] S.L. Beaucage, M.H. Caruthers, *Tetrahedron Letters* **1981**, *22,* 1859-1862.

[21] N.D. Sinha, J. Biernat, J. Mcmanus, H. Koster, *Nucleic Acids Res.* **1984**, *12*, 4539-4557.

[22] F.D. Lewis, X.Y. Liu, *Journal Of The American Chemical Society* **1999**, *121*, 11928-11929.

[23] M. Traetteberg, E.B. Frantsen, *Journal Of Molecular Structure* **1975**, *26*, 69-76.

[24] C.H. Choi, M. Kertesz, *Journal Of Physical Chemistry A* **1997**, *101*, 3823-3831.

[25] M. Zuker, *Methods In Enzymology* **1989**, *180*, 262-288.

[26] M. Ghosh, N. Rumpal, U. Varshney, K.V. Chary, *Eur. J. Biochem.* **2002**, *269*, 1886-1894.

[27] N.B. Ulyanov, W.R. Bauer, T.L. James, *J. Biomol. Nmr* **2002**, *22*, 265-280.

[28] W. Bannwarth, A. Treciak, *Helvetica Chimica Acta* **1987**, *70*, 175-186.

11. Conclusions and Outlook

We have shown that simple flexible non-nucleosidic polyaromatic residues can be used as base surrogates. Phenanthrene, phenanthroline and pyrene derivatives can be incorporated into oligodeoxynucleotides to give structurally stable hybrids. The aromatic residues contribute to the stability of the duplex via interstrand stacking interactions. Models of interstrand stacked polyaromatic residues were developed on the basis of circular dichroism, thermal denaturation, electrophoretic mobility and fluorescence experiments. While we could show that factors, such as dipole moment, aromatic interaction area and the length of the linkers play a role, the contributions of the individual factors are difficult to determine. As commonly observed with nucleic acids, sequence effects (nearest neighbors) seem to have a significant influence.

The interstrand stacking properties of the base surrogates find applications in the structural stabilization of DNA containing an abasic site, in the design of hairpin mimics and in the controlled generation of excimers. The latter aspect opens the possibility of developing a novel type of molecular beacon, which is based on hybridization induced formation of pyrene excimers.

Further studies in this area are already ongoing in our group. They include the synthesis and investigation of oligomeric derivatives of other types of non-nucleosidic building blocks. A further aspect is the improvement in the control of excimer formation by interstrand stacking. If excimer formation can be completely suppressed in a stem loop structure, this may lead to excimer-based molecular beacons.

Curriculum Vitae

1976	Born on the 5th of July in Binningen (BL, Switzerland)
1983-1987	Elementary school in Zielebach (BE)
1988-1991	High school in Utzenstorf (BE)
1991-1996	High school in Burgdorf (BE), Matura Typus C
1996-2001	Undergraduate studies in chemistry at the Department of Chemistry and Biochemistry, University of Bern. Diploma work in the group of Prof. Dr. J.-L- Reymond.
2001-	Ph.D. thesis in the group of Prof. Dr. R. Häner.

Bern, Mai 2005 Simon M. Langenegger